

SIMULATING THE BIRTH ENVIRONMENT OF **CIRCUMSTELLAR DISCS**

SIMULATING THE BIRTH ENVIRONMENT OF CIRCUMSTELLAR DISCS

FRANCISCA CONCHA-RAMIREZ

A PhD THESIS BY
**FRANCISCA
CONCHA-RAMIREZ**

Simulating the birth environment of circumstellar discs

Simulating the birth environment of circumstellar discs

Proefschrift

ter verkrijging van
de graad van doctor aan de Universiteit Leiden,
op gezag van rector magnificus prof. dr. ir. H. Bijl,
volgens besluit van het college voor promoties
te verdedigen op 6 april 2021
klokke 15.00 uur

door

Francisca Andrea Concha Ramírez

geboren te Temuco, Chile
in 1988

Promotiecommissie

| | | |
|----------------|---|--|
| Promotor: | Prof. dr. S.F. Portegies Zwart | |
| Co-promotor: | Dr. M.R. Hogerheijde | |
| Overige leden: | Prof.dr. H.J.A. Röttgering Prof.dr. J.S. Kaastra Prof.dr. C.W.M. Fridlund Dr. E. Sellentin Prof.dr. C. Dominik Dr. E. Kokubo Prof.dr. S. Pfalzner | University of Leiden University of Leiden University of Leiden University of Leiden University of Amsterdam University of Tokyo Forschungszentrum Jülich |

Cover design by Francisca Concha-Ramírez.

The background colour of the cover is *Cosmic Latte* [#FFF8E7, RGB (255, 248, 231)], the average colour of the Universe (Baldry et al. 2002). This colour is obtained by averaging the light emitted by 20,000 galaxies from the 2dF Survey (Colless et al. 2001).

*There is no thing as a single-issue struggle
because we do not live single-issue lives.*

Audre Lorde

| | |
|--|-----------|
| 1. Introduction | 1 |
| 1.1. Star clusters | 3 |
| 1.1.1. Formation and evolution | 3 |
| 1.1.2. Evolutionary time scales and radii | 6 |
| 1.2. Circumstellar discs | 7 |
| 1.2.1. Formation and evolution | 8 |
| 1.2.2. Disc masses and sizes | 10 |
| 1.3. Effects of the environment on circumstellar disc evolution | 11 |
| 1.3.1. Dynamical truncations | 12 |
| 1.3.2. External photoevaporation | 13 |
| 1.3.3. Ram pressure stripping | 16 |
| 1.3.4. Supernovae | 17 |
| 1.4. Numerical simulations | 18 |
| 1.4.1. N-body codes | 18 |
| 1.4.2. Smoothed-particle hydrodynamics | 19 |
| 1.4.3. AMUSE | 19 |
| 1.5. This thesis | 20 |
| 2. Viscous evolution of circumstellar discs in young star clusters | 25 |
| 2.1. Introduction | 26 |
| 2.2. Methods | 27 |
| 2.2.1. Evolution of isolated viscous discs | 27 |
| 2.2.2. Gas in the cluster | 29 |
| 2.2.3. Dynamical disc truncation | 30 |
| 2.2.4. Numerical implementation | 30 |
| 2.3. Results | 31 |
| 2.3.1. Initial conditions | 31 |
| 2.3.2. The effect of gas in the cluster | 33 |
| 2.3.3. Evolution of the circumstellar discs | 33 |
| 2.3.4. Comparison with observations | 34 |
| 2.4. Discussion | 38 |
| 2.5. Summary and conclusions | 41 |
| 3. External photoevaporation constrains time-scale for planet formation | 43 |
| 3.1. Introduction | 44 |
| 3.2. Model | 46 |
| 3.2.1. Viscous growth of circumstellar discs | 46 |
| 3.2.2. Dynamical truncations | 47 |
| 3.2.3. External photoevaporation | 47 |
| 3.2.4. Initial conditions | 51 |
| 3.3. Results | 54 |
| 3.3.1. Disc mass loss in time | 54 |
| 3.3.2. Disc lifetimes | 57 |
| 3.4. Discussion | 60 |
| 3.4.1. Disc survival and consequences for planet formation | 60 |
| 3.4.2. Influence of initial conditions | 61 |
| 3.4.3. Model caveats | 62 |
| 3.5. Conclusions | 64 |
| 3.A. Resolution of the discs | 64 |

| | |
|---|------------|
| 4. Effects of stellar density on photoevaporation of circumstellar discs | 67 |
| 4.1. Introduction | 68 |
| 4.2. Model | 69 |
| 4.2.1. Stars and circumstellar discs | 70 |
| 4.2.2. External photoevaporation | 70 |
| 4.2.3. Initial conditions | 71 |
| 4.2.4. Model caveats | 72 |
| 4.3. Results | 73 |
| 4.3.1. Disc fractions and lifetimes | 75 |
| 4.3.2. Disc masses | 77 |
| 4.4. Discussion | 80 |
| 4.5. Conclusions | 80 |
| 5. Evolution of circumstellar discs in young star-forming regions | 83 |
| 5.1. Introduction | 84 |
| 5.2. Model | 86 |
| 5.2.1. Molecular cloud collapse and star formation | 86 |
| 5.2.2. Stellar dynamics and circumstellar discs | 87 |
| 5.2.3. Initial conditions | 91 |
| 5.3. Results | 91 |
| 5.3.1. Star formation and cluster evolution | 91 |
| 5.3.2. Disc masses | 96 |
| 5.4. Discussion | 100 |
| 5.5. Summary and conclusions | 103 |
| Bibliography | 106 |
| Bibliography | 107 |
| English summary | 123 |
| Nederlandse samenvatting | 127 |
| Resumen en español | 131 |
| List of publications | 135 |
| Curriculum Vitae | 137 |
| Acknowledgements | 139 |

1 | Introduction

How unique is the solar system? Until relatively recently, the solar system was the only example of a planetary system we knew, and the concept of planets in distant regions of the galaxy belonged to the realm of science fiction. While the sheer number of stars in the universe hinted that our eight planets might not be an exception to the rule, we did not have any confirmation of the existence of other planets, or any clues of how these systems could look like. Until the late 20th Century, the solar system was most certainly unique, at least to the best of our knowledge.

Since the first discovery of a planet orbiting a Sun-like star in 1995 (Mayor & Queloz 1995), observational surveys have revealed an incredible variety of planetary systems. As of February 2021, 4685 planets¹ around stars other than the Sun, or exoplanets, have been detected. Somewhat surprisingly, the discovery of so many new planetary systems has not made our own look any less unique. If there is one thing that all planetary systems seem to have in common is their unlikeness.

The current image we have of star and planet formation has its origins in the 18th Century, in particular in the nebular hypothesis first developed by French polymath and mathematician Pierre-Simon Laplace, and German philosopher Immanuel Kant. The premise was simple: Kant (1755) conjectured that the back then newly-observed nebulae (e.g. Halley 1715) were locations of star and planet formation. A similar conclusion was reached independently by Laplace (1796), who also argued that it was the collapse of these nebulae which brought on the formation of a star, along with the material around it forming the shape of a disc. It was not until 1978 when this premise surfaced again in the work of Prentice (1978). The first detection of a circumstellar disc, around the star β Pictoris, was reported in Smith & Terrile (1984).

The first observations of resolved circumstellar discs were in the Orion nebula, where their dark silhouettes against the bright nebulous background were imaged by the Hubble Space Telescope (O'dell & Wen 1994). Nowadays, modern telescopes such as the Very Large Telescope (VLT) and the Atacama Large Millimetre/submillimeter Array (ALMA), both located in the magnificently beautiful Atacama desert in the north of Chile, have opened our eyes to the detailed substructure of these discs, allowing us to see planet formation as it happens.

¹Data from <http://exoplanet.eu> last accessed on 19 February 2021

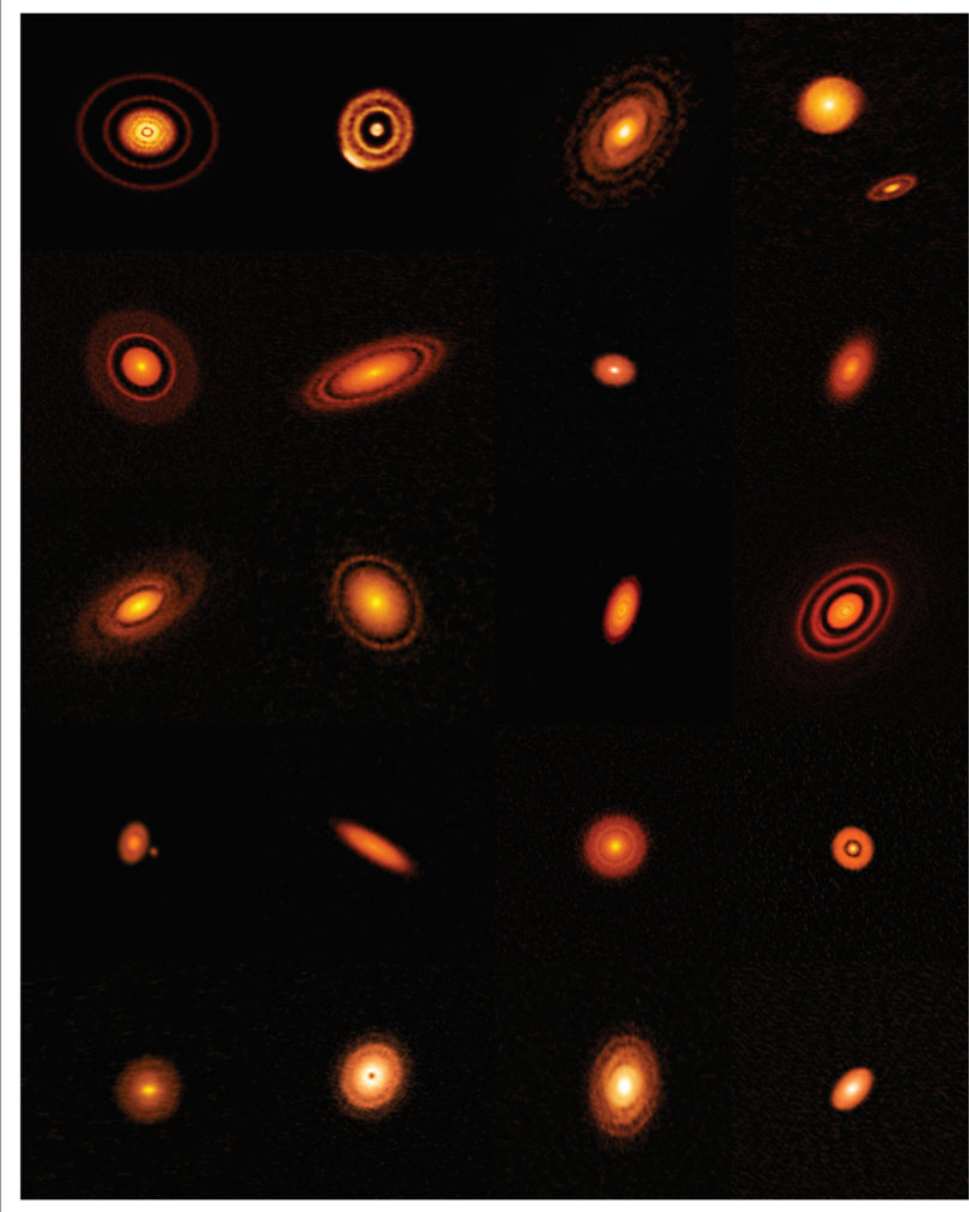


Figure 1.1: A sample of discs from ALMA's highest resolution survey, the Disc Substructures at High Angular Resolution Project (DSHARP). ALMA (ESO/NAOJ/NRAO), S. Andrews *et al.*; NRAO/AUI/NSF, S. Dagnello.

Further observations of circumstellar disc populations suggest that the environment in which they are immersed can have important repercussions for their potential to form planets. If planets do eventually form, their composition and dynamical configurations are likely to be shaped by the surroundings of their original discs. To answer the question of how unique the solar system is, we then have to take a step back in time, and look not just at the current configuration of our home system, but also at the conditions during its formation.

This thesis looks to quantify the effects that the star formation environment has over the young circumstellar discs. To do this, we perform numerical simulations of circumstellar disc which are affected by several ambient mechanisms that have been observed in star forming regions. We look to determine how these processes influence the mass reservoir of the discs, and how they constrain their potential to form planets. In the following Sections of this Chapter we set the scientific context for this work. In Section 1.5 we outline the goals and following Chapters of the thesis.

1.1. Star clusters

Star clusters are studied from many different areas in astrophysics. Beyond being of interest for their inner stellar dynamics and stellar evolution processes, star clusters are probes for star formation in distant galaxies and can provide insights into galaxy assembly (see Kruijssen 2014, Forbes et al. 2018, for recent reviews on this topic). In this thesis we focus our interest in star clusters as the birth sites of stars and circumstellar discs.

There is not a single definition of star cluster. Portegies Zwart et al. (2010) define a star cluster simply as a group stars which are gravitationally bound. According to Lada & Lada (2003) star clusters are defined as groups of stars which are gravitationally bound and whose stellar mass density is enough to keep the conglomerate stable against the tidal field of the galaxy and passing interstellar clouds, assuming virial equilibrium. Adams & Myers (2001) propose an additional criterion that the number of stars in the cluster is enough so that it does not evaporate in 10^8 Gyr, which is typical lifetime of open clusters in the field. Krumholz & McKee (2020) follow the simple definition of Trumpler (1930) and define star clusters as stellar groups which are not dominated by dark matter (separating them from galaxies) and with a mean stellar density that is at least a few times higher than the background. This allows to define star clusters very generally and remarks the fact that, while different types of clusters exist (see below), their dynamics and evolution are similar. There is no evidence that the different types of star clusters actually form differently (Elmegreen & Efremov 1997, Krumholz & McKee 2020).

Stars clusters are generally divided into three broad categories: globular clusters, open clusters, and associations. Globular clusters are generally massive ($M_c \gtrsim 10^5 M_\odot$) and old ($\gtrsim 10$ Gyr), containing hundreds of thousands of stars (Portegies Zwart et al. 2010). Open clusters are younger ($\lesssim 0.3$ Gyr) and less massive ($M_c \lesssim 10^3 M_\odot$), and generally contain a few hundred stars. Stellar associations are unbound conglomerates with a less than a hundred stars (Adams & Myers 2001; Gieles & Portegies Zwart 2011).

1.1.1. Formation and evolution

Stars form from the collapse of a giant molecular cloud. These clouds are located in large complexes in the spiral arms of galaxies. The masses of individual clouds can go up to $10^6 M_\odot$ and sizes up to 100 pc (Larson 2003). These clouds are not homogeneous in density, and they present substructure in the form of clumps and filaments arranged in a partly hierarchical fashion which can be approximated with fractal models (e.g. Scalo 1990, Elmegreen

& Falgarone 1996; Elmegreen et al. 2000; Williams et al. 2000; Bate 2010; Hacar et al. 2013; Chevance et al. 2020; Krause et al. 2020). These clumps have masses ranging from $\sim 1 M_{\odot}$ to several thousand solar masses, and sizes from 0.1 pc to several parsec (Larson 2003). The irregular shapes of the clouds and their substructure suggest that these arrangements might be modelled by turbulent flows (Falgarone et al. 1991; Falgarone & Phillips 1991).

Depending on their mass, the clumps within giant molecular clouds can form individual stars, small multiple systems, or large star clusters (e.g. Lada et al. 1993; Larson 1995; Williams et al. 2000; Lada & Lada 2003; Bate 2012). The star formation process remains the same across these different scales, and it begins with the collapse of a clump. Regardless of their substructure, molecular clouds have typical temperatures of $\sim 10 - 20$ K across their range of different densities (e.g. Larson 1985; Masunaga & Inutsuka 2000). The combination of low, constant temperature and high densities in the clumps make them Jeans unstable (Jeans 1902), meaning that a small gravitational instability can grow exponentially and cause the clump to fragment into smaller and smaller pieces in a chain reaction-like effect. The fragmentation will continue as long as the gas can cool efficiently (e.g. Hoyle 1953; Hunter 1964, 1977; Field et al. 2008; Vázquez-Semadeni et al. 2019).

As the fragmentation continues, some of the smallest pieces will reach densities high enough to form a star. This point-like source will be surrounded by an envelope of infalling material. These high density points, which can now be referred to as protostars, have initial masses $\sim 10^{-2} M_{\odot}$ and will continue growing by accreting material from the envelope (e.g. Larson 1969; Appenzeller & Tscharnutter 1975; Winkler & Newman 1980; Masunaga & Inutsuka 2000; Wuchterl & Tscharnutter 2003). It is at this moment when circumstellar disc begin to form. In the present section we will continue describing the star cluster formation process, and resume describing disc formation in Section 1.2.1.

The total angular momentum in a giant molecular cloud is too large to be contained in a single star (e.g. Mestel & Spitzer 1956; Mestel 1965; Spitzer 1968; Bodenheimer et al. 2000). As such, the fragmentation process results not only in the formation of individual stars, but also in stellar aggregates. The substructure present in the clouds plays an important role in establishing the kinematics and structure of young clusters (e.g. Klessen et al. 2000; Klessen & Burkert 2000; Kruijssen et al. 2012).

There are two main scenarios of star cluster formation: *in-situ* formation and conveyor belt formation (e.g. Longmore et al. 2014; Krumholz & McKee 2020). The differences between the two concern mostly the extent of the initial gas compared with the radius of the final cluster. *In-situ* formation refers to the cluster forming rapidly from a clump or cloud of gas. The size of the initial gas cloud will be the same as the final radius of the cluster. This mechanism requires for star formation to happen very quickly, in about one dynamical timescale (see Section 1.1.2) (Longmore et al. 2014). The conveyor belt scenario considers the initial gas to be much more extended than the final cluster, probably by several cluster radii. The clumps and filaments present in the cloud accrete gas from the outer regions and direct it to the protostars.

Regardless of the formation scenario, the young stellar clusters are still embedded in leftover gas. In an ideal system, all the gas in the molecular cloud would turn into stars. However, several mechanisms that arise from the star formation process itself can reduce the amount of gas available to form stars. Protostellar outflows (e.g. Matzner & McKee 2000; Bally 2016; Offner & Chabrier 2017), photoionization feedback (e.g. Williams & McKee 1997; Matzner 2002; Murray & Rahman 2010), radiation pressure (e.g. Fall et al. 2010; Murray & Rahman 2010; Grudić et al. 2018), and stellar feedback such as wind and supernovae (e.g. Vink et al. 2001; Pelupessy & Portegies Zwart 2012; Offner & Arce 2015) can all reduce the amount of gas available for star formation. To form bound clusters, $\sim 30\%$ to 50% of the



Figure 1.2: Trapezium cluster in optical (left) and infrared (right) wavelengths. The stars embedded in the gas are only visible with infrared instruments. NASA; K.L. Luhman (*Harvard-Smithsonian Center for Astrophysics, Cambridge, Mass.*); G. Schneider, E. Young, G. Rieke, A. Cotera, H. Chen, M. Rieke, R. Thompson (*Steward Observatory, University of Arizona, Tucson, Ariz.*); C.R. O'Dell and S.K. Wong (*Rice University*).

gas must be turned into stars before feedback mechanisms begin (Lada et al. 1984; Goodwin 1997; Clarke et al. 2000). During the embedded stage the stars in the clusters are only visible in infrared wavelengths (Figure 1.2).

In young star clusters, 50% to 90% of the total mass can be comprised of leftover gas (e.g. Lada & Lada 1991; Clarke et al. 2000), whereas it is not present in older systems (e.g. Lada & Lada 1995; Portegies Zwart et al. 2010). The removal of the leftover gas has important consequences in the dynamics of the cluster. In particular, the initial gas fraction and the rate at which the gas is expelled are important. Losing $\sim 50\%$ of the gas in a short time scale compared with the cluster crossing time (see Section 1.1.2) results in the cluster becoming unbound (e.g. Clarke et al. 2000; Elmegreen et al. 2000; Portegies Zwart et al. 2010). If the gas expulsion lasts several crossing times, the cluster can adapt to the slow changes in potential and survive as a bound system, keeping most of its stars (e.g. Lada et al. 1984; Baumgardt & Kroupa 2007; Pelupessy & Portegies Zwart 2012).

After the gas is completely dispersed from the clusters, their evolution continues to be dominated purely by gravity and stellar evolution. Eventually, clusters lose mass due to both internal and external processes. Stellar evolution causes stars to lose $\sim 20\%$ of their mass in supernova explosions. This mass loss occurs until ~ 40 Myr of evolution. These explosions can cause the stellar remnants to escape the cluster, due to the velocity kicks (e.g. Faucher-Giguère & Kaspi 2006; Kruijssen 2009). The tidal field of the galaxy can greatly increase mass loss by removing stars from the cluster (e.g. Takahashi & Portegies Zwart 2000; Baumgardt & Makino 2003; Lamers et al. 2010). On longer timescales ($t \gtrsim 100$ Myr) mass loss is dominated by dynamical relaxation, also known as evaporation or dissolution. This effect is related to the kinetic energy distribution trying to compensate for high-energy stars being kicked out of the cluster. This causes stars to escape the cluster through tidal streams (e.g. Spitzer 1940; Fujii & Portegies Zwart 2011; Gnedin et al. 2014; Madrid et al. 2017; Lucas et al. 2018; Dinnbier & Kroupa 2020). The cluster stars then dissipate into the field.

1.1.2. Evolutionary time scales and radii

The dynamical evolution of star clusters is studied through a series of time scales and radii. The definitions of these parameters are generally different for theoretical analyses than for observations. This is because several quantities, such as the total mass or the potential energy, are impossible to measure from observations. In this section we deal with theoretical definitions, since these are the ones used in the following chapters of this thesis.

The dynamical time scale, or crossing time, corresponds to the time that it takes for a particle to cross the system and is defined as (Spitzer 1988):

$$t_{\text{dyn}} = \frac{R_c}{v}, \quad (1.1)$$

where R_c is the cluster radius and v is the mean velocity of a star. From the virial theorem, this expression can be rewritten as:

$$t_{\text{dyn}} = \sqrt{\frac{R_c^3}{GM_c}}, \quad (1.2)$$

where G is the universal gravitational constant and M_c is the mass of the cluster. The dynamical time scale indicates the time in which the system reaches dynamical equilibrium.

Another important time scale is the relaxation time scale. This is the time in which the initial orbits of the stars have been erased by distant interactions with other stars. The relaxation time scale is the time within which global characteristics of the cluster change. It is defined as (Spitzer 1988):

$$t_{\text{relax}} = \frac{N}{6 \ln(N)} t_{\text{dyn}}. \quad (1.3)$$

For a star cluster with $N = 1,000$, the relaxation time scale is $t_{\text{relax}} \sim 10$ Myr. This is several Myr shorter than the average lifetime of an open cluster. This means that interactions between stars are important during the life of such a cluster and there is significant dynamical evolution. These types of systems are called collisional. On the other hand, a galaxy like the Milky Way ($N \sim 10^{11}$) has a relaxation time scale $t_{\text{relax}} \sim 10^7$ Gyr, so the interactions between stars are not relevant in defining its dynamical evolution. Galaxies are known as collisionless systems.

Star clusters tend to be round and symmetrical, so being able to calculate their radius is useful to follow their evolution. Several definitions of cluster radius exist. The virial radius corresponds to the radius within which the cluster is in virial equilibrium. It is defined as:

$$R_{\text{vir}} = \frac{GM_c^2}{2|U|}, \quad (1.4)$$

where U is the total potential energy of the system.

The radius of the core of the cluster can be defined theoretically in two ways. When the central density and velocity dispersion are known, the core radius can be defined as (King 1966):

$$R_{\text{core}} = \sqrt{\frac{3 < v^2 >}{4\pi G\rho}}, \quad (1.5)$$

where $\langle v^2 \rangle$ is the velocity dispersion and ρ is the central density. When these values are not easy to obtain, the core radius can be defined using density-weighted nearest neighbours distances (Casertano & Hut 1985):

$$R_{\text{core}} = \sqrt{\frac{\sum_i \rho_i^2 r_i^2}{\sum_i \rho_i^2}}, \quad (1.6)$$

where ρ_i is the local number density around star i and r_i is its distance to the k nearest neighbours. In numerical simulations, both definitions of R_{core} behave similarly.

1.2. Circumstellar discs

Circumstellar discs are a natural outcome of the star formation process. These discs contain the building blocks for future planetary systems. Their different evolutionary paths can help us understand the planet formation process and the diversity of planetary systems we observe today.

Circumstellar discs are geometrically thin (vertical scale height $h \ll r$) and have masses $M_{\text{disc}} \ll M_*$. This means that they can be modelled within the theory of thin accretion discs (Pringle 1981). In particular, they can be described by the similarity solutions for accretion discs by Lynden-Bell & Pringle (1974). In this frame, the discs are defined by their initial characteristic radius, initial mass, the viscosity at specific radii, and the radial dependence of the viscosity. The characteristic radius of a disc is defined as:

$$R_d(t) = \left(1 + \frac{t}{t_v}\right)^{\frac{1}{2-\gamma}} R_c(0), \quad (1.7)$$

where γ is the radial dependency exponent for the viscosity and t_v is the viscous time scale of the disc at $t = 0$. The mass of the disc is defined as:

$$M_d(t) = M_d(0) \left(1 + \frac{t}{t_v}\right)^{\frac{1}{2\gamma-4}}. \quad (1.8)$$

The viscous time scale, the time within which angular momentum is redistributed by viscosity, is given by:

$$t_v = \frac{R_c(0)}{3(2-\gamma)^2 \nu_c}, \quad (1.9)$$

where ν_c is the disc viscosity, defined as:

$$\nu_c = \alpha \frac{c_s^2}{\Omega} = \alpha \frac{k_b T \sqrt{R^3}}{\mu m_p \sqrt{GM_*}}. \quad (1.10)$$

Here, α is the viscosity turbulence parameter (Shakura & Sunyaev 1973), c_s is the isothermal sound speed, $\Omega = \sqrt{GM/R^3}$ is the keplerian velocity, k_b is the Boltzmann constant, μ is the mean molecular weight of the gas, m_p is the proton mass, T is the disc midplane temperature at R , and M_* is the mass of the host star. Finally, the surface density of the discs is defined by Lynden-Bell & Pringle (1974) as:

$$\Sigma(R, t = 0) = \Sigma_0 \frac{R_c}{R} \exp\left(\frac{-R}{R_c}\right), \quad (1.11)$$

| Class | Physical properties |
|-------|---|
| 0 | $M_{\text{env}} > M_* > M_{\text{disc}}$ |
| I | $M_* > M_{\text{env}} \sim M_{\text{disc}}$ |
| II | $M_{\text{disc}}/M_* \sim 1\%, M_{\text{env}} \sim 0$ |
| III | $M_{\text{disc}}/M_* \ll 1\%, M_{\text{env}} \sim 0$ |

Table 1.1: Classification of young stellar objects. Adapted from Williams & Cieza (2011)

where R_c is the characteristic radius of the disc as described in Eq. 1.7, and

$$\Sigma_0 = \frac{M_d}{2\pi R_c^2(1 - \exp(R/R_c))}. \quad (1.12)$$

The evolution of circumstellar discs is dependent on their viscosity ν_c , which in turn depends on the turbulence parameter α and the radial dependence γ . From Equations 1.10 and 1.9 it can be seen that higher values of α result in shorter viscous time scales, meaning rapidly evolving discs. Discs with lower α evolve slower. Values for both parameters have been estimated observationally. Analysing accretion rates in the Taurus and Chamaeleon I molecular cloud complexes, Hartmann et al. (1998) find a value of $\gamma \gtrsim 1$. The limit $\gamma \sim 1$ corresponds to a value of α that is constant all over the disc. With their observed disc sizes, they estimate $\alpha \sim 10^{-2}$. Isella et al. (2009) observe resolved discs in several different regions and find cases for $\gamma > 0$, $\gamma \sim 0$, and even $\gamma < 0$ for some discs. The $\gamma \sim 0$ case corresponds for constant viscosity through the discs. In the discs with $\gamma < 0$ viscosity decreases with radius, which is the opposite of what is expected from the models. They derive values of α ranging from 5×10^{-1} to 10^{-4} . Other surveys have found similar ranges (e.g. Andrews et al. 2010; Mulders & Dominik 2012; Trapman et al. 2020).

1.2.1. Formation and evolution

As a direct consequence of angular momentum conservation during the star formation process (Section 1.1.1), circumstellar discs form within the first 10^4 years after the collapse of a molecular cloud (Yorke et al. 1993; Hueso & Guillot 2005). While the initial collapse of a clump in a molecular cloud begins into a point source, distant material with higher angular momentum falls inward toward the newly formed protostar (e.g. Bate 2011). This material will eventually form a disc around the protostar. Initially, the young disc will be surrounded by gas and dust, in what is usually referred to as the embedded stage. At this point, the young star and circumstellar disc are categorised as a Class 0 young stellar object (see Table 1.1), which have lifetimes ~ 0.2 Myr (Dunham et al. 2015).

The material which surrounds the disc is accreted into the disc itself or dispersed through outflows and jets (e.g. Elmegreen & Scalo 2004; Scalo & Elmegreen 2004; Nakamura & Li 2012; Bally 2016). As the envelope starts to dissipate, the system evolves into a Class I object. This stage lasts ~ 0.5 Myr (Evans et al. 2009; Williams & Cieza 2011). The star formation process is effectively over by the end of the Class I phase, and the originally protostellar disc can now be considered protoplanetary. When the dispersal of the envelope is complete and the star at the center of the disc becomes optically visible it is referred to as a Class II object.

The time scales on which discs evolve are too short compared to the lifetime of their host stars. It is not possible to observe ongoing evolutionary processes, and a demographic approach is required to quantify properties of the discs. By observing populations of Class II

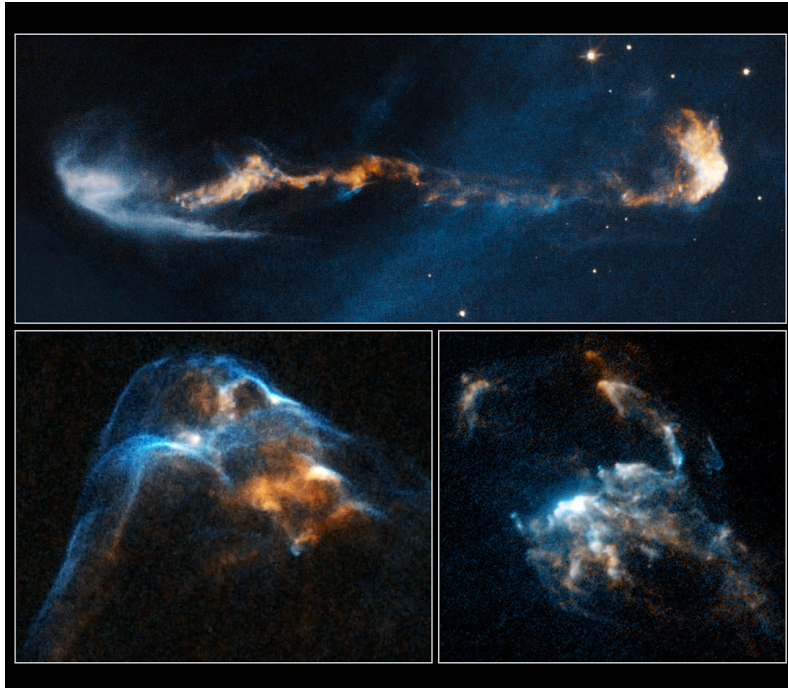


Figure 1.3: Protostellar jets and outflows in HH47 (top panel, Vela constellation), HH34 and HH2 (bottom panels, Orion nebula). *NASA, ESA, and P. Hartigan (Rice University)*.

objects in star forming regions of different ages and densities it is possible to paint a picture of disc evolution.

One of the most important properties of circumstellar discs are their lifetimes, since these set the time available for planet formation. Currently, the best way to estimate disc lifetimes is to measure disc fractions in regions of different ages. The presence of a disc around a star is detected as an infrared excess. The first statistical study of the number of discs in a star forming region was performed by Strom et al. (1989) in Taurus-Auriga. They found that $\sim 80\%$ of stars with ages $\lesssim 1$ Myr have infrared excesses indicating the presence of discs, while less than 10% of stars older than 10 Myr do. Haisch et al. (2001) study the disc fractions in three star clusters (NGC 2264, NGC 2362, and NGC 1960) and find a half-life ≤ 3 Myr for the discs, and a mean lifetime of ~ 6 Myr. From a series of Spitzer Space Telescope surveys, Mamajek (2009) model the decrease in disc fractions in several regions as an exponential decay with a typical time scale of 2.5 Myr. Similar estimates have been found from several other star forming regions and star clusters (e.g. Lada et al. 2006; Sicilia-Aguilar et al. 2006; Winston et al. 2007; Hernández et al. 2007; Gutermuth et al. 2008; Sung et al. 2009; Ansdell et al. 2016, 2017).

Disc dispersal is the result of the interplay of many different processes. While there are several environmental effects which can accelerate it (see Section 1.3), within this section we limit our discussion only to internal causes.

The first mechanism leading to mass loss is the viscous evolution of the discs. The distribution of angular momentum causes both the expansion of the disc and accretion onto the host star (Armitage 2011; Williams & Cieza 2011). Measurements of stellar accretion rates show that Class II objects are constantly accreting mass into the star from the discs. A $\sim 1 M_{\odot}$ young star can accrete up to 10% of its mass during the first Myr of the Class II phase,

with accretion rates $10^{-8} - 10^{-7} \text{ M}_\odot \text{ yr}^{-1}$ (Hartmann et al. 1998, 2016). These accretion rates decrease with stellar age (e.g. Sicilia-Aguilar et al. 2010; Manara et al. 2012, 2016) and decline even further in transition discs, which are on the verge of completely being depleted of gas (Kim et al. 2016; Najita et al. 2015). This decline with age is expected from accretion theory (Hartmann et al. 1998). However, disc dispersal through accretion only would imply an indefinite viscous expansion of the outer regions of the discs. Since there is no observational evidence for this, there must be other processes aiding in mass dissipation (Gorti et al. 2009).

Another elemental process that causes mass depletion in discs is planet formation. Observational and theoretical studies have shown that planet formation must start within 0.1 to 1 Myr after star formation for discs to still be massive enough to form rocky planets and the cores of gas giants (e.g. Greaves & Rice 2010; Williams 2012; Najita & Kenyon 2014; Manara et al. 2018; Tychoniec et al. 2020, Chapters 3, 4, and 5 of this thesis). Resolved observations of circumstellar discs have shown gaps and spiral arms that are likely produced by young planets (e.g. Isella et al. 2012; Andrews et al. 2016; van Boekel et al. 2017; Marino et al. 2018, 2019; van der Marel et al. 2018; Francis & van der Marel 2020; Huang et al. 2020). Numerical models have confirmed that these structures can be originated by planet formation (e.g. Bae et al. 2018; Dong et al. 2019).

An internal mechanism that can accelerate disc dispersal is photoevaporation from the host star. Internal photoevaporation is the process through which high-energy photons coming from the host star heat the disc surface, causing gas to evaporate (e.g. Luhman et al. 2010; Ercolano et al. 2011; Gorti et al. 2009). Internal photoevaporation is dominated by X-ray photons (Owen et al. 2012). The bulk of the internal photoevaporation mass loss occurs in the inner 20 au of the discs (Font et al. 2004; Owen et al. 2010). This process can then also constrain the time available to form planetary systems (Gorti et al. 2015). However, photoevaporation seems to be more efficient when the radiation comes from nearby stars. We expand on this process on Section 1.3.

1.2.2. Disc masses and sizes

Circumstellar discs are formed by gas and dust and, unlike in the interstellar medium, these two components are decoupled. Most of the mass in solids is in the shape of dust grains of sizes $\sim 1 \text{ mm}$ and larger, which are not mixed with the gas (Bergin & Williams 2018). To determine disc masses and sizes, both of these constituents need to be addressed separately.

The gas is generally much harder to detect than the dust. This is because its main constituent, molecular hydrogen, is affected by several physical processes which make it very weak or even undetectable in most of the disc (Field et al. 1966; Carmona et al. 2008). Other molecules can be used as tracers of molecular hydrogen, such as carbon monoxide and hydrogen deuteride. However, the abundance of these molecules has to be determined with very high precision to be used as a tracer for molecular hydrogen (Bergin & Williams 2018). As such, total disc masses are generally estimated from disc dust masses.

Dust masses are measured by proxy. The millimetre wavelength flux measure can be transformed into a disc dust mass using the relation:

$$M_{\text{dust}} = \frac{F_\nu d^2}{\kappa^2 B_\nu(T_{\text{dust}})} \quad (1.13)$$

where F_ν is the millimetre flux, κ is the estimated opacity, B_ν is the Plank function and T_{dust} is the temperature of the disc midplane, assumed constant and $\approx 20 \text{ K}$ (Andrews & Williams 2005). From the dust mass, a gas mass is calculated by assuming a 100:1 gas-to-dust ratio. This ratio is derived from the interstellar medium (Goldsmith et al. 1997).

There is a big range of observed disc masses, and they seem to greatly depend on the age (see Section 1.2.1) and environment (see Section 1.3) of the discs. In surveys of the youngest star forming regions, such as Chamaeleon I and the Lupus clouds, total disc masses span a range from $\sim 10^{-1}$ to $10 M_{\text{Jup}}$ (Ansdel et al. 2016; Pascucci et al. 2016; Ansdel et al. 2017). In older regions, such as Upper Scorpio, the average disc mass is $\sim 1 M_{\text{Jup}}$ (Barenfeld et al. 2016).

Measuring disc sizes requires the discs to be resolved, making it more complicated than disc masses. Surveys at high angular resolution, such as those carried out by ALMA, allow for measurements of disc dust sizes. However, radial drift of dust means that the measured dust sizes are likely to be more compact than the gas discs. Gas disc sizes are measured through the rotational line emission from molecules such as carbon monoxide and cyanogen (e.g. Barenfeld et al. 2017; Facchini et al. 2017; Ansdel et al. 2018; Trapman et al. 2019). Ansdel et al. (2018) find the ratio of gas radius to dust radius to be $\sim 1.5 - 3$. Dust disc sizes in the Lupus clouds have been found to range from ~ 40 au to ~ 300 au (Ansdel et al. 2018). In Upper Scorpio, the median disc dust radius is 21 au (Barenfeld et al. 2017).

1.3. Effects of the environment on circumstellar disc evolution

Demographic studies of circumstellar discs show great variations between regions of different ages and stellar densities. In regions where massive stars are present, the number of discs and their masses decrease the closer they are to an OB-type star. Several studies have found diminishing disc fractions, disc masses, and disc sizes with decreasing distance to θ^1 Ori C, an O6 type star in the Trapezium cluster (e.g. Vicente & Alves 2005; Mann & Williams 2010; Mann et al. 2014; Eisner et al. 2018). In particular, there is a lack of discs with dust masses higher than $9M_{\oplus}$ within 0.03 pc of θ^1 Ori C. At projected distances larger than 0.3 pc from the star, the disc population is more similar to those of low mass star forming regions (Vicente & Alves 2005; Mann et al. 2014). Similar effects are reported by Ansdel et al. (2017) in the σ Orionis region, where disc masses lessen with decreasing distance to the OB triple star system at its center. No massive discs are detected within the 0.5 pc around these massive stars. van Terwisga et al. (2020) find evidence for two distinct disc populations in the NGC 2024 region: one population, located close the massive star IRS 1, appears to have fewer discs and lower disc masses than the second population, embedded in a dense molecular gas ridge. Several other surveys have revealed evidence of environmental effects in various regions, such as NGC 6611 (Guarcello et al. 2009), Pismis 24 (Fang et al. 2012), NGC 1977 (Kim et al. 2016), and Cygnus OB2 (Guarcello et al. 2016).

Disc mass distributions in low mass star forming regions are found to be statistically indistinguishable from each other. This is the case for Lupus, Taurus, and the Orion Molecular Cloud 2 (Ansdel et al. 2016; van Terwisga et al. 2020), suggesting that in low stellar densities the discs evolve similarly and mostly unperturbed. These regions, together which others such as Chamaeleon I and Ophiuchus (Williams et al. 2019), represent relatively young and sparse locations of star formation, with estimated ages of 1 – 5 Myr. The discs masses in all of these regions are in average higher than those in Orion, even though their ages are comparable. Older regions, such as Upper Scorpio (~ 10 Myr, Barenfeld et al. 2016), have less discs than younger ones and the discs are less massive and smaller (Barenfeld et al. 2016, 2017).

While it is known that disc mass decreases with age due to viscous evolution (see Section 1.2.1), these observations suggest that the stellar density of the star forming region and

the presence of massive stars in the vicinity can also affect disc mass distributions. These differences in disc populations can be attributed to a series of environmental effects which are described below.

1.3.1. Dynamical truncations

While star-star collisions are rare, the cross sections of circumstellar discs are much larger than those of stars, so their probability of being perturbed dynamically by another star in a crowded environment is non negligible (Pfalzner 2003). Given that the encounters themselves are very short-lived, the observational evidence of dynamical encounters is limited to the imprints they can leave on the discs. Population studies of discs in dense stellar regions, in particular those in which the size of the discs can be resolved, have shown that the average disc size decreases with increasing local stellar density (e.g. Vicente & Alves 2005; de Juan Ovelar et al. 2012). This was proposed as a result of dynamical encounters truncating the discs.

With the advent of modern telescopes such as ALMA and the VLT it has been possible to observe the eventual consequences of dynamical encounters directly. A fascinating assortment of disc substructure is now coming to light, such as spiral arms, tidal tails, and misaligned inner and outer discs. These could be explained by close encounters with passing stars (e.g. Reche et al. 2009; Christiaens et al. 2014; Salyk et al. 2014; Kuffmeier et al. 2020; Kraus et al. 2020; Ménard et al. 2020). Cabrit et al. (2006) suggest that the ~ 600 au trailing “tail” of material observed in the disc of RW Aur A was likely caused by the recent fly-by of its companion, RW Aur B. Numerical simulations by Dai et al. (2015) confirm that this might indeed have been the case, since the arms seen in RW Aur A look like the ones that form when a star passes nearby the disc in their simulations. New observations by Rodriguez et al. (2018) reveal more substructure within the disc of RW Aur A, and the authors argue that this might be the result of several, cumulative close encounters. Winter et al. (2018c) model the dust emission structure surrounding the triple system HV Tau and the disc of DO Tau, and suggest that it corresponds to the remainders of the discs surrounding both system after they experienced a close encounter about 0.1 Myr ago.

Furthermore, it has been proposed that the young protoplanetary disc of the solar system was truncated in such an encounter. This argument is based on the sharp edge of the solar system at ~ 30 au, which can be attributed to an encounter with a star of around a solar mass at a periastron distance of ~ 100 au (Adams 2010; Breslau et al. 2014; Pfalzner et al. 2018). Additional evidence for this encounter is given by the orbits of the *Sednitos*, a family of a dozen (known) solar system objects including the dwarf planet Sedna, which have extraordinary wide orbits ($a > 150$ au) and a perihelion distance much larger than the Earth’s. Jílková et al. (2015) show that the orbits of the *Sednitos* can be explained by their origin being a capture from the planetesimal disc of a nearby passing star. Pfalzner et al. (2018) show that a fly-by of a star with mass 0.3 to $1 M_\odot$ at perihelion distances between 50 and 150 au could cause such characteristics, and that the *Sednitos* could have originally belonged to the solar system and their orbits have been excited by such an encounter.

The first numerical studies regarding the effects that a nearby star could have on a circumstellar disc were performed in the context of binary star formation and evolution (e.g. Paczynski 1977; Pringle 1989; Clarke & Pringle 1991). It was a natural step to expand these analyses into the realm of larger stellar systems, where the perturber is a point mass in an unbound orbit. Clarke & Pringle (1993) perform numerical simulations of prograde, retrograde coplanar and orthogonal approaches of a star to a circumstellar disc. They investigated the fate of the debris resulting from these encounters: how much remains bound, how much is unbound, and how much stays in the neighbourhood of the disc. They find that a pro-

grade coplanar encounter is the most destructive, that disc matter down to about $0.5r_{enc}$ is left unbound after the encounter, and that a considerable amount of matter is captured by the perturbing star.

Several numerical simulations have continued to explore the effects of dynamical encounters over circumstellar discs (e.g. Korycansky & Papaloizou 1995; Hall et al. 1996; Bonnell & Kroupa 1998; Pfalzner 2003; Bate et al. 2003; Pfalzner et al. 2005b,a; Breslau et al. 2014; Vincke et al. 2015; Vincke & Pfalzner 2016). Scally & Clarke (2001) simulate a region akin to the Trapezium cluster and keep track of all the encounters occurring in 12 Myr. They find that it is likely for each star in their model to experience at least one encounter closer than 1×10^3 au during the 1×10^6 Myr estimated disc lifetimes. However, they determine that only 3% to 4% of the discs can be destroyed by encounters alone. They consider an encounter to be destroying if the perturber comes closer than 100 au. Further analyses have shown that, unlike the assumptions by Scally & Clarke (2001), it is not only one very close encounter that can destroy a disc, but actually a series of further encounters can have a cumulative effect (Pfalzner et al. 2006). Further models have shown that dynamical encounters might not only truncate the discs but also harden their surface density (Rosotti et al. 2014), lead to the formation of spiral arms, and cause accretion bursts into the stars due to material being pushed inwards on the disc. Pfalzner et al. (2005a) show that these bursts of accretion are common in regions such as the Orion Nebula Cluster.

In recent years, newer simulations suggest that while dynamical encounters do play a role in shaping circumstellar discs, they are not the most efficient or most important method for disc destruction in high stellar density environments. Winter et al. (2018b) perform a comparison of disc mass loss rates caused by external photoevaporation and dynamical truncations. They find that, while some discs do get truncated in close encounters, the mass loss due to external photoevaporation is orders of magnitude higher. Winter et al. (2018a) find that even the cumulative effect of many distant dynamical encounters does not lead to a great amount of mass loss. As will be discussed in Section 1.3.2 and Chapters 3, 4, and 5 of this thesis, the relative importance of dynamical encounters as a means for efficient disc destruction is still up for debate, in particular when compared to external photoevaporation.

1.3.2. External photoevaporation

Photoevaporation is the process by which high energy photons heat the surface of a circumstellar disc and evaporate material from it. These photons can originate from the host star or from nearby massive stars in the vicinity of a disc. The former process is known as internal photoevaporation (see Section 1.2.1), and the latter as external photoevaporation. Given that external photoevaporation is the one directly related to the star formation environment, in this section and throughout this thesis the main focus is on that mechanism.

There are several observational clues of external photoevaporation removing mass in circumstellar discs. The first observations correspond to *proplyds*, cometary tail-like structures of ionized gas that form in discs when close to a massive star. The first proplyds were observed in the Orion nebula (O'dell & Wen 1994; O'dell 1998; Vicente & Alves 2005; Eisner & Carpenter 2006; Mann et al. 2014; Kim et al. 2016) and several subsequent studies confirmed that their structures could be explained by the massive stars in the region stripping mass from the discs through radiation (e.g. Richling & Yorke 1997; Johnstone et al. 1998; Störzer & Hollenbach 1999; Adams et al. 2004). The demographic differences across star forming regions enumerated at the beginning of this section also show that discs closer to bright stars are less massive than discs located in sparser regions. While in high density regions dynamical encounters might contribute to disc dispersal, observations seem to point to proximity to an OB star resulting in declining disc masses.



Figure 1.4: Proplyds in the Orion nebula observed with the Hubble Space Telescope. *NASA/ESA, L. Ricci (ESO)*.

Photoevaporation can occur from a combination of far ultraviolet (FUV), extreme ultraviolet (EUV), and X-ray photons. EUV radiation ionizes and heats disc surfaces up to $\sim 10^4$ K, while FUV and X-ray heat gas up to temperatures from ~ 100 to 3,000 K but keep it neutral. FUV photons dissociate gas molecules, generating a photodissociation region of neutral gas which the EUV radiation can not penetrate. Because of this, FUV radiation is the main driver of external photoevaporation (Johnstone et al. 1998; Adams et al. 2004).

The thermal pressure from the photons pushes the gas outward. The bulk of the mass loss occurs from the outer regions of the discs, beyond a critical radius r_g at which the sound speed of the heated gas equals the escape speed from the gravitational field of the host star. This radius is defined as:

$$r_g = \frac{GM_* <\mu>}{kT} \approx 100 \text{ au} \left(\frac{T}{1,000 \text{ K}} \right)^{-1} \left(\frac{M_*}{M_\odot} \right) \quad (1.14)$$

where M_* is the mass of the host star and $<\mu>$ is the average mass of the gas particles (Adams et al. 2004). Early theoretical models of photoevaporation assumed that mass loss due to photoevaporation occurred only at radii $r > r_g$ (e.g. Hollenbach et al. 1994; Johnstone et al. 1998; Störzer & Hollenbach 1999), and that as such it would result only in disc truncation. Adams et al. (2004) show that mass is still removed from the inner regions of the discs, but the effects of external photoevaporation do cause the discs to deplete from the outside in. While the thermal pressure affects the behaviour of the gas, dust grains with radii ≤ 1 cm (Adams et al. 2004) can get entrapped in the photoevaporation wind and also be removed from the discs. However, dust quickly agglomerates to sizes larger than the critical radius and turns resilient to photoevaporation (Haworth et al. 2018a).

Studies of single discs as well as clustered regions show disc masses to be strongly dependent on the background radiation fields, as a direct consequence of external photoevaporation. The intensity of the radiation fields is generally defined in terms of Habing units (G_0), with $1 G_0 \approx 1.6 \times 10^{-3}$ erg cm $^{-2}$ s $^{-1}$ being the average flux in the local interstellar medium (Habing 1968). Adams et al. (2004) find that discs around stars $M_* \approx 0.5 M_\odot$ are evaporated down to ~ 15 au in less than 10 Myr when exposed to moderate radiation fields of $\sim 3,000 G_0$, but that even discs around stars of a solar mass or higher are destroyed in that time scale for radiation fields $\sim 3 \times 10^4 G_0$. Anderson et al. (2013) find that disc dispersal is nearly always dominated by external photoevaporation in FUV fields $\sim 3,000 G_0$. Newer models have shown that even lower radiation fields can be destructive to circumstellar discs. Facchini et al. (2016) show that discs of size ~ 150 au are subject to strong mass loss due to photoevaporation in radiation fields as low as $\sim 30 G_0$. This dependence on background radiation fields can be directly linked to a dependence on local stellar density.

Several numerical models have been developed to analyse the effects of external photoevaporation in clustered environments. Scally & Clarke (2001) model a region similar to the centre of the ONC and find external photoevaporation to cause important mass loss on disc radii larger than 10 au. According to their mass loss rates, for planets to be able to form beyond that radii, they should already be assembled within 2 Myr of the formation of the disc. They also find external photoevaporation to be dominant over dynamical truncations as a means for disc destruction. Similar results are obtained by Adams et al. (2006) and Fatuzzo & Adams (2008), who statistically estimate the FUV background radiation fields in simulated star clusters, and find values enough to truncate discs down to ~ 30 au within 10 Myr. Fatuzzo & Adams (2008) argue that 25% of the disc population loses planet-forming potential in a star cluster similar to those found in the solar neighbourhood ($N_* = 1,000 - 2,000$).

Newer models have confirmed the relative importance of external photoevaporation as a method for disc dispersal, in particular in clustered environments. Winter et al. (2018b)

find that in regions where the local stellar density is enough for dynamical truncations to be possible ($N_* \gtrsim 10^4 \text{ pc}^{-3}$), the discs are also exposed to FUV fields $\sim 3,000 G_0$ which causes the destruction of even the most massive discs ($M_{\text{disc}} = 0.1 M_\odot$) within 3 Myr. They conclude that it is highly unlikely to have clustered environments where dynamical truncations dominate over external photoevaporation. In follow up work, Winter et al. (2020b) perform simulations of regions of different densities and compare the effects of external photoevaporation and dynamical truncations. They find photoevaporation to be the dominant mass loss process in regions similar to the Central Molecular Zone of the Milky Way (surface density $\Sigma_0 = 10^3 M_\odot \text{ pc}^{-2}$) as well as in densities closer to the solar neighbourhood ($\Sigma_0 = 12 M_\odot \text{ pc}^{-2}$). In the dense regions, external photoevaporation evaporates 90% of circumstellar discs within 1.0 Myr. Similar results are reported by Nicholson et al. (2019), who find 50% of discs are evaporated due to external photoevaporation within 1.0 Myr in regions of density $\sim 100 M_\odot \text{ pc}^{-3}$. Chapters 3, 4, and 5 of this thesis obtain similar disc dispersion timescales for external photoevaporation, and confirm that this process seems to be dominant over dynamical truncations even in high density regions.

As proximity to massive stars is the defining factor of external photoevaporation, the extent of the effects of radiation depend greatly on the spatial distribution of the star forming regions. In particular, the presence of gas can shield the circumstellar discs from radiation, allowing them to live for longer. van Terwisga et al. (2020) report the discovery of two distinct disc populations in the NGC 2024 region. One is a population of low mass discs, similar to the ones observed in regions with higher stellar densities such as the ONC. They are affected by the radiation of the massive stars IRS 1 and IRS 2b, and their low masses can be explained by external photoevaporation. The second population of discs is embedded in a dense ridge of molecular gas, and the disc masses are higher and similar to those of low density regions such as Lupus or Taurus. The authors argue that is possible for these discs to be more massive because the gas protects them from external photoevaporation. Winter et al. (2019a) reproduce the observed disc population in the Cygnus OB2 region by considering the presence of gas in the early stages of the cluster. The gas absorbs some of the radiation coming from massive stars, shielding the discs from photoevaporation during their first million years of evolution.

Numerical and observational evidence points to external photoevaporation being the most important environmental mechanism affecting the evolution of circumstellar discs. Its effects are one of the main foci of this thesis and are explored in Chapters 3, 4, and 5.

1.3.3. Ram pressure stripping

The star formation process results not only in stars and circumstellar discs, but also in leftover gas, which can linger for several million years before eventually being expelled due to stellar feedback (Portegies Zwart et al. 2010). This gas can have important effects on the stellar dynamics of the region (see Section 1.1) and on the evolution of the circumstellar discs. As was discussed in Section 1.3.2, gas can shield the discs from external photoevaporation, reducing their mass loss rates and extending their lifetimes. However, the presence of gas can also truncate the discs via ram pressure stripping.

Ram pressure stripping was first investigated in the context of galaxies moving through the intra (galaxy) cluster medium. Depending on the gravitational force, the drag from the gas can remove material from the outer parts of the discs. Theoretical truncation radii have been calculated for galaxies (Gunn & Gott 1972; Mori & Burkert 2000) and later expanded to discs moving through the interstellar medium (Chevalier 2000; Moeckel & Throop 2009; Wijnen et al. 2017a). After ram pressure has stripped the outer regions, the subsequent disc evolution is dominated by a redistribution of angular momentum. This is caused by the

accretion of material with zero azimuthal angular momentum from the interstellar medium onto the disc, which decreases the local momentum on its surface. This process increases the surface density of the discs and shrinks them further. However, this shrinking is much less pronounced than during the stripping phase (Wijnen et al. 2017a).

Wijnen et al. (2016) find ram pressure stripping shrinks initially 100 au discs down to ~ 20 au within 2.500 yr of evolution. Furthermore, Wijnen et al. (2017b) find ram pressure stripping to be the dominant disc truncation mechanism when compared to dynamical encounters, in embedded clusters where 30% of the mass is in stars, regardless of the total mass of the cluster. The inner regions of the disc are not affected by the ram pressure. However, Moeckel & Throop (2009) find more modest mass loss rates in discs affected by ram pressure stripping, and they estimate that this process might lead to mass losses of no more than $\sim 2\%$ the initial mass of the discs.

1.3.4. Supernovae

A nearby supernova explosion can affect a circumstellar disc in two main ways: the blast of the explosion can remove mass from the disc through ram pressure stripping (Chevalier 2000) and it can also enrich the young disc with short-lived radionuclides (SLRs), such as ^{26}Al and ^{60}Fe . The excess of SLRs in meteorites with respect to the average interstellar medium suggests that these isotopes were not inherited at the moment of the formation of the solar system disc, but were actually injected through a later event (e.g. Russell et al. 2006; Gounelle & Meibom 2008).

Close & Pittard (2017) perform simulations of a supernova explosion located at 0.3 pc of a circumstellar disc. They find that low mass discs ($M_d \sim 0.1 M_{Jup}$) can only survive such an event if they face the blast of the supernova edge-on, but even in that case they lose $\sim 60\%$ of their initial mass. In simulations where discs are inclined with respect to the blast direction, they can lose up to 90% of their mass within 100 years. Higher mass discs ($M_d \sim 1.0 M_{Jup}$) can lose up to 30% of their mass in the blast. This mass loss occurs through ram pressure stripping during the first 100 years, in what the authors deem a period of instantaneous stripping. This quick mass loss is followed by a longer, moderate ablation period which lasts until ~ 200 yr after the explosion. While the intensity of the ablation decreases in time, through this period the mass loss rates are still 2 orders of magnitude higher than those of external photoevaporation.

Portegies Zwart et al. (2018) study the effects that a nearby supernova explosion can have on a circumstellar disc around a solar mass star and initial radius 100 au. They find that the disc is almost completely stripped of its mass if the supernova occurs at a distance of 0.05 pc. At distances from 0.15 to 0.4 pc the discs are truncated down to ~ 50 au. There is mass loss between 10 and 50 au, but the inner 10 au region remains unperturbed. However, they find that in their models the SLRs enrichment is too low to explain the excess observed in the solar system meteorites.

Ansdell et al. (2020) present a survey of discs in the λ Orionis region, in which there is evidence of a supernova explosion ~ 1 Myr ago. They find that, while no discs are observed within 0.3 pc from the estimated location of the explosion, the rest of the discs seem to follow the expected mass distributions from simple age evolution processes, given that this is an older region (age ~ 5 Myr). They suggest that a supernova occurring several million years into disc evolution might not be destructive enough to remove planet forming potential from the discs, except for the ones located extremely close to the explosion.

1.4. Numerical simulations

The nature of astrophysical phenomena makes it practically impossible to analyse our subjects of study directly. The invention of the telescope revolutionized astronomy, and the modern telescopes of today have opened our eyes to a wonderful array of observations that Lippershey and Galilei could not have dreamed of. And yet, all we can observe are nothing but instantaneous snapshots of extremely complicated and convoluted processes which, save for particular exceptions, evolve in timescales of millions of years.

While pure theory can give us a mathematical understanding of astrophysical phenomena, there is a different comprehension that comes from seeing the processes evolve before our eyes. It is in this sense that numerical simulations provide an invaluable asset to astrophysicists: by bridging the gap between observations and theory. Processes that in nature take several million years can be simulated in weeks in a computer. While many assumptions have to be made to be able to create computational simulations, the insight that numerical models provide make them an essential piece of modern astrophysics.

This thesis deals with astrophysical simulations of processes that occur at many different time and spatial scales. To be able to model the complex systems that compose this work, we make use of the Astrophysical MULTipurpose Software Environment (AMUSE), which allows to bring together numerical codes for many different astrophysical processes. In the following sections we explain some general numerical methods relevant to this thesis and introduce the AMUSE framework.

1.4.1. N-body codes

Gravitational interactions between particles are described by Newton's equations of motion. These equations allow us to determine the position and velocity of a particle at any given time:

$$\ddot{\mathbf{r}}_i = -G \sum_{j=1, j \neq i}^N m_j \frac{\mathbf{r}_i - \mathbf{r}_j}{|\mathbf{r}_i - \mathbf{r}_j|^3} \quad (1.15)$$

where \mathbf{r}_i is the position of particle i with respect to an inertial frame, m_i is its mass, and G is the universal gravitational constant [Newton 1687]. Analytical solutions for this system of equations are known only for $N = 2$ and particular cases of $N = 3$ (the restricted three-body problem). However, for any instances of $N > 3$, the equations of motion must be solved numerically.

N-body codes refer to a category of numerical solvers in which each astrophysical object (or sometimes a group of objects) is deemed as one single particle, and the equations of motion are solved numerically for each of the N particles. In astrophysics, N-body integrators are generally used to model planetary systems (e.g. Spurzem et al. 2009; Cai et al. 2017; van Elteren et al. 2019; Torres et al. 2019), stellar dynamics (e.g. Casertano & Hut 1985; Scally & Clarke 2001; Fujii & Portegies Zwart 2016; Portegies Zwart 2016), and galaxy formation and dynamics (e.g. Springel et al. 2005; Boylan-Kolchin et al. 2009; Klypin et al. 2011; Baugh et al. 2019).

At the core of an N-body solver is the time discretization used to iterate over Eq. 1.15. The most used method to solve the system of equations is known as the predictor-corrector scheme. This is an implicit method, meaning that the equation to calculate the state of the system at time $t + \delta t$ actually contains the expression $t + \delta t$. These implicit equations are solved iteratively. First, the predictor step uses Taylor series to expand $t + \delta t$ and extrapolate

positions and velocities at time t . The accelerations and higher derivatives are then recalculated with the extrapolated values, and a combination of old and new accelerations are used to predict higher derivatives. Finally, the corrector step uses these new derivatives to refine the predictions by adding terms to the Taylor expansion. The highest exponent in the Taylor expansion is usually referred to as the order of the integrator.

Different types of N-body codes exist. Pure N-body codes allow for no free parameters other than the time step for the iterations. These codes generally scale with N as $O(N \log N)$. Direct N-body codes make use of additional parameters to speed-up the calculations and usually make use of regularizations to resolve close multiple systems, making them appropriate for very dense, collisional simulations. However, these types of codes scale as $O(N^2)$. Approximate N-body codes relax constraints on the calculations, such as precision, to achieve very fast results. These codes are usually based on tree calculations and particles meshes, and they usually scale as $O(N \log N)$ with some of them even reaching $O(N)$.

1.4.2. Smoothed-particle hydrodynamics

While N-body codes are useful for modelling many astrophysical systems, it is clear that they scale with the number of physical particles. If what we want to model is a fluid or gas, such as a molecular cloud, N-body codes are not the most appropriate. Modelling each gas particle as a particle in an N-body code is not computationally feasible. For such cases, smoothed-particle hydrodynamics (SPH) codes are a better alternative.

There are two types of SPH codes. Lagrangian codes are based on particles, but the definition of an SPH particle is different than that of an N-body code. An SPH particle is a discrete element of fluid, but it does not directly represent a physical particle. The properties of an SPH particle, such as its position and velocity, are calculated as the weighted average of the surrounding particles. Each SPH particle is defined by a smoothing length, which determines the weight given to the surrounding particles. This weight decreases steeply around each particle, greatly reducing the number of calculations between elements. The second type of SPH codes correspond to Eulerian methods, where the hydrodynamics differential equations are solved in a grid.

Hydrodynamics codes are used to model several phenomena in astrophysics, such as supernovae explosions, stellar mergers, star formation and stellar feedback (e.g. Bate [1998], Klessen et al. [1998], Bate et al. [2003], Bate [2012], Pelupessy & Portegies Zwart [2012], Fujii & Portegies Zwart [2015], Dobbs et al. [2020]), and galaxy formation and large scale cosmological structure (e.g. Hernquist et al. [1996], Springel & Hernquist [2003], Schaye et al. [2015], Mitchell et al. [2018]).

1.4.3. AMUSE

The Astrophysical MUltipurpose Software Environment (AMUSE²) is a python framework which allows for integration of several independent numerical codes, facilitating their combination and allowing to model more complex physical systems (Portegies Zwart et al. [2009], [2013], Pelupessy et al. [2013], Portegies Zwart & McMillan [2018]). The AMUSE project is motivated and built on three core principles (Portegies Zwart & McMillan [2018]):

1. Provide an homogeneous and physically motivated interface for existing codes for astrophysical simulations

²<http://amusecode.org>

2. Integrate multiple community codes from four fundamental physical domains: stellar evolution, gravitational dynamics, hydrodynamics, and radiative transfer
3. Allow to design new simulation experiments by combining the community codes in different ways

Currently, AMUSE incorporates more than 60 community codes. The open source and community oriented philosophy of the project allows for anybody to contribute by creating an AMUSE interface to integrate new astrophysical simulation codes. In the context of this thesis, AMUSE was used to couple codes for stellar dynamics and stellar evolution together with an implementation for viscous disc evolution and photoevaporation. The AMUSE interface used to integrate the viscous evolution code, VADER (Krumholz & Forbes 2015, see Chapter 3 for more information), was developed for the simulations performed in Chapters 3, 4, and 5 of this thesis.

1.5. This thesis

The goal of this thesis is to quantify the effects that the star formation environment has over the evolution of young circumstellar discs. In particular, the focus is on external photoevaporation and dynamical truncations, and on how these two mechanisms compare in terms of mass loss rates. We evaluate the significance of each effect by analysing the resulting distributions of disc masses, and we perform comparisons with disc masses observed in star forming regions.

This work has been developed through numerical simulations of star forming regions. Our models consider stellar dynamics, stellar evolution, viscous disc evolution, external and internal photoevaporation, and dust evolution in the discs. All the astrophysical codes necessary to assemble the simulations developed for this thesis were bridged together using the AMUSE framework (Section 1.4.3).

In **Chapter 2** we simulate young star clusters which are embedded in gas. We use a background potential to implement the gravitational effects of the gas, and a semi-analytical model for the viscous evolution of the discs. We then evolve the stellar dynamics of the region for 2 Myr, during which the discs are susceptible to truncation due to close encounters with other stars. We study the resulting distributions of disc sizes under three scenarios: clusters with no gas, with constant gas throughout the entire simulation, and with gas expulsion starting at 1 Myr. We also perform a basic comparison to disc distributions observed in several star forming regions.

In **Chapter 3** we compare the effects of dynamical truncations against external photoevaporation, in terms of mass loss. We introduce a new model for the discs, which uses a viscous evolution code. For modelling external photoevaporation we use a pre-computed grid of mass loss rates, which allows us to determine the mass loss in every time step depending on the radius of the disc and its distance to a massive star. We model star clusters of densities $50 \text{ M}_\odot \text{ pc}^{-3}$ and $100 \text{ M}_\odot \text{ pc}^{-3}$ and evolve the stellar dynamics (including dynamical encounters), stellar evolution, viscous evolution of the discs, and external photoevaporation.

In **Chapter 4** we use the model from Chapter 3 to quantify the local stellar densities for which external photoevaporation severely constrains disc lifetimes. We investigate a larger parameter space of number stellar densities than in Chapter 3 and look at the disc mass distributions after 2 Myr of evolution. We compare our results to observations of disc masses in different star forming regions.

In **Chapter 5** we improve on the initial conditions of previous models by simulating not only the disc evolution, but also the star formation process. We implement a simple model of

giant molecular cloud collapse and star formation to obtain primordial positions, velocities, and masses of the stars. We then use these as initial conditions for our stellar dynamics and disc evolution model. In this Chapter we also expand our circumstellar disc model by adding the effects on internal photoevaporation and dust evolution inside the disc.

The results of this thesis show that mass loss due to external photoevaporation dominates over dynamical encounters in all the simulated stellar regions. External photoevaporation is extremely efficient in evaporating circumstellar discs, completely depleting the mass of $\sim 50\%$ of the initial discs in low density regions (Chapter 3) and up to 90% of the discs in high density regions (Chapter 4) after 2 Myr of evolution.

* * *

Remember that all models are wrong; the practical question is how wrong do they have to be to not be useful.

George E. P. Box

2

The viscous evolution of circumstellar discs in young star clusters

F. Concha-Ramírez; E. Vaher; S. Portegies Zwart
Monthly Notices of the Royal Astronomical Society
Volume 482, Issue 1, p.732-742 (2019)

STARs with circumstellar discs may form in environments with high stellar and gas densities that affect the discs through processes like truncation from dynamical encounters, ram pressure stripping, and external photoevaporation. Circumstellar discs also undergo viscous evolution that leads to disc expansion. Previous work indicates that dynamical truncation and viscous evolution play a major role in determining circumstellar disc size and mass distributions. However, it remains unclear under what circumstances each of these two processes dominates. Here, we present results of simulations of young stellar clusters taking viscous evolution and dynamical truncations into account. We model the embedded phase of the clusters by adding leftover gas as a background potential that can be present through the whole evolution of the cluster, or expelled after 1 Myr. We compare our simulation results to actual observations of disc sizes, disc masses, and accretion rates in star-forming regions. We argue that the relative importance of dynamical truncations and the viscous evolution of the discs changes with time and cluster density. Viscous evolution causes the importance of dynamical encounters to increase in time, but the encounters cease soon after the expulsion of the leftover gas. For the clusters simulated in this work, viscous growth dominates the evolution of the discs.

*

2.1. Introduction

Stars are formed in clustered environments (Clarke et al. 2000; Lada & Lada 2003). Circumstellar discs develop shortly after star formation (Williams & Cieza 2011), when they are still embedded in the dense star and gas surroundings of the cluster. In these environments, discs can be disturbed by different processes such as truncations due to close stellar encounters (Rosotti et al. 2014; Vincke et al. 2015; Portegies Zwart 2016), external photoevaporation due to nearby bright O type stars (O'dell 1998; Scally & Clarke 2001; Guarcello et al. 2016; Haworth et al. 2017), accretion and ram pressure stripping (Wijnen et al. 2016; 2017a), and nearby supernovae (Pelupessy & Portegies Zwart 2012). Circumstellar discs can also present viscous evolution (Lynden-Bell & Pringle 1974). As the typical viscous time scales of T Tauri stars seem to be on the order of 10^5 yr (Hartmann et al. 1998; Isella et al. 2009), circumstellar discs are likely to undergo considerable viscous growth during the first few million years of cluster evolution.

Studying the processes that affect the distribution of circumstellar discs in young star clusters helps to understand the development of planetary systems like our own. Different processes, however, can dominate the evolution of clusters at different times and cluster densities. Young clusters are still embedded in the gas from which they formed. Gas expulsion, which can be the result of feedback from massive stars such as winds and supernovae explosions, leaves the cluster in a supervirial state that leads to its expansion and possible dissolution (Tutukov 1978). Vincke & Pfalzner (2016) carried out simulations including the effect of truncations by stellar encounters before and after gas expulsion. They show that taking the early gas expulsion into account in their simulations increases the rate of stellar encounters, because the larger total mass increases the stellar velocity dispersion.

Most approaches to study the interaction of the circumstellar discs with their surrounding cluster have focused on a static size for the disc which can only decrease by the influencing external processes (e.g. Scally & Clarke (2001); Pfalzner et al. (2006); Olczak et al. (2006, 2010); Vincke et al. (2015); Portegies Zwart (2016)). In contrast, Rosotti et al. (2014) considered the viscous evolution of the discs along with truncations by dynamical encounters, by combining N-body simulations with smoothed particle hydrodynamics (SPH) to represent the growth of the discs. However, due to the numerical cost of their simulation, their study was limited to 100 stars of $1M_\odot$ each distributed in a Plummer sphere, only half the stars had a circumstellar disc, and their simulations were run for just 0.5 Myr.

The purpose of this work is to analyse the combined effect of viscous disc evolution and the presence of gas on the dynamics and circumstellar disc distributions in young star clusters. We look to understand the relative importance of such processes during different stages of cluster evolution. We include the viscous evolution of the circumstellar discs semi-analytically using the similarity solutions developed by Lynden-Bell & Pringle (1974). We also consider disc truncations caused by dynamical encounters between stars in the cluster. Additionally, we model the presence of gas in the cluster, as a means to represent the embedded phase, and the further expulsion of said gas. We carry out our simulations using the AMUSE framework (Portegies Zwart et al. 2013; Pelupessy et al. 2013). All the code used for the simulations, data analyses, and figures of this paper is available in a Github repository¹.

Thanks to modern observational techniques, circumstellar discs have been observed and characterized inside many open star clusters and star forming regions, such as Chamaeleon I (Pascucci et al. 2016; Mulders et al. 2017; Manara et al. 2017), σ Orionis (Maucó et al. 2016; Ansdell et al. 2017), the Lupus clouds (Alcalá et al. 2014; Ansdell et al. 2016, 2018), the Orion Trapezium cluster (Vicente & Alves 2005; Mann & Williams 2009; Robberto et al. 2004), and

¹<http://doi.org/10.5281/zenodo.1465931>

the Upper Scorpio region (Barenfeld et al. 2016, 2017). From these observations, the size and mass of the discs and the accretion rate onto their central star can be calculated. This brings an opportunity to calibrate the results obtained by simulations, by offering a way to compare simulated disc distributions with observed ones.

2.2. Methods

2.2.1. Evolution of isolated viscous discs

[Lynden-Bell & Pringle] (1974) showed that for a thin disc in which viscosity has a radial power-law dependence and no time dependence, there exists a similarity solution to which all initial mass distributions will asymptotically approach. The description of the similarity solutions used in this work is largely based on the one provided by [Hartmann et al.] (1998), who applied the similarity solutions to explain the observed accretion rates of T Tauri stars.

The similarity solutions of viscous discs are characterised by four independent parameters:

1. γ - the radial viscosity dependence exponent.
2. $M_d(0)$ - the initial disc mass.
3. $R_c(0)$ - the initial characteristic disc radius, outside of which $1/e \approx 37\%$ of the disc mass initially resides.
4. t_v - the viscous time scale at $R_c(0)$. It is possible to instead specify ν_c , the viscosity at $R_c(0)$.

For the present work, the modelled discs will be represented by three properties: their characteristic radius, the mass of the disc, and the accretion rate from the disc to the central star. These are the properties derived from observations, allowing us to compare them directly with the simulation results.

According to the model developed by [Lynden-Bell & Pringle] (1974), the characteristic radius of the disc as a function of time t is given by

$$R_c(t) = \left(1 + \frac{t}{t_v}\right)^{\frac{1}{2\gamma}} R_c(0). \quad (2.1)$$

The disc mass as a function of time is

$$M_d(t) = M_d(0) \left(1 + \frac{t}{t_v}\right)^{\frac{1}{2\gamma-4}} \quad (2.2)$$

and the radial cumulative mass distribution of the disc as a function of time is

$$M_d(R, t) = M_d(t) \left(1 - e^{-\Gamma}\right). \quad (2.3)$$

Here

$$\Gamma = \left(\frac{R}{R_c(0)}\right)^{2-\gamma} \left(1 + \frac{t}{t_v}\right)^{-1} \quad (2.4)$$

The accretion rate of matter to the star as a function of time is

$$\dot{M}_{acc}(t) = -\frac{dM_d(t)}{dt} = \frac{M_d(0)}{(4-2\gamma)t_v} \left(1 + \frac{t}{t_v}\right)^\Delta. \quad (2.5)$$

Here $\Delta = \frac{5-2\gamma}{2\gamma-4}$. The viscous time scale t_v relates to the characteristic viscosity of the disc v_c by

$$t_v = \frac{R_c(0)^2}{3(2-\gamma)^2 v_c}. \quad (2.6)$$

The disc viscosity can be written as

$$\nu(R) = \alpha \frac{c_s^2}{\Omega} = \alpha \frac{k_B T \sqrt{R^3}}{\mu m_p \sqrt{GM_*}}. \quad (2.7)$$

Here α is the turbulent mixing strength (Shakura & Sunyaev 1973), $c_s = \sqrt{\frac{k_B T}{\mu m_p}}$ is the isothermal sound speed, $\Omega = \sqrt{\frac{GM_*}{R^3}}$ is the Kepler frequency, k_B is the Boltzmann constant, T is the disc temperature at distance R from the star, μ is the mean molecular weight of the gas in atomic mass units, m_p is the proton mass, G is the constant of gravity, M_* is the mass of the central star and the mass of the disc is assumed to be insignificant. Considering the temperature of the disc as a radial power law $T \propto R^{-q}$,

$$\nu_c = \alpha \frac{k_B T R_c(0)^{\frac{3}{2}-q}}{\mu m_p R^{-q} \sqrt{GM_*}}, \quad (2.8)$$

and

$$t_v = \frac{\mu m_p R_c(0)^{\frac{1}{2}+q} \sqrt{GM_*}}{3\alpha (2-\gamma)^2 k_B T R^q}. \quad (2.9)$$

Relating T_d with an estimate of stellar luminosity $L_* = L_*(M_*)$ allows us to write $t_v = t_v(M_*, \alpha, \gamma, q, R_c(0))$. While t_v is an independent parameter for the similarity solutions, we parametrize it as a function of γ and $R_c(0)$ in our implementation, on physical grounds. We use the zero age main sequence stellar luminosities for stars with metallicities $Z = 0.02$ from Hurley et al. (2000) that are available in the package SeBa, which is incorporated into AMUSE.

If it is observed that $\dot{M}_{acc}(t) \propto t^{-\eta}$, then the viscosity exponent γ can be defined as:

$$\gamma = \frac{4\eta - 5}{2\eta - 2}, \quad (2.10)$$

where we assumed that γ is the same for all discs. Previous work by Hartmann et al. (1998), Sicilia-Aguilar et al. (2010) and Antoniucci et al. (2014) have found the value of η to be in the range $1.2 \lesssim \eta \lesssim 2.8$. Furthermore, Andrews et al. (2010) found a value of $\gamma = 0.9 \pm 0.2$ in the Ophiuchus star forming region, independent of the disc masses or stellar properties. In general $\gamma = 1$, which corresponds to $\eta = 1.5$, seems to be in agreement with most observed discs and is thus the value we adopt in this work.

Equation (2.9) shows that the viscous time scale depends on the turbulence parameter α and on the temperature profile of the disc. A value of $\alpha \sim 10^{-2}$ was found by Hartmann et al. (1998) from observations of T Tauri stars. Isella et al. (2009) suggest that α might range from 10^{-4} to 0.5 , while Andrews et al. (2010) found $\alpha \sim 10^{-3} - 10^{-2}$ in the Ophiuchus star forming region. Mulders & Dominik (2012) found that $\alpha \sim 10^{-4}$ for circumstellar discs around stars of all masses, but by assuming slightly different circumstellar dust properties $\alpha \sim 10^{-2}$ could also fit the observations. In figure 2.1 we show the viscous time scales obtained in our model for three different values of the turbulence parameter: $\alpha = 10^{-4}$, $\alpha = 5 \times 10^{-3}$, and $\alpha = 10^{-2}$. It can be seen that the two highest values of the turbulence parameter lead to viscous time scales that agree with observations, up to moderately massive stars. Motivated by this, we adopt two values for this parameter: $\alpha = 10^{-2}$, in what we refer to as fast viscous evolution,

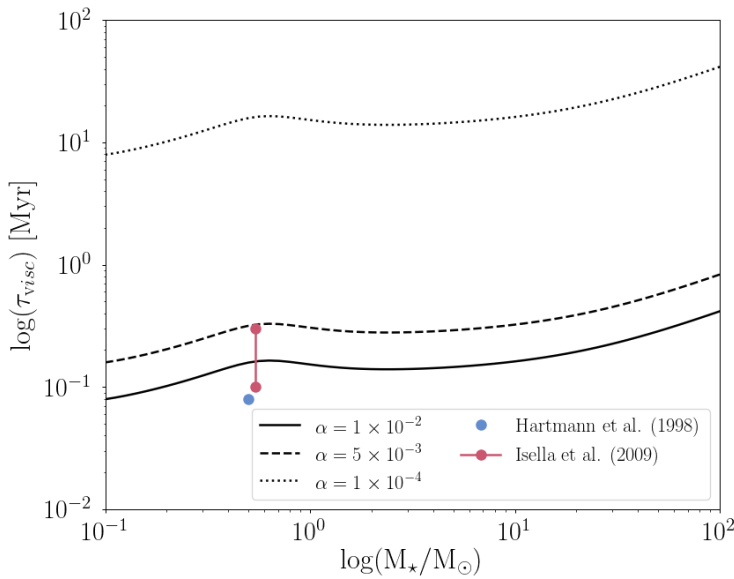


Figure 2.1: Viscous time scales in our model as a function of stellar mass, for different values of the turbulence parameter α . Observational estimates for circumstellar discs around T Tauri stars by Hartmann et al. (1998) and Isella et al. (2009) are shown for comparison.

and $\alpha = 5 \times 10^{-3}$ in what we call slow viscous evolution. The viscosity parameters chosen are in good agreement with estimates for the viscous time scale, t_v . Hartmann et al. (1998) found a value of $t_v \sim 8 \times 10^4$ yr for a typical T Tauri star. Isella et al. (2009) estimate, based on their observations, that $t_v \sim 10^5$ yr – 3×10^5 yr.

Values of α should be considered only an approximation. In reality, disc parameters related to the viscosity —like the viscosity exponent γ and the turbulence parameter α — should be expected to vary among stars of equal mass, age, and observed accretion rates; even within the same disc, different parts of it may show different viscosity parameters (Pinte et al. 2016).

2.2.2. Gas in the cluster

The presence of gas in the cluster is modelled semi-analytically with a background potential in the N -body computations. We adopt the gas and gas expulsion parameters from Lüghausen et al. (2012). The distribution of the gas corresponds to a Plummer sphere with the same Plummer radius as the stars in the cluster. The initial mass of the gas, $M_g(0)$, is taken to be twice the mass of the stars, which corresponds to a star formation efficiency of 1/3.

In the runs with gas expulsion, the mass of the gas as a function of time is given by

$$M_g(t) = \begin{cases} M_g(0) & t \leq t_D, \\ \frac{M_g(0)}{\varphi} & t > t_D, \end{cases} \quad (2.11)$$

with $\varphi = 1 + (t - t_D)/\tau$, and where t_D is the time at which gas expulsion begins. The gas expulsion timescale corresponds to the time it takes for the cluster to lose half its gas once

gas expulsion has begun, and it is given by

$$\tau = \frac{R_P}{1 \text{ pc}} \times 0.1 \text{ Myr}, \quad (2.12)$$

where R_P is the Plummer radius of the cluster.

2.2.3. Dynamical disc truncation

The semi-analytical model used in this work assumes that, between encounters, discs evolve according to the similarity solution described in section 2.2.1. A close enough stellar encounter introduces a discontinuity in the disc parameters, but after that the disc is assumed to continue evolving as an isolated viscous disc.

The work by Rosotti et al. (2014) encourages us to adopt the commonly used approximation that an encounter truncates circumstellar discs at one third of the encounter distance in the case of equal mass stars. In addition, we use the mass dependence from Bhandare et al. (2016). The combination of these two models gives us the characteristic radius of a circumstellar disc immediately after an truncating encounter:

$$R'_c = \frac{r_{\text{enc}}}{3} \left(\frac{M}{m} \right)^{0.2}, \quad (2.13)$$

where r_{enc} is the encounter distance, M is the mass of the star with the disc in question, and m is the mass of the encountered star.

Equation (2.2) gives the disc mass immediately before the encounter. This mass is lower than the initial disc mass, because some of it has been accreted onto the star. In our model this mass difference is added to the stellar mass. If the encounter is assumed to not remove mass from the inner part of the disc, then the disc mass inside the new initial characteristic radius just after the encounter can be assumed to be equal to the mass inside that radius just before the encounter. Equation (2.3) and the properties of characteristic radius can then be used to find the disc mass immediately after the encounter as

$$M'_d = \frac{M_d(R'_c, t)}{1 - \frac{1}{e}} \simeq 1.6 M_d(R'_c, t), \quad (2.14)$$

where t is the time from the last discontinuity of the disc parameters.

According to equation (2.6) and the underlying assumption $v \propto R^\gamma$, the new viscous timescale of the disc will be

$$t'_v = \left(\frac{R'_c}{R_c(0)} \right)^{2-\gamma} t_v. \quad (2.15)$$

In our model, the relative change in disc mass and accretion rate in an encounter is determined by γ and the truncation radius relative to the disc characteristic radius just before the encounter, $R'_c/R_c(t)$. If the disc is truncated, its viscous time scale decreases and the disc starts evolving faster. We ignore the orientation of the discs, so the equation for truncation radius is the average truncation radius over all disc inclinations.

2.2.4. Numerical implementation

We use the 4th-order Hermite N -body code ph4, which is incorporated into the AMUSE framework. The softening length is $\epsilon = 100$ au and the time step parameter is $\eta = 10^{-2}$. The simulations start in virial equilibrium and last for 2 Myr.

Collisional radii for each star in the cluster are defined depending on the stellar mass and the theoretical size of the disc evolving in isolation, given by equation 5.13. The initial collisional radius for each star is given by the distance at which the most massive star in the cluster can truncate its disc. The collisional radii of all stars are updated every 2,000 yr, to account for the viscous evolution of the discs. Two stars are considered to be in an encounter if the distance between them is less than the sum of their collisional radii. The encounter distance between the stars is then computed by analytically solving the two body problem. If the encounter is strong enough as to truncate the discs, disc parameters of both stars are updated as described in section 2.2.3. After each encounter, the collisional radii of both stars are set to $0.49r_{\text{enc}}$ in order to prevent the N -body code from detecting the same encounter multiple times during the same 2,000 yr window.

2.3. Results

2.3.1. Initial conditions

Cluster properties

Simulations were run for clusters with 1,500 stars. The stellar masses are randomly sampled from a Kroupa initial mass distribution (Kroupa 2001) with lower mass limit $0.1M_{\odot}$ and upper mass limit $100M_{\odot}$. The stars are initially distributed in a Plummer sphere (Plummer 1911) with Plummer radius 0.5 parsec. All stars are assumed to be single and coeval.

All simulations were carried out for 2.0 Myr. We define three different gas scenarios for the simulations:

1. No gas
2. Gas presence
3. Gas expulsion starting at 1.0 Myr

Each simulation was run for two values of the turbulence parameter: $\alpha = 10^{-2}$ and $\alpha = 5 \times 10^{-3}$.

Disc properties

Based on the observations of low mass stars carried out by Isella et al. (2009) and the estimations obtained by Hartmann et al. (1998), the initial characteristic radius R_c of the circumstellar discs was chosen to be

$$R_c(0) = R' \left(\frac{M_*}{M_{\odot}} \right)^{0.5} \quad (2.16)$$

with $R' = 30$ AU.

Circumstellar discs with masses larger than 10% of the mass of their star are the most likely to be gravitationally unstable (Kratter & Lodato 2016). According to hydrodynamical simulations of collapsing gas clouds, the disc-to-star mass ratios of embedded protostars are large enough for gravitational instabilities to occur (Vorobyov 2011), but these instabilities lead to accretion bursts that quickly decrease the mass ratios (Armitage et al. 2001, Kratter & Lodato 2016). Based on this we chose the initial disc masses to be

$$M_d(0) = 0.1M_* \quad (2.17)$$

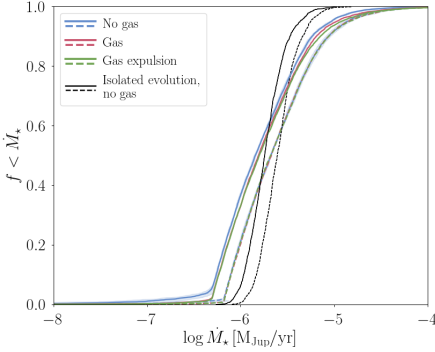
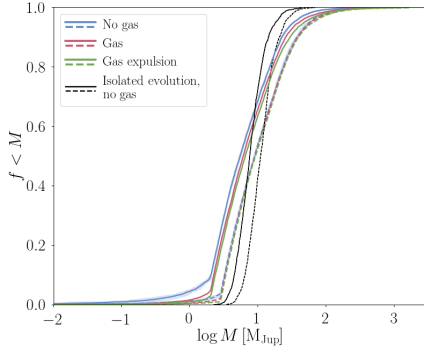
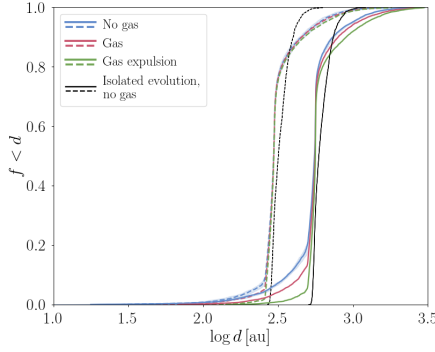


Figure 2.2: Cumulative distributions of the mean disc size (top panel) and mass (center), and the accretion rate onto central star (bottom panel) at the end of the simulations. The colors indicate the different mode of gas loss in the simulation (see legend in the top left corner), and in black we show the results of isolated disc evolution (viscous growth only, no truncations). The solid lines correspond to fast viscous disc evolution ($\alpha = 10^{-2}$) and the dashed lines to slow viscous evolution ($\alpha = 5 \times 10^{-3}$). The shaded areas around the blue curves indicate the dispersion around the mean value averaged over 5 simulations. For clarity we only show this uncertainty interval for the blue curves, but the others are comparable.

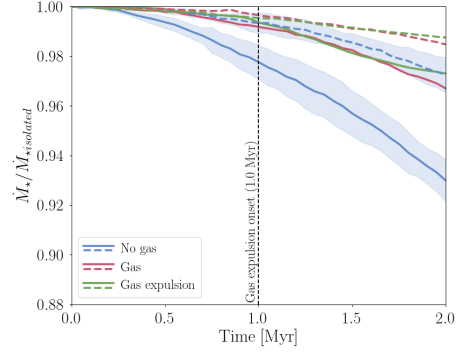
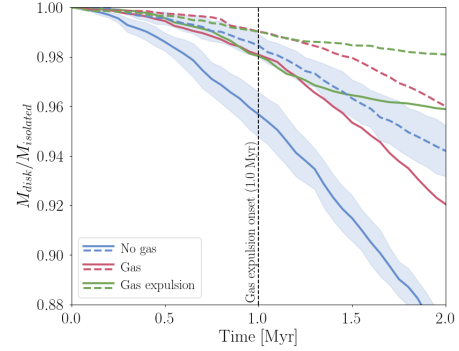
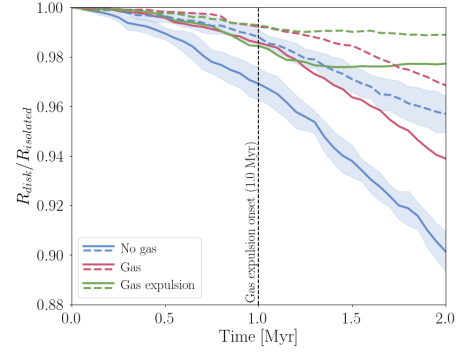


Figure 2.3: Evolution of the mean disc size (top panel) and mass (center), and accretion rate onto central star (bottom panel) compared to the isolated disc case. By definition, values closer to 1 are similar to the isolated case. The colors indicate the different mode of gas loss in the simulation (see legend in the lower left corner). The solid lines correspond to fast viscous disc evolution ($\alpha = 10^{-2}$) and the dashed lines to slow viscous evolution ($\alpha = 5 \times 10^{-3}$). The dashed black vertical line shows the gas expulsion onset, 1.0 Myr. The shaded areas around the blue curves indicate the dispersion around the mean value averaged over 5 simulations. For clarity we only show this uncertainty interval for the blue curves, but the others are comparable.

2.3.2. The effect of gas in the cluster

In Fig. 2.2 we present the cumulative distributions for the mean values of sizes and masses of the circumstellar discs, and the accretion rates onto the central star. The three different colors in each of the panels present one of our choices of how the gas is removed from the cluster. In black we show the results of isolated evolution, where discs are subject to viscous growth but no dynamical truncations. In addition, we present the results for two choices of the turbulence parameter α with solid and dashed lines.

Changing the value of α has quite a pronounced effect on the size distribution of the discs, in the sense that a low value (of 5×10^{-3}) results in smaller discs. This difference is mainly caused by the faster intrinsic growth of the discs for high values of α . For rather viscous discs, $\alpha = 10^{-2}$, some difference in the mean size is noticeable near ~ 500 au, in the sense that for the simulations without gas the discs are on average somewhat smaller than in the other simulations. This is caused by more frequent encounters in the former simulations. The gas expulsion tends to drive the early evaporation of the cluster, which leads to larger discs on average because the latter effect terminates the dynamical disc-truncation process. The mean sizes of the discs in the simulation with gas but without expulsion tend to be in between the other two distributions, because some truncation leads to a subsequent faster viscous growth of the discs, as shown in equation 2.15.

The same behaviour can be seen for the average disc masses and accretion rates onto the central star (Fig. 2.2, middle and bottom panel respectively). In the simulations without gas, there are more discs with masses $\lesssim 2 M_{\text{Jup}}$ than in the other simulations. Again this difference is diminished in the slow viscous evolution case. For the accretion rates the different simulations yield the same final distributions, except for a negligible higher amount of discs with $\dot{M} < \sim 2 \times 10^{-8} M_{\text{Jup}}/\text{yr}$ in the cases without gas. Unlike the case for the average disc radius, using different values of α in the simulations yields comparable results for the final distributions of both average disc masses and accretion rates. The two values for the turbulence parameter used in our simulations yield final values of disc mass and accretion rates that differ by less than an order of magnitude.

2.3.3. Evolution of the circumstellar discs

During the 2.0 Myr of the simulations, both the viscous growth of the discs and their truncations due to dynamical encounters occur simultaneously. The final disc size, mass, and accretion rate distributions are the result of the combination of these two processes. In Figure 2.3 we show the normalized disc parameters compared to the isolated case, averaged over 5 simulations for each of the gas scenarios. The normalized disc parameters correspond to the actual value for each parameter, divided by the value of the isolated case (viscous growth only, no truncations). By construction, the normalized disc parameters have a value of 1 if there are no dynamical truncations taking place. In a cluster where dynamical truncations are taken into account, we can expect the normalized disc parameters to deviate from 1. The behaviour seen in this case is in agreement with the final parameter distributions shown in Section 2.3.2. In the top panel of Figure 2.3 it can be seen how, for the simulations without intracluster gas and for initial disc parameters as specified in Section 2.3.1, fast viscous evolution results in discs about 10% smaller than in the isolated case, while for the slow viscous evolution this value drops to less than 5%. It can also be seen how the expulsion of the leftover gas allows the discs to simply continue their viscous evolution without being further perturbed by dynamical truncations. These normalized parameters show that the size of the discs in the first Myr of cluster evolution is dominated by the viscous growth, rather than by dynamical truncations. The dynamical encounters experienced by the discs are not enough

to truncate them to values largely different from the isolated case. Specially in the case of slow viscous growth, this process seems to be the only one driving the evolution of the discs.

For the disc mass and the accretion rate of the central star (center and bottom panels of Fig. 2.3, respectively), similar behaviours are observed in the curves, also in agreement with the cumulative distributions in Fig. 2.2. Again, the different values of α used in our simulations result in a negligible difference in disc mass and accretion rate.

2.3.4. Comparison with observations

Observations of circumstellar discs in young clustered environments can help us understand how representative our simulations are. We compared our results with observations of star forming regions and stellar associations. Given the different ages, stellar densities, and general characteristics of the star formation regions mentioned above, we do not look to reproduce precisely their disc distributions using only our approximate model. We carry out this comparison as a way to determine if our model yields reasonable results within the varied collection of young star forming regions.

Observational data

We compared our simulation results with observations of star forming regions and stellar associations. The ages, distances, and stellar densities of the observed regions used in this work can be found in Table 2.1. Given the diverse nature of the observational data used in this work, we give detailed descriptions of the specific observations used for disc sizes, disc masses, and stellar accretion rates.

For the disc radii, we used gas measurements when available. Gas discs are particularly important, because gas dominates the dynamics of the whole disc and gas discs are expected to be larger than dust discs by a factor of ~ 2 (Ansdell et al. 2018), since dust can decouple from the gas and drift to the inner regions of the discs. Due to observational constraints, however, gas discs are much more difficult to observe than the compact, sub-mm/mm dusty ones. For this work, we limit ourselves to gaseous radii for discs in the Lupus clouds and Upper Scorpio star forming regions, as noted below.

Given that the chemistry of CO and other tracers of disc mass may be affected by rapid loss of gas or carbon depletion, we chose to use dust masses for our comparisons, scaling them to total disc masses by using the 1:100 dust-to-gas ratio determined by Bohlin et al. (1978), which assumes that protoplanetary discs inherit this ratio from the interstellar medium. Recent observations, however, suggest that the dust-to-gas ratio might actually be much lower (Ansdell et al. 2016; Miotello et al. 2017). The implications of this to our analyses are further discussed in section 5.4.

Trapezium cluster For disc sizes in the Orion Trapezium cluster we used a sample of 135 bright proplyds and 14 disc silhouettes from Vicente & Alves (2005), corresponding to dust radii. The dust mass distribution of circumstellar discs in the Trapezium were obtained from Mann & Williams (2009). The stellar mass accretion rates were obtained from Robberto et al. (2004).

Lupus clouds Gas radii for 22 circumstellar discs in the Lupus star forming region were obtained from Ansdell et al. (2018). Dust masses for 22 discs were obtained from Tazzari et al. (2017). Stellar mass accretion rates were obtained from Alcalá et al. (2014).

Table 2.1: Observational values and obtained similar simulations for the observed star forming regions. References: ^(a)Hillenbrand & Hartmann ⁽¹⁹⁹⁸⁾, ^(b)Muench et al. ⁽²⁰⁰²⁾, ^(c)Hillenbrand ⁽¹⁹⁹⁷⁾, ^(d)Schulz et al. ⁽²⁰¹⁵⁾, ^(e)Comerón ⁽²⁰⁰⁸⁾, ^(f)Merin et al. ⁽²⁰⁰⁸⁾, ^(g)Luhman ⁽²⁰⁰⁷⁾, ^(h)Roccatagliata et al. ⁽²⁰¹⁸⁾, ⁽ⁱ⁾Boulanger et al. ⁽¹⁹⁹⁸⁾, ^(j)Sacco et al. ⁽²⁰¹⁷⁾, ^(k)Sherry et al. ⁽²⁰⁰⁴⁾, ^(l)Schaefer et al. ⁽²⁰¹⁶⁾, ^(m)Caballero ⁽²⁰⁰⁸⁾, ⁽ⁿ⁾Carpenter et al. ⁽²⁰⁰⁶⁾, ^(o)Preibisch & Mamajek ⁽²⁰⁰⁸⁾, ^(p)Luhman & Mamajek ⁽²⁰¹²⁾

| | Trapezium | Lupus clouds | Chamaeleon I | σ Orionis | Upper Scorpio |
|---|--------------------|---------------------------------|------------------|------------------|-------------------|
| Age (Myr) | $\sim 1^{(a)}$ | $1 - 3^{(e)}$ | $2 - 3^{(g)}$ | $3 - 5^{(k)}$ | $5 - 11^{(n)}$ |
| Distance (pc) | $450^{(b)}$ | $200 \text{ (Lupus III)}^{(e)}$ | $\sim 190^{(h)}$ | $385^{(l)}$ | $145 \pm 2^{(p)}$ |
| R (pc) | $1^{(c)}$ | $\sim 52^{(f)}$ | $4^{(i)}$ | $3^{(m)}$ | $15^{(p)}$ |
| N | $\sim 2,000^{(c)}$ | $\sim 12,700^{(f)}$ | $\sim 240^{(j)}$ | $340^{(m)}$ | $863^{(q)}$ |
| ρ_N (stars pc ⁻³) | $\sim 250^{(d)}$ | ~ 500 | ~ 0.9 | ~ 3 | ~ 0.05 |
| Simulation N | 750 | 1,000 | 25 | 25 | 25 |
| Simulation ρ_N (stars pc ⁻³) | 1816.09 | 509.35 | 35.25 | 35.25 | 35.25 |
| Disc size | 2×10^{-3} | 2×10^{-3} | 10^{-4} | 10^{-4} | 10^{-4} |
| Simulation α | Disc mass | 10^{-4} | 10^{-2} | 10^{-4} | 10^{-2} |
| | Accretion rate | 10^{-4} | 10^{-2} | 10^{-2} | 10^{-4} |

Chamaeleon I Dust radii for 87 circumstellar discs in the Chamaeleon I star forming region were obtained from Pascucci et al. (2016). Dust masses for 93 sources were obtained from Mulders et al. (2017). Accretion rates for this region were taken from Manara et al. (2017).

σ Orionis Measurements of dust radii and stellar accretion rates for 32 sources in this star forming region were obtained from Maucó et al. (2016). Dust masses for 92 sources were taken from Ansdell et al. (2017).

Upper Scorpio Gas radii for 57 sources in the Upper Scorpio star forming region were taken from Barenfeld et al. (2017). Dust masses for the circumstellar discs were obtained from (Barenfeld et al. 2016).

Preparing simulation results for comparison

In the previous sections we represented the size of a disc with its characteristic radius, which encloses $\approx 63\%$ of its mass (Equation 5.13). As a way to do a parallel with actual observations of circumstellar disc sizes, we follow Tazzari et al. (2017) in fitting the outer radius of a disc at the point where 95% of the mass of the disc is enclosed. To perform the comparisons with observations, we redefined our simulated disc radii as to contain 95% of the disc mass, as follows. Equation 2.4 can be rewritten as

$$\Gamma = \left(\frac{R}{(1 + t/t_v)^{1/(2-\gamma)} R_c(0)} \right)^{2-\gamma}.$$

Using Equation 5.13, this can be rewritten as

$$\Gamma = \left(\frac{R}{R_c(t)} \right)^{2-\gamma}.$$

The radius R_M that encompasses the mass M can be found by solving Equation 2.3, from which we obtain

$$\left(\frac{R_M}{R_c(t)} \right)^{2-\gamma} = \ln \left(\frac{1}{1 - M/M_d(t)} \right).$$

Since we are using $\gamma = 1$ in our simulations, this further simplifies to

$$R_M = R_c(t) \ln \left(\frac{1}{1 - M/M_d(t)} \right)$$

so the radius $R_{0.95}$ that encompasses 95 % of the disc mass is

$$R_{0.95} = \ln(20)R_c(t) \approx 3R_c(t)$$

Comparison

The observed star forming regions have distinct ages and stellar densities. This is taken into account when we compare them with simulations. The comparisons were performed as follows: first, the stellar densities of the observed regions were obtained from the literature (observational parameters can be found in Table 2.1). We performed new simulations with the same initial conditions mentioned in section 2.3.1, except now with number of stars

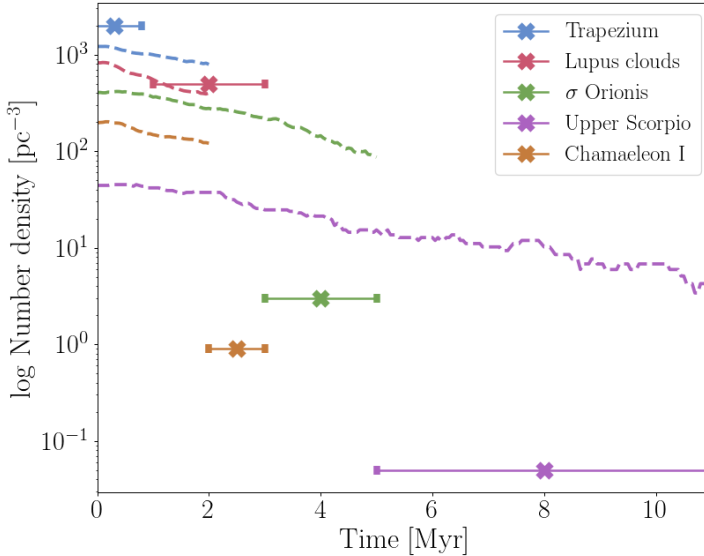


Figure 2.4: Observed stellar densities of star clusters, along with the most similar simulation. Simulations are plotted at the time comparable to the estimated age of the corresponding cluster (dashed lines in the same colors). The process carried out to find the most similar simulations is described in section 2.3.4. References for the observational values can be found in Table 2.1.

$N=[25, 50, 100, 125, 250, 500, 750, 1,000, 1,250, 1,500, 1,750, 2,000, 2,250, 2,500, 5,000]$ and with values of $\alpha=[10^{-4}, 2 \times 10^{-3}, 5 \times 10^{-3}, 7 \times 10^{-3}, 10^{-2}]$, to allow the observations to be compared with simulated clusters spanning a wider range of parameter space for N and α than the one used for our previous results. Given that the star forming regions with the largest estimated ages are the ones with lowest stellar densities (see Table 2.1), additional simulations with $N=[25, 50, 100, 125]$ were run for 11 Myr. For each observed star forming region, we went through the different simulations and looked at the stellar density at the point in time corresponding to the estimated age for the observed star forming region. The simulation which resulted on the closest stellar density to the one of the observed region was selected as the most similar one.

For the selected stellar density, there are different values of the turbulence parameter α . This means an additional step is needed to determine the simulation result closest to each star forming region. A Kolmogorov–Smirnov (KS) test was performed between the observed and simulated distributions of disc size, disc mass, and accretion rate. A separate KS test was carried out for each of these parameters.

In Figure 2.4 we show the observational values for stellar density, along with the comparable simulation for each observation. The regions with higher stellar densities (the Trapezium cluster and the Lupus clouds) find good matches in our simulations. For the clusters with lower densities (Chamaeleon I, σ Orionis, and Upper Scorpio), even the simulations with the lowest densities are not a good match.

Given that the results for different gas scenarios in section 2.3.3 show that disc evolution is dominated by viscous growth rather than dynamical truncations, we are interested in determining if our model is nevertheless able to reproduce the observed distributions of disc

sizes, masses, and accretion rates. In Figure 2.5 we show the cumulative distributions for disc size, disc mass, and accretion rates for each observed cluster (solid lines) together with its corresponding simulation (dashed line). The simulation curves are plotted at the point in time coinciding with the estimated age of the clusters. The closest resemblance of one of our simulations to an observation is obtained for the Trapezium cluster. The simulation closest to the Lupus region curve both under and over estimates disc sizes. Our model tends to underestimate disc sizes for the top region of the Upper Scorpio observations. This can be related to the fact that gaseous radii were considered for these regions, which leads to large disc sizes (Ansdel et al. 2018). For Upper Scorpio, however, as reported in Barenfeld et al. (2017) only 4 discs of their sample turn out to have large gas discs. For most of the Upper Scorpio data, as well as for the Chamaeleon I data, our model overestimates disc sizes.

Regarding the disc masses, in the center panel of Figure 2.5 it can be seen that good simulation matches are found for the Lupus clouds and Chamaeleon I. The masses for Upper Scorpio and σ Orionis are overestimated by our simulations, whereas the masses for the Trapezium cluster are underestimated.

2.4. Discussion

We carried out simulations to understand how the combined effect of viscous disc evolution and leftover gas from the star formation process affect the development of circumstellar discs in star clusters. The discs are subject to viscous growth and can be truncated by dynamical interactions with nearby stars.

In our simulations we ignore various physical mechanisms that can alter the size and mass of circumstellar discs and cluster dynamics over its bound life-time. These effects include the tidal field of the galaxy, stellar evolution, and radiative feedback processes. Initially, our clusters are composed of single stars each of which has a relatively massive but small (~ 30 au) disc, in which orientation is ignored and truncation radius is defined as the average over all inclinations.

Photoevaporation of a circumstellar disc can be caused both by the central star or by nearby OB stars present in the clusters. The influence of external UV radiation can have an important effect on the outer parts of the circumstellar discs, causing mass loss and further diminishing their radii (Scally & Clarke 2001; Guarcello et al. 2016).

Other mechanisms neglected in our model are ram-pressure stripping and face-on accretion on discs. Wijnen et al. (2016, 2017a) demonstrated that face-on accretion of ambient gas in embedded star-forming regions can cause circumstellar discs to contract, while the ram pressure exerted by the interstellar medium strips the outer parts of the discs. Nearby supernovae could also have important repercussions on the morphology and mass of circumstellar discs (Close & Pittard 2017; Portegies Zwart et al. 2018), but since our clusters are very young we ignore this effect.

Encounters between stars with discs could result in the exchange of disc-material from one to the other and affect the shape and mass of both discs (Jilková et al. 2016). Such encounters also tend to harden the surface density of the discs, making their density profiles diverge from the similarity solutions (Hall 1997).

In Figure 2.6 we present a schematic overview of the various processes that can affect the final characteristics of circumstellar discs in young star clusters. We take values for viscous growth and dynamical truncations based in our results. We also include ram pressure stripping, stellar feedback from winds and supernovae, and external photoevaporation with values obtained from literature. This figure is intended as a guideline to visualize how incomplete our understanding of the processes that happen inside young star clusters still

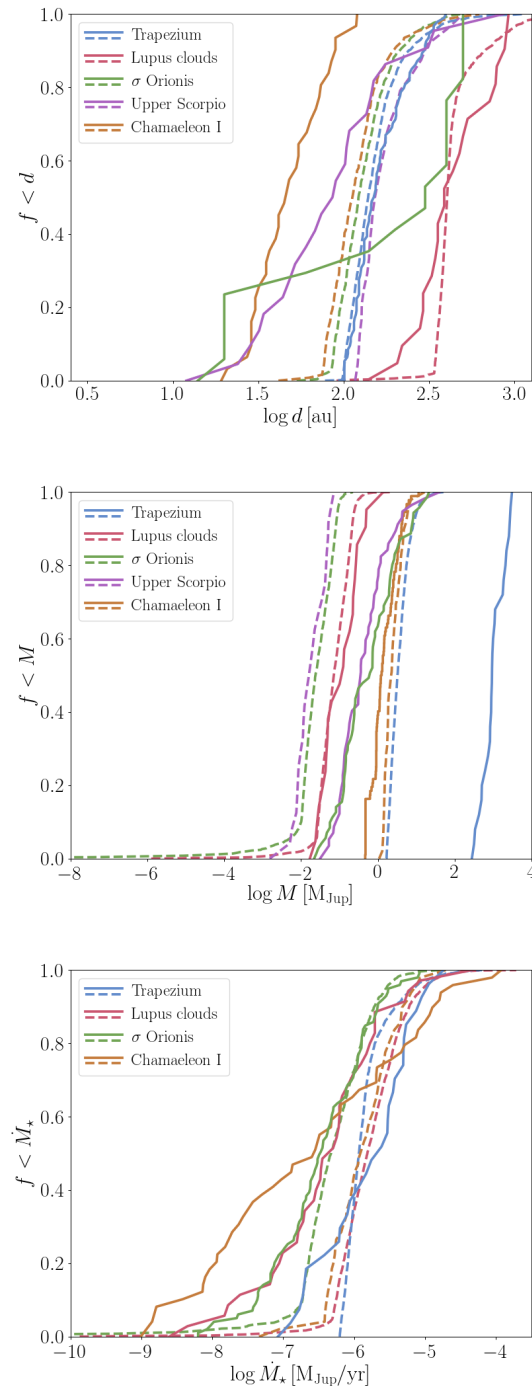


Figure 2.5: Observed cumulative distributions for the mean disc size (top panel) and mass (center), and accretion rate onto central star (bottom panel) for observed clusters (solid lines) along with the most similar simulation result (dashed lines) obtained at the time comparable to the estimated age of the corresponding cluster. Accretion rates measurements for the discs on the Upper Scorpio region were not available at the time of this paper.

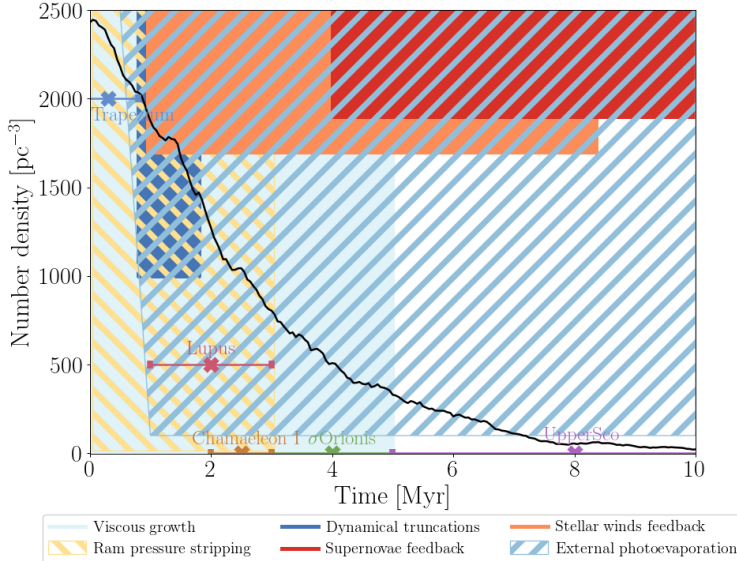


Figure 2.6: Physical processes in embedded clusters and their corresponding time scales and density scales. The cluster density shown corresponds to one of our simulations for $N = 1,500$, $\alpha = 5 \times 10^{-3}$. References: Ram pressure stripping Wijnen et al. (2016, 2017a); Dynamical truncations Portegies Zwart (2016); Vincke & Pfalzner (2016); Wijnen et al. (2017a); Supernovae feedback Pelupessy & Portegies Zwart (2012); Parker et al. (2014); Stellar winds feedback Pelupessy & Portegies Zwart (2012); External photoevaporation Adams (2010); Anderson et al. (2013); Facchini et al. (2016).

is. These processes need to be better constrained in parameter space before we can further discuss which ones dominate in the existing observations of young star forming regions.

Stellar density for a simulation with $N = 1,500$, $\alpha = 5 \times 10^{-3}$ is shown as a guide. Our simulations run only for 2.0 Myr, and after that the clusters are not dense enough for dynamical truncations to be important. We expand the influence of viscous growth up to 5.0 Myr. This is the point when the diversity in spectral-energy distributions of observed circumstellar discs settles down and discs are predominantly weak. This means that they could have dissipated or that gas depletion or planet formation could be taking place (Hillenbrand 2008; Gorti et al. 2016). In our model, as well as in the literature, dynamical truncations do not appear to be a critical process for disc shrinking, in particular when encounters with other stars are distant and when the discs are also affected by external photoevaporation due to bright OB stars (Rosotti et al. 2018; Winter et al. 2018a,b). External photoevaporation can also start in early stages of cluster evolution (~ 0.5 Myr) and carry on for almost the whole life of the bright OB stars generating the strong UV radiation (Adams 2010). Discs can be expected to always be destroyed by external photoevaporation within 10 Myr (Anderson et al. 2013). Based on the work of Facchini et al. (2016) we extend external photoevaporation down to $N = 100$ stars, since their results show that discs with radius > 150 au can endure intense mass loss even for very low ambient far UV fields ($G_0 \sim 30$).² We set the start of external photoevaporation effects at 1.0 Myr for low stellar densities, because this is the point where the average disc size for our isolated discs reaches 150 au. Feedback effects of supernovae start after ~ 4 Myr. At stellar densities $\gtrsim 1.900 \text{ pc}^{-3}$ it can affect the evolution of the discs and even destroy them (Pelupessy & Portegies Zwart 2012; Parker et al. 2014).

² $G_0 = 1.6 \times 10^{-3} \text{ erg s}^{-1} \text{ cm}^{-2}$, the interstellar FUV value

Winds from nearby stars can affect their Neighbors from times as early as 0.96 Myr; however, stellar densities $\gtrsim 1.500 \text{ pc}^{-3}$ are needed for this to affect the evolution of the discs (Pelupessy & Portegies Zwart 2012). Ram pressure stripping and face-on accretion affect the discs all through the embedded phase of young star clusters, even for very low stellar and gas densities (Wijnen et al. 2016, 2017a).

The discrepancy between observations and simulation results could reflect not only the need to include more physical processes. The initial conditions chosen for the simulations could also not be representative of real clusters. It is possible that young stellar clusters present substructure, in which the local stellar density might be higher and in turn lead to more dynamical encounters (Goodwin & Whitworth 2004).

We overlook the presence of primordial binaries in our initial conditions, which could also contribute to the overestimation of our disc sizes. Cox et al. (2017) show that discs around binary stars tend to be smaller than their isolated counterparts, and they tend to be less bright. Neglecting primordial binaries is a rather strong assumption, because they tend to have a strong effect on the disc-size distribution and their survivability in the cluster. We realize that our simulations tend to overestimate disc sizes, but observations may as well underestimate disc sizes, in particular of the outer extended regions of discs where they have a low surface density.

The different descriptions of observed disc radii and masses used together in section 2.3.4 may also explain why we do not see consistency in the over and underestimation of these parameters in our simulations. Having a uniform description of the observational data would be ideal to perform a more accurate comparison. Thanks to Gaia DR2 (Brown et al. 2018), the distances to the star forming regions considered in this work are being calculated more precisely (e.g. Roccatagliata et al. 2018), which could also reflect differences in disc sizes from the ones here reported. The first-order approach obtained in this paper, however, serves as a good guideline as to where to direct future developments.

2.5. Summary and conclusions

We studied the effect of viscous growth and dynamical truncations of circumstellar discs inside young star clusters. We used a semi-analytic model to include the viscous evolution of the discs, and a background potential to implement the gas in the cluster. We studied three scenarios for the gas: no gas in the cluster, constant gas through the cluster's evolution, and gas expulsion halfway through the cluster's evolution. For this, we ran simulations with number of stars $N = 1,500$, turbulence parameter $\alpha = 10^{-2}$ and $\alpha = 5 \times 10^{-3}$, and spanning 2.0 Myr of cluster evolution.

Our simulations result in similar distributions for average disc size, disc mass, and accretion rate onto the central star, independent of the gas in the cluster. Although clusters without leftover gas result in a higher amount of discs with radius $\lesssim 500 \text{ au}$, in our simulations gas presence does not seem to largely shape the final distribution of circumstellar disc parameters. In an environment where dynamical truncations were important in shaping the sizes of the circumstellar discs, we would expect the presence of gas to make a difference in the final disc size distribution, since stars still embedded in leftover gas have higher velocity dispersions (Vincke & Pfalzner 2016) which in turn leads to more dynamical encounters. In the parameter space spanned by our simulations, dynamical truncations are overtaken by viscous growth in determining the size of the circumstellar discs.

The different values of the turbulence parameter are reflected in the resulting sizes of circumstellar discs. Simulations with fast viscous growth ($\alpha = 10^{-2}$) return bigger discs, but these discs are still not large enough to be affected by dynamical encounters. The size of the

circumstellar discs in our simulations is only defined by the inherent viscous growth of the discs. Dynamical truncations do not play an important role in the determination of the final disc sizes and masses.

We performed a comparison of our simulation results with observational data of circumstellar disc sizes, masses, and stellar accretion rates in several young star forming regions. To better match the stellar densities of the observed regions, we expanded the parameter space of our simulations to number of stars $N=[25, 50, 100, 125, 250, 500, 750, 1,000, 1,250, 1,500, 1,750, 2,000, 2,250, 2,500, 5,000]$ and values of $\alpha=[10^{-4}, 2 \times 10^{-3}, 5 \times 10^{-3}, 7 \times 10^{-3}, 10^{-2}]$. We also adjusted the definitions of size and mass of our simulated discs to suit the descriptions of the observed discs.

Low values of the turbulence parameter ($\alpha=10^{-4}$) are not enough to reproduce the small circumstellar disc sizes observed in the star forming regions. Simulations with higher values of α ($\alpha=5 \times 10^{-3}$ and higher) differ even more from the observed disc distributions. The stellar density of the simulated clusters is not enough for dynamical encounters to actively truncate the discs and reproduce observed circumstellar disc sizes. Dynamical truncations by themselves are not relevant enough to shape the observed distributions of circumstellar disc sizes and masses. Other processes are at play in terms of counteracting the viscous growth of the discs.

Compared to observations, our model both under and overestimates different disc parameters, but does not show a consistent behaviour related to the data. This could be due to the physical processes ignored in this work, or to an incorrect selection of initial conditions. It is also important to note that the observational data is not uniformly characterized, which could contribute to the incongruence with simulation results. The distributions of disc parameters obtained by our simulations, if not accurate, still fall within ranges in agreement with the ones spanned by observations of different star forming regions.

* * *

3 | External photoevaporation of circumstellar discs constrains the time-scale for planet formation

F. Concha-Ramírez; M. J. C. Wilhelm;
S. Portegies Zwart; T. J. Haworth

Monthly Notices of the Royal Astronomical Society
Volume 490, Issue 4, p.5678–5690 (2019)

PLANET-FORMING circumstellar discs are a fundamental part of the star formation process. Since stars form in a hierarchical fashion in groups of up to hundreds or thousands, the UV radiation environment that these discs are exposed to can vary in strength by at least six orders of magnitude. This radiation can limit the masses and sizes of the discs. Diversity in star forming environments can have long lasting effects in disc evolution and in the resulting planetary populations. We perform simulations to explore the evolution of circumstellar discs in young star clusters. We include viscous evolution, as well as the impact of dynamical encounters and external photoevaporation. We find that photoevaporation is an important process in destroying circumstellar discs: in regions of stellar density $\rho \sim 100 \text{ M}_\odot \text{ pc}^{-3}$ around 80% of discs are destroyed before 2.0 Myr of cluster evolution. In regions of $\rho \sim 50 \text{ M}_\odot \text{ pc}^{-3}$ around 50% of discs are destroyed in the same timescale. Our findings are in agreement with observed disc fractions in young star forming regions and support previous estimations that planet formation must start in timescales $< 0.1 - 1 \text{ Myr}$.

*

3.1. Introduction

Circumstellar discs develop as a result of the star formation process (Williams & Cieza 2011). Since a non negligible fraction of stars are not born in isolation (Bressert et al. 2010; King et al. 2012), and gas left over from the star formation process can linger for a few Myr (Portegies Zwart et al. 2010), during their first stages of evolution the discs remain embedded in an environment that is dense in gas and neighbouring stars. These conditions can be hostile for the discs in a myriad of ways: they can be subject to dynamical truncations (Vincke et al. 2015; Portegies Zwart 2016; Vincke & Pfalzner 2016) or be affected by processes related to stellar evolution, such as stellar winds (Pelupessy & Portegies Zwart 2012), supernovae explosions (Close & Pittard 2017; Portegies Zwart et al. 2018), and photoevaporation due to bright OB stars in the vicinity (e.g. Guarcello et al. 2016; Haworth et al. 2017). The surrounding gas can also shrink the discs through ram pressure stripping (Wijnen et al. 2016, 2017a). Since planet formation related processes seem to start very quickly in circumstellar discs ($< 0.1 - 1$ Myr, Najita & Kenyon (2014); Manara et al. (2018)), understanding the mechanisms that affect disc evolution is directly connected to understanding planetary system formation and survival. The Sun was probably born within a star cluster (Portegies Zwart et al. 2009), so discerning how the cluster environment affects the evolution of the discs can help us comprehend the origins of the Solar System.

There are several observational indications that the environment of circumstellar discs shortly after their formation is unfavourable for their survival. Discs have been observed to be evaporating in several young star forming regions (e.g. Fang et al. 2012; de Juan Ovelar et al. 2012; Mann et al. 2014; Kim et al. 2016; van Terwisga et al. 2019). Moreover, observations indicate that disc fractions decline in regions close to an O-type star (e.g. Balog et al. 2007; Guarcello et al. 2007, 2009, 2010; Fang et al. 2012; Mann et al. 2014; Guarcello et al. 2016). Fatuzzo & Adams (2008) estimate an FUV radiation field of up to $G_0 \approx 1,000$ in star clusters of $N > 1,000$ stars¹, while Facchini et al. (2016) show that discs of radius ~ 150 au are subject to photoevaporation even in very low FUV fields ($G_0 = 30$). In regions of high stellar density, nearby stars can also affect disc size and morphology by dynamical interactions. Observational evidence of the imprints of dynamical truncations has been reported in several nearby stellar clusters (Olczak et al. 2008; Reche et al. 2009; de Juan Ovelar et al. 2012). Tidal stripping that can be explained by disc-star interactions has been observed in the RW Aurigae system (Cabrit et al. 2006; Rodriguez et al. 2018; Dai et al. 2015) and in the T Tauri binary system AS 205 (Salyk et al. 2014). There is also evidence that the Solar System might have been affected by a close encounter with another star during its early stages (Jílková et al. 2015; Pfalzner et al. 2018).

Circumstellar discs are not only affected by external processes, but also by their internal viscous evolution. The combination of outwardly decreasing angular velocity together with outwardly increasing angular momentum causes shear stress forces inside the discs. As a consequence mass is accreted from the innermost regions of the disc onto its host star, whereas the outermost regions expand (Lynden-Bell & Pringle 1974). Tazzari et al. (2017) propose that the measured offsets in sizes and masses of discs in the Lupus clouds versus discs in the Taurus-Auriga and Ophiuchus regions can be explained as observational evidence of viscous spreading. However Rosotti et al. (2019) argue that current surveys do not yet have the sufficient sensitivity to properly detect this phenomenon.

Different approaches have been implemented to study the effects of these processes on the lifetime of circumstellar discs. External photoevaporation has been modelled with radiation hydrodynamics codes that solve flow equations through the disc boundaries, together

¹ G_0 is the FUV field measured in units of the Habing flux, 1.6×10^{-3} erg s⁻¹ cm⁻² (Habing 1968).

with photodissociation region codes to obtain the temperature profiles of the discs (e.g. Haworth et al. 2016; Facchini et al. 2016). This method has been coupled with α -disc models to account for viscous evolution of the disc (e.g. Adams et al. 2004; Anderson et al. 2013; Gorti et al. 2015; Rosotti et al. 2017). Haworth et al. (2018a) introduce the concept of pre-computing photoevaporation mass losses in terms of the surface density of the discs, an approach that we expand on in section 3.2.3. Winter et al. (2019a) model the environment of Cygnus OB2 and use the photoevaporation mass loss rate to constrain the timescale for gas expulsion in the young star forming region. Nicholson et al. (2019) perform simulations of star forming regions where FUV photoevaporation is implemented in post-processing, and find a very short lifetime for the discs (< 2 Myr) in moderate and low density regions ($\lesssim 100 M_{\odot} pc^{-3}$).

Regarding dynamical effects, close encounters on a single N-body disc of test particles have been investigated in several studies (e.g. Breslau et al. 2014; Jílková et al. 2016; Bhandare et al. 2016; Pfalzner et al. 2018). Winter et al. (2018a,b) use a ring of test particles around a star to obtain linearized expressions of the effect that a stellar encounter can have on the mass and morphology of the disc, and then use them to simulate the disc using a smoothed particles hydrodynamics (SPH) code. A different approach for studying these effects is evolving the stellar dynamics of the cluster separately, and applying the effects of dynamical encounters afterwards (e.g. Olczak et al. 2006, 2010; Malmberg et al. 2011; Steinhausen & Pfalzner 2014; Vincke et al. 2015; Vincke & Pfalzner 2016, 2018). Directly adding SPH discs to a simulation of a massive star cluster is computationally expensive, since a high resolution is needed over long time scales. The closest effort corresponds to the work by Rosotti et al. (2014), in which individual SPH codes are coupled to half of the $1 M_{\odot}$ stars in a cluster with 100 stars. This allows them to study the effects of viscous spreading of the discs and dynamical truncations in a self-consistent way, but they are limited by the computational resources needed for this problem. Parametrized approaches have also been developed, where the cluster dynamics and effects of truncations (Portegies Zwart 2016) and viscous spreading (Concha-Ramírez et al. 2019a) are considered simultaneously.

Concha-Ramírez et al. (2019a) investigate the effect of viscous growth and dynamical truncations on the final sizes and masses of protoplanetary discs inside stars clusters using a parametrized model for the discs. They show that viscous evolution and dynamical encounters are unable to explain the compact discs observed in star forming regions. They argue that other processes must affect the early evolution of the discs. Here we expand the model by improving the description of the viscous discs and by adding external photoevaporation due to the presence of bright nearby stars.

We model the circumstellar discs using the Viscous Accretion Disc Evolution Resource (VADER) (Krumholz & Forbes 2015). This code solves the equations of angular momentum and mass transport in a thin, axisymmetric disc. Dynamical truncations are parametrized, and the mass loss due to external photoevaporation is calculated using the Far-ultraviolet Radiation Induced Evaporation of Discs (FRIED) grid (Haworth et al. 2018b). This grid consists of pre-calculated mass loss rates for discs of different sizes and masses, immersed in several different external FUV fields. We use the Astrophysical Multipurpose Software Environment (AMUSE)² (Portegies Zwart & McMillan 2018) framework to couple these codes along with cluster dynamics and stellar evolution. All the code developed for the simulations, data analyses, and figures of this paper is available in Github³.

²<http://amusecode.github.io/>

³<https://doi.org/10.5281/zenodo.3537675>

3.2. Model

3.2.1. Viscous growth of circumstellar discs

We implement circumstellar discs using the Viscous Accretion Disc Evolution Resource (VADER) by Krumholz & Forbes (2015). VADER is an open source viscous evolution code which uses finite-volume discretization to solve the equations of mass transport, angular momentum, and internal energy in a thin, axisymmetric disc. An AMUSE interface for VADER was developed in the context of this work and is available online.

For the initial disc column density we use the standard disc profile introduced by Lynden-Bell & Pringle (1974):

$$\Sigma(r, t = 0) = \Sigma_0 \frac{r_c}{r} \exp\left(\frac{-r}{r_c}\right), \quad (3.1)$$

with

$$\Sigma_0 = \frac{m_d}{2\pi r_c^2 (1 - \exp(-r_d/r_c))}, \quad (3.2)$$

where r_c is the characteristic radius of the disc, r_d and m_d are the initial radius and mass of the disc, respectively, and Σ_0 is a normalization constant. Considering $r_c \approx r_d$ (Anderson et al. 2013), the density profile of the disc is:

$$\Sigma(r, t = 0) \approx \frac{m_d}{2\pi r_d (1 - e^{-1})} \frac{\exp(-r/r_d)}{r}. \quad (3.3)$$

This expression allows the disc to expand freely at the outer boundary while keeping the condition of zero torque at the inner boundary r_i .

To establish the radius of the discs we set the column density outside r_d to a negligible value $\Sigma_{\text{edge}} = 10^{-12} \text{ g cm}^{-2}$. The FRIED grid that we use to calculate the photoevaporation mass loss (see section 3.2.3) is a function of disc radius and outer surface density. There is a numerical challenge in determining what the disc outer surface density and radius actually are, since there is a large gradient in it down to the Σ_{edge} value. Computing a mass loss rate for a very low outer surface density in this steep gradient would return an artificially low result. Considering this we define the disc radius as the position of the first cell next to Σ_{edge} , as shown in Figure 3.1.

The temperature profile of the discs is given by

$$T(r) = T_m \left(\frac{r}{1 \text{ au}} \right)^{-1/2}, \quad (3.4)$$

where T_m is the midplane temperature at 1 au. Based on Anderson et al. (2013) we adopt $T_m = 300 \text{ K}$.

Each disc is composed of a grid of 50 logarithmically spaced cells, in a range between 0.5 and 5.000 au. In Appendix 3.A we show that the resolution is enough for our calculations. The discs have a Keplerian rotation profile and turbulence parameter $\alpha = 5 \times 10^{-3}$. The fact that the outer radius of the grid is much larger than the disc sizes (which were initially around 100 au, see section 3.2.4) allows the discs to expand freely without reaching the boundaries of the grid. The mass flow through the outer boundary is set to zero in order to maintain the density Σ_{edge} needed to define the disc radius. The mass flow through the inner boundary is considered as accreted mass and added to the mass of the host star.

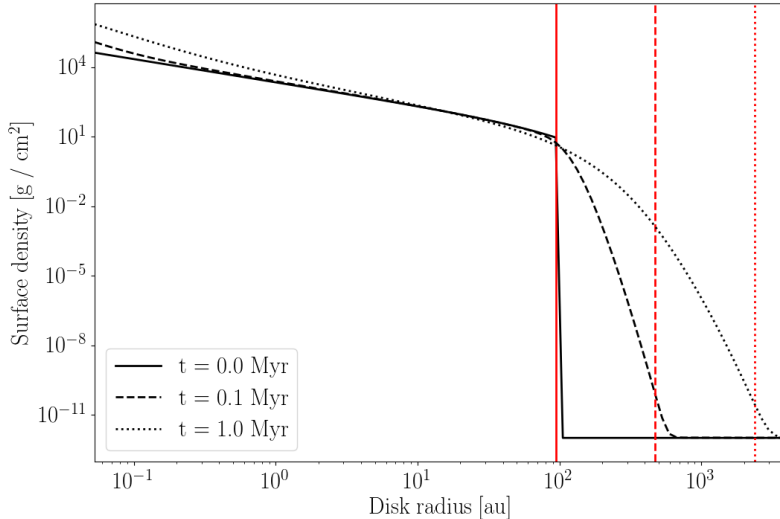


Figure 3.1: Definition of disc radius. The black lines show the disc profile and the corresponding red lines show the measured disc radius. Solid lines represent a disc initialized with $R = 100$ au. The dashed lines show the same disc after 0.1 Myr of isolated evolution, and the dotted lines after 1.0 Myr of isolated evolution.

3.2.2. Dynamical truncations

A close encounter between discs induces a discontinuity in their evolution. To modify the discs we calculate parametrized truncation radii. For two stars of the same mass, Rosotti et al. (2014) approximated the truncation radius to a third of the encounter distance. Together with the mass dependence from Bhandare et al. (2016), the dynamical truncation radius takes the form:

$$r' = \frac{r_{enc}}{3} \left(\frac{m_1}{m_2} \right)^{0.32}, \quad (3.5)$$

where m_1 and m_2 are the masses of the encountering stars.

To implement truncations we first calculate the corresponding truncation radius caused by the encounter, according to equation 3.5. We consider all the mass outside this radius to be stripped from the disc. To define r' as the new disc radius we change the column density of all the disc cells outside r' to the edge value $\Sigma_{\text{edge}} = 10^{-12}$ g cm⁻².

3.2.3. External photoevaporation

A circumstellar disc can be evaporated by radiation coming from its host star or from a bright star in the vicinity. The heating of the disc surface can lead to the formation of gaps at different locations, which can cause the progression to a transition disc (e.g. Clarke et al. 2001; Gorti et al. 2009). The radiation can also truncate the disc by removing material from the outer, loosely-bound regions (e.g. Adams et al. 2004).

Models of internal photoevaporation have shown that most of the mass loss in this case occurs in the inner 20 au of the disc (Font et al. 2004; Owen et al. 2010). Radiation from the

host star can evaporate material from the outskirts of the disc, however [Owen et al. (2010)] show that more than 50% of the total mass loss occurs in the 5 – 20 au region. In [Font et al. (2004)] around 90% of the mass loss occurs within the inner 18 au of the disc. Given that the mass loss rate from the outer disc is typically comparable to or larger than that from the inner disc, we expect external photoevaporation to dominate in the outer regions. External photoevaporation has been shown to be more effective in evaporating the discs than radiation from the host star (e.g. [Johnstone et al. (1998); Adams & Myers (2001)]). Truncation by external photoevaporation can also result in changes of the viscosity parameter α , which further affects the viscous evolution of the discs ([Rosotti et al. (2017)]). In this work we ignore the effects of photoevaporation on internal disc structure, and deal exclusively with disc survival rates. Because of this and the discussion above we focus on external photoevaporation due to bright stars in the vicinity.

OB-type stars emit heating radiation in the form of extreme-ultraviolet (EUV), far-ultraviolet (FUV), and X-rays. In the case of external photoevaporation the dispersal of disc material is dominated by the FUV photons ([Armitage (2000); Adams et al. (2004); Gorti & Hollenbach (2009)]). The main part of our work deals with photoevaporation due to FUV photons; in addition we also incorporate the effect of EUV photons (see Eq. 5.4).

The amount of mass lost from the discs as a result of external photoevaporation depends on the luminosity of the bright stars in the cluster. This luminosity, together with the distance from each of the massive stars to the discs, is used to obtain the amount of radiation received by each disc. We can then calculate the amount of mass lost. Below we explain what we consider to be massive stars and how we calculate the mass loss rate.

FUV luminosities

We follow [Adams et al. (2004)] in defining the FUV band ranging from 6 eV up to 13.6 eV, or approximately from 912 Å to 2070 Å. We calculate the FUV radiation of the stars in the simulations based on their spectral types. Given the presence of spectral lines in this band, we use synthetic stellar spectra rather than relying on black body approximations. The spectral library used is UVBLUE ([Rodríguez-Merino et al. (2005)]), chosen for its high coverage of parameter space and high resolution, spanning the appropriate wavelength ranges. It spans a three dimensional parameter space of stellar temperature, metallicity, and surface gravity.

We use the UVBLUE spectral library to precompute a relation between stellar mass and FUV luminosity. We do this by considering all the stars in the cluster to have solar metallicity ($Z = 0.02$). We then select the temperature and surface gravity spectra closer to the zero age main sequence value of each star, according to the parametrized stellar evolution code SeBa ([Portegies Zwart & Verbunt (1996); Toonen et al. (2012)]). Given that the masses and radii of the stars are known, using the chosen spectra we build a relationship between stellar mass and FUV luminosity. This relation takes the shape of a segmented power law, as is shown in Figure 3.2. A similar fit was obtained by [Parravano et al. (2003)]. In runtime the stars are subject to stellar evolution and the FUV luminosity for each star was calculated directly from this fit using the stellar mass.

The mass range of the fit in Figure 3.2 is $0.12 - 100 M_{\odot}$, however, we are only interested in the range $1.9 - 50 M_{\odot}$. As is further explained in section 3.2.3, we only consider stars with masses higher than $1.9 M_{\odot}$ to be emitting FUV radiation, and $50 M_{\odot}$ is the theoretical upper limit for the stellar mass distribution. Stars with masses $\leq 1.9 M_{\odot}$ are given discs and are affected by the massive stars. The massive stars are also subject to stellar evolution, which is implemented with SeBa through the AMUSE interface. The FUV luminosity of each massive star is calculated in every time step, from the precomputed fit, after evolving the stellar

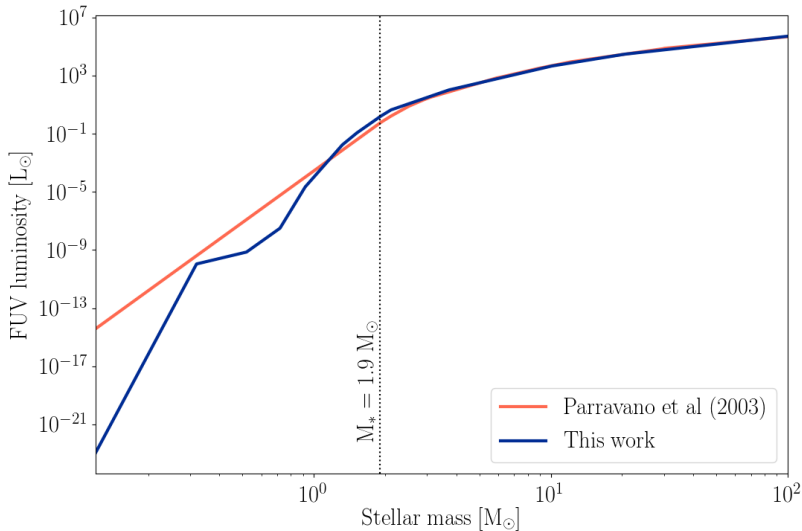


Figure 3.2: FUV luminosity vs. stellar mass fit calculated from the ZAMS spectra. $M_* = 1.9 M_\odot$ is the lower mass limit of the FRIED grid, and the lower mass limit for the stars to be considered emitting FUV radiation in our simulations (see Section 3.2.3 for details).

evolution code. The low mass stars are not subject to stellar evolution.

Mass loss rate due to external photoevaporation

To calculate the mass loss due to FUV external photoevaporation we use the Far-ultraviolet Radiation Induced Evaporation of Discs (FRIED) grid developed by Haworth et al. (2018b). The FRIED grid is an open access grid of calculations of externally evaporating circumstellar discs. It spans a five dimension parameter space consisting of disc sizes (1 – 400 au), disc masses ($10^{-4} – 10^2 M_{Jup}$), FUV fields ($10 – 10^4 G_0$), stellar masses ($0.05 – 1.9 M_\odot$) and disc outer surface densities. The seemingly three dimensional grid subspace of disc mass, edge surface density, and disc radius is in fact two dimensional, as any combination of disc radius and disc mass has only one edge density associated with it. Because of this, we only take into account a four dimensional grid of radiation field strength, host star mass, disc mass, and disc radius.

Following the stellar mass ranges of the FRIED grid we separate the stars in the simulations into two subgroups: *massive stars* and *low mass stars*. Massive stars are all stars with initial masses higher than $1.9 M_\odot$, while low mass stars have masses $\leq 1.9 M_\odot$. Only the low mass stars have circumstellar discs in the simulations. The massive stars are considered as only generating FUV radiation and affecting the low mass stars. In this way we make sure that we stay within the stellar mass limits of the FRIED grid. Low mass stars ($\lesssim 1 M_\odot$) have a negligible UV flux (Adams et al. 2006), so this approximation holds well for our purposes. Calculation of the FUV radiation emitted by the massive stars is further explained in section 3.2.3. These star subgroups are considered only for the calculation of FUV radiation and photoevaporation mass loss. In the gravity evolution code the two subgroups are undistinguishable.

The FRIED grid allows to take a circumstellar disc with a specific mass, size, and density,

around a star with a certain mass, and from the FUV radiation that it receives, obtain the photoevaporation mass loss. However, the parameters of the simulated discs do not always exactly match the ones in the grid. We perform interpolations over the grid to calculate the mass losses of the discs in the simulations. Because of computational constraints, we perform the interpolations on a subspace of the grid, such that it contains at least one data point above and below the phase space point of the disc in each dimension. The high resolution of the FRIED grid ensures that this interpolation is performed over an already smooth region.

When a massive star approaches a circumstellar disc, external photoevaporation is dominated by EUV radiation. Following Johnstone et al. (1998) we define a distance limit below which EUV photons dominate:

$$d_{min} \approx 5 \times 10^{17} \left(\frac{\epsilon^2}{f_r \Phi_{49}} \right)^{-1/2} r_{d_{14}}^{1/2} \text{ cm} \quad (3.6)$$

where $\left(\frac{\epsilon^2}{f_r \Phi_{49}} \right)^{1/2} \approx 4$, $r_{d_{14}} = \frac{r_d}{10^{14} \text{ cm}}$ with r_d the disc radius, and $5 \times 10^{17} \text{ cm} \sim 3 \times 10^4 \text{ au} \sim 0.16 \text{ pc}$. When a star with a disc is at a distance $d < d_{min}$ from a massive star we calculate the mass loss using equation (20) from Johnstone et al. (1998):

$$\dot{M}_{EUV} = 2.0 \times 10^{-9} \frac{(1+x)^2}{x} \epsilon r_{d_{14}} M_\odot \text{ yr}^{-1} \quad (3.7)$$

with $x \approx 1.5$ and $\epsilon \approx 3$. During most of their evolution, however, the circumstellar discs in the simulations experience photoevaporation only due to FUV photons. Since we do not consider interstellar gas and dust in the clusters, we do not account for extinction in the calculation of the radiation received by each small star.

Disc truncation due to photoevaporation

Once the mass loss due to photoevaporation is calculated for every disc, the discs are truncated at a point that coincides with the amount of mass lost in the process. We take the approach of Clarke (2007) and remove mass from the outer edge of the disc. We do this by moving outside-in from the disc edge and removing mass from each cell by turning its column density to the edge value $\Sigma_{\text{edge}} = 10^{-12}$ defined in section 3.2.1. We stop at the point where the mass removed from the disc is equal to the calculated mass loss.

We consider a disc to be completely evaporated when it has lost 99% of its initial mass (Anderson et al. 2013) or when its mean column density is lower than 1 g cm^{-2} (Pascucci et al. 2016). From this point forward the star continues its dynamical evolution normally, but is no longer affected by massive stars.

Summary of cluster evolution

The code runs in major time steps, which represent the time scale on which the various processes are coupled. Within each of these macroscopic time steps (1.000 yr), internal evolutionary processes such as stellar evolution and gravitational dynamics proceed in their own internal time steps (500 yr and 1.000 yr respectively). Throughout each macroscopic time step, we perform the following operations:

1. Gravitational dynamics code is evolved.
2. We check the stars for dynamical encounters:
 - 2.a If a dynamical encounter occurs, we determine the truncation radius for each disc.

- 2.b We update the radius and mass of the discs.
- 3. Stellar evolution code is evolved.
- 4. Photoevaporation process is carried out as follows. For each massive star:
 - 4.a We calculate the distance d from the massive star to each low mass star.
 - 4.b If $d < d_{min}$ (see Eq. 5.4) we calculate the mass loss \dot{M}_{EUV} .
 - 4.c If $d \geq d_{min}$ the massive star's FUV luminosity L_{FUV} is calculated (see section 3.2.3).
 - 4.d Using d and L_{FUV} we calculate l_{FUV} , the amount of FUV radiation received by the low mass star.
 - 4.e Using l_{FUV} together with the low mass star's mass, disc mass, and disc radius, we build a sub-grid of the FRIED grid and interpolate over it to calculate the mass loss \dot{M}_{FUV} .
 - 4.f The total mass loss in the time step is calculated using \dot{M}_{EUV} and \dot{M}_{FUV} .
 - 4.g The mass is removed from the disc by moving outside-in and removing mass from the cells.
 - 4.h The disc mass and radius are updated.
- 5. Discs are checked for dispersal. If a disc has been dispersed (see section 3.2.3) the code for the disc is stopped and removed and the star continues evolving only as part of the gravitational dynamics code.
- 6. Simulation runs until 5 Myr of evolution or until all the discs are dispersed, whichever happens first.

We present a scheme of this process and of the photoevaporation in Figures 3.3 and 3.4 respectively.

3.2.4. Initial conditions

Discs

The initial radii of the circumstellar discs are given by:

$$R_d(t = 0) = R' \left(\frac{M_*}{M_\odot} \right)^{0.5} \quad (3.8)$$

where R' is a constant. The youngest circumstellar discs observed to date have diameters that range from ~ 30 au (e.g. Lee et al. 2018) to $\sim 120 - 180$ au (e.g. Murillo et al. 2013; van 't Hoff et al. 2018). Based on this we choose $R' = 100$ au, which for our mass range $0.05 - 1.9 M_\odot$ for stars with discs results in initial disc radii between ~ 22 au and ~ 137 au.

The initial masses of the discs are defined as:

$$M_d(t = 0) = 0.1 M_* \quad (3.9)$$

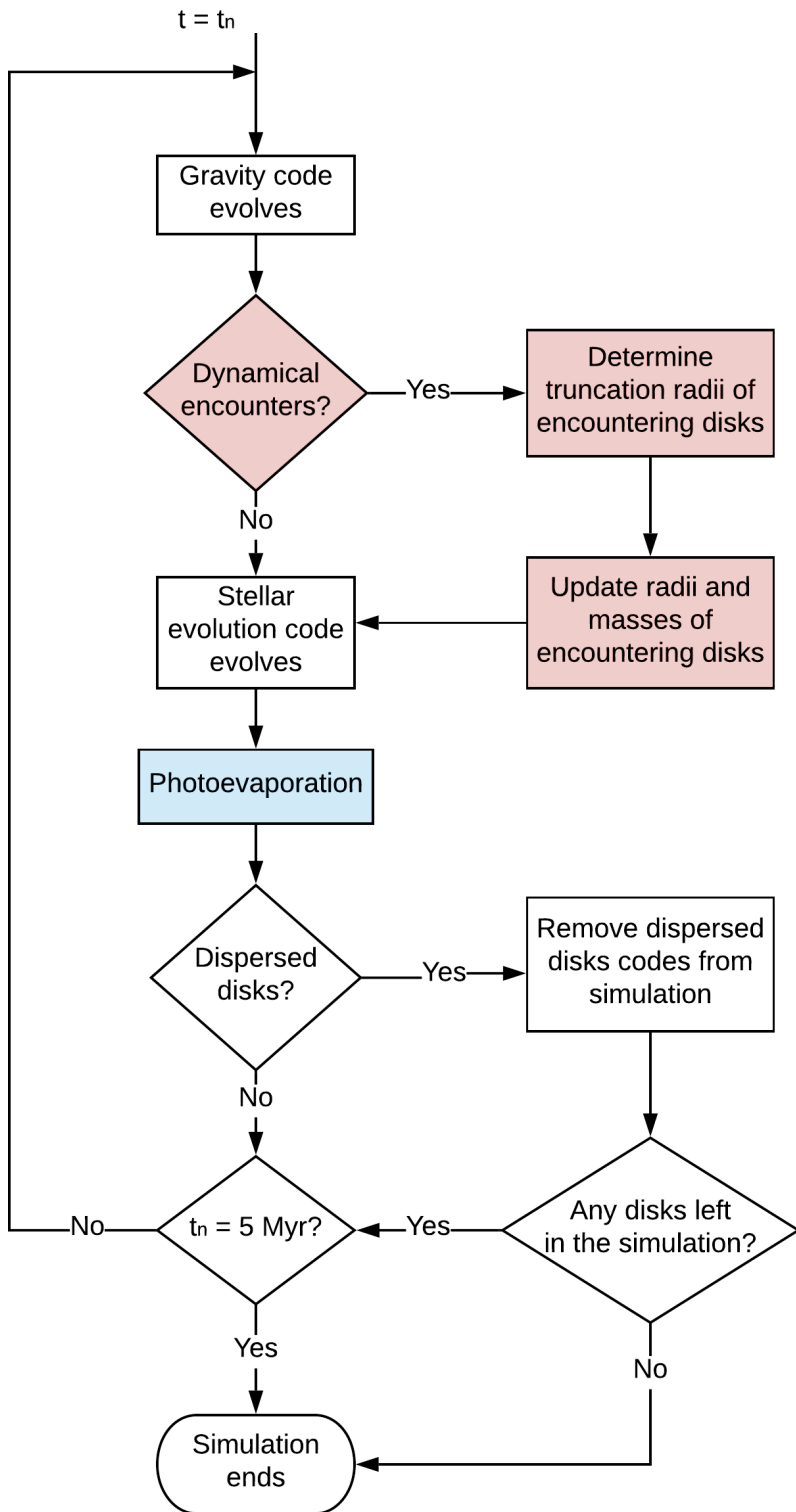


Figure 3.3: Operations performed in each macroscopic time step. Within each macroscopic time step t_n , internal evolutionary processes such as stellar evolution and gravitational dynamics proceed in their own internal time steps.

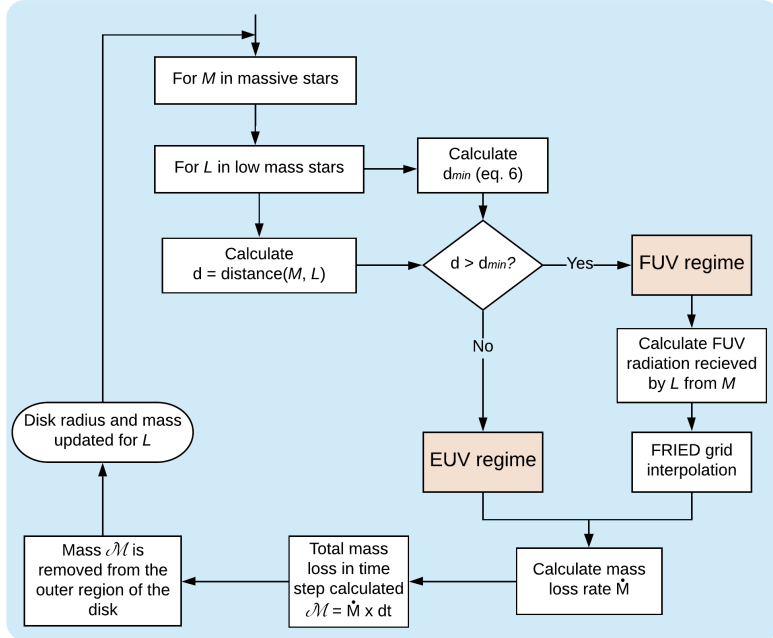


Figure 3.4: Flowchart of the photoevaporation process.

| Region | Sim. # | Low mass stars | $\bar{M}_{\text{low mass}} [M_{\odot}]$ | Massive stars | $\bar{M}_{\text{massive}} [M_{\odot}]$ |
|--------------|--------|----------------|---|---------------|--|
| ρ_{100} | 1 | 97% | 1.18 ± 0.17 | 3% | 4.08 ± 2.69 |
| | 2 | 99% | 0.24 ± 0.30 | 1% | 3.43 |
| | 3 | 96% | 0.24 ± 0.31 | 4% | 4.51 ± 2.59 |
| ρ_{50} | 1 | 94% | 0.27 ± 0.33 | 6% | 5.94 ± 5.65 |
| | 2 | 96% | 0.25 ± 0.31 | 4% | 3.51 ± 0.26 |
| | 3 | 99% | 0.24 ± 0.27 | 1% | 4.90 |

Table 3.1: Stellar mass properties in each simulation run.

Cluster

We perform simulations of young star clusters with stellar densities $\rho \sim 100 M_{\odot} \text{ pc}^{-3}$ and $\rho \sim 50 M_{\odot} \text{ pc}^{-3}$ using Plummer sphere spatial distributions (Plummer 1911). We will refer to these distributions as ρ_{100} and ρ_{50} , respectively. All the regions are in virial equilibrium (viral ratio $Q = 0.5$).

Stellar masses are randomly drawn from a Kroupa mass distribution (Kroupa 2001) with maximum mass $50 M_{\odot}$. The mean mass of the distribution is $\bar{M}_* \approx 0.3 M_{\odot}$. In Table 3.1 we show the details of the stellar masses in each simulation.

The simulations end at 5 Myr or when all the discs are dispersed, whichever happens first.

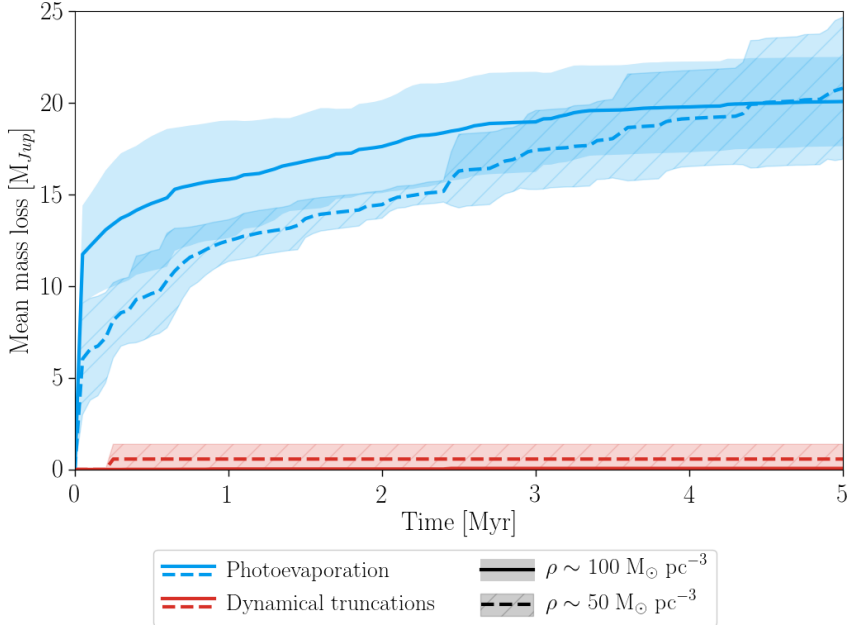


Figure 3.5: Mean mass loss in time due to external photoevaporation (blue) and dynamical truncations (red). The solid and dashed lines correspond to the ρ_{100} and ρ_{50} regions, respectively. The shaded areas indicate the standard deviation of the simulations.

3.3. Results

3.3.1. Disc mass loss in time

As a way to quantify the mass loss effect of each of the processes included in the simulations, we measure the mass loss due to external photoevaporation and dynamical truncations separately. In Figure 3.5 we show the mass loss over time for external photoevaporation and dynamical truncations. The solid and dashed lines correspond to the mean mass loss among all stars in the ρ_{100} and ρ_{50} regions, respectively. The shaded areas show the extent of the results in the different simulation runs.

The mass lost from the circumstellar discs is dominated by external photoevaporation over the entire lifetime of the simulated clusters. Dynamical truncations only have a local effect on truncating disc radii and masses, whereas photoevaporation is a global effect influencing all discs in the cluster.

The amount of FUV radiation received by each disc and the ensuing mass loss are variable. The effect depends on the proximity to massive stars, which changes with time as the stars orbit in the cluster potential. For the ρ_{100} region the average FUV radiation over 5 Myr of evolution was $\sim 475 G_0$, with a minimum of $10 G_0$ and a maximum of $\sim 10^4 G_0$. For the ρ_{50} region the average over 5 Myr was $\sim 56 G_0$, minimum $\sim 2 G_0$ and maximum $267 G_0$. These values are only shown as an indicative of the environment that the simulation discs were dispersed in, however a short exposure to a strong FUV field can be instantly more destructive than a sustained low FUV field. The FUV field can also vary in time due to processes intrinsic to star formation, such as a massive star being embedded during its early stages (e.g. Ali & Harries 2019). In our simulations, however, photoevaporation is driven by

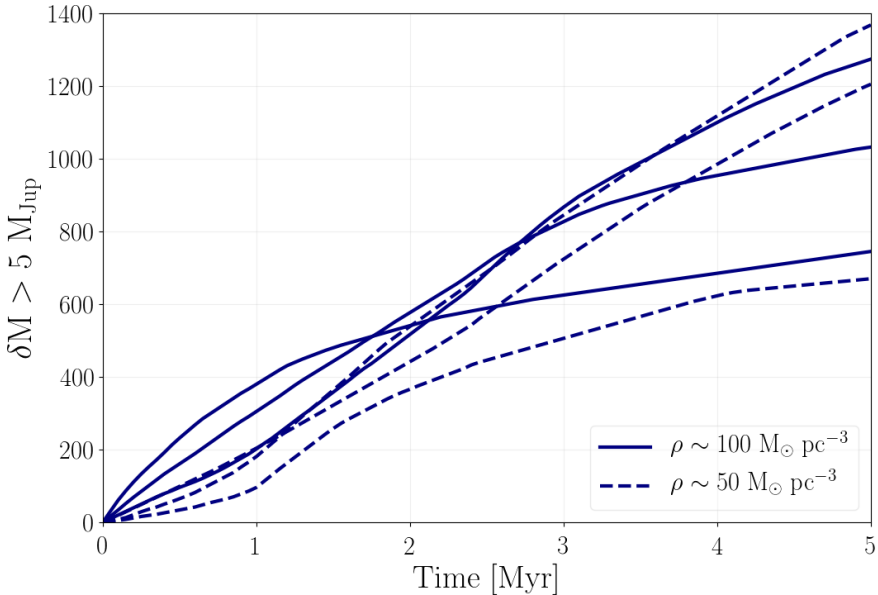


Figure 3.6: Cumulative distribution of discs that lose more than $5 M_{\text{Jup}}$ in time in each simulation. The solid lines correspond to the ρ_{100} region simulations and the dashed lines to the ρ_{50} region simulations.

the background FUV field. In Figure 3.6 we show the cumulative distributions of discs that lose more than $5 M_{\text{Jup}}$ in time. It can be seen that large mass losses are not driven by close encounters with bright stars but by the environmental FUV radiation. From Figure 3.6 it can be seen that before 2 Myr of evolution the discs in ρ_{100} lose mass more strongly than the ones in ρ_{50} . However, starting around 2 Myr and until the end of the simulations there is large scatter in the mass loss behaviour for each region. This is related to the dynamics of each cluster. For ρ_{100} the crossing time is $t_{\text{cross}} = 1.20 \pm 0.04$ Myr, and for ρ_{50} the crossing time is $t_{\text{cross}} = 0.98 \pm 0.09$ Myr. This results in the fact that, after one crossing time, all the stars in the clusters have been affected by the radiating stars similarly, causing the scatter in the mass loss effects. While the density of each cluster defines the effects of photoevaporation in the early evolutionary stages, after one crossing time the initial density of the region is not as important and photoevaporation works uniformly.

In Figure 3.7 we show the time step of maximum mass loss for each disc. It can be seen that, other than the effect of switching on the simulation at the beginning (see section 3.4.2), there is not a particular time at which a disc loses much mass. In Figure 3.8 we show how the cumulative distributions of disc masses at different moments in the simulation. The solid lines correspond to ρ_{100} the dashed lines to ρ_{50} . Each line corresponds to the total discs in all simulations. It can be seen that disc mass distributions decrease monotonically.

It is important to note that the FRIED grid has a lower limit of $10 G_0$ for the FUV field, which is higher than the minimum experienced in the ρ_{50} region. However, more than 90% of the stars in these simulations are within the limits of the grid at all times. In the few cases where stars were outside the limits of the grid, the mass loss obtained reflects a lower bound defined by the grid, but this does not affect our results.

Photoevaporation mass loss can have different effects over the gas and dust components

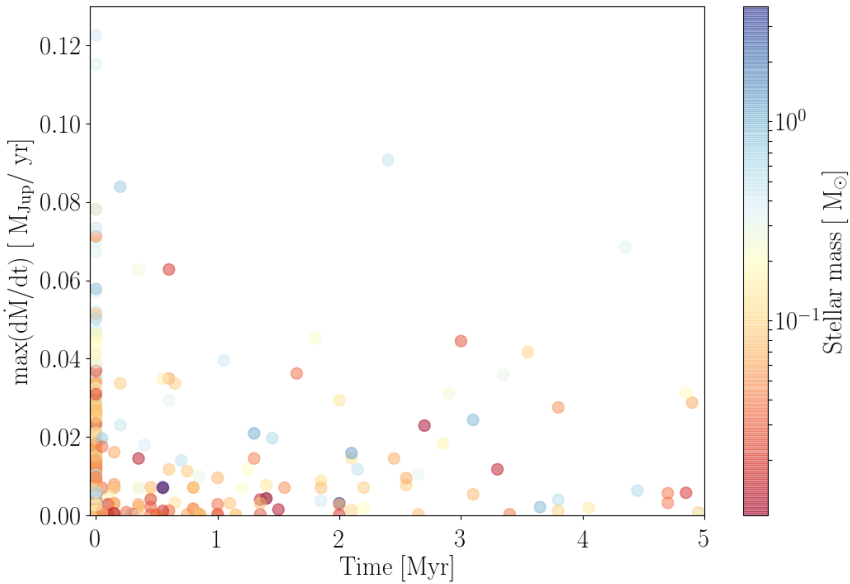


Figure 3.7: Maximum mass loss per time step for every disc. Each point corresponds to one disc in a simulation. The position of each point in time corresponds to its moment of maximum mass loss. This moment in time is not necessarily when the disc was dispersed.

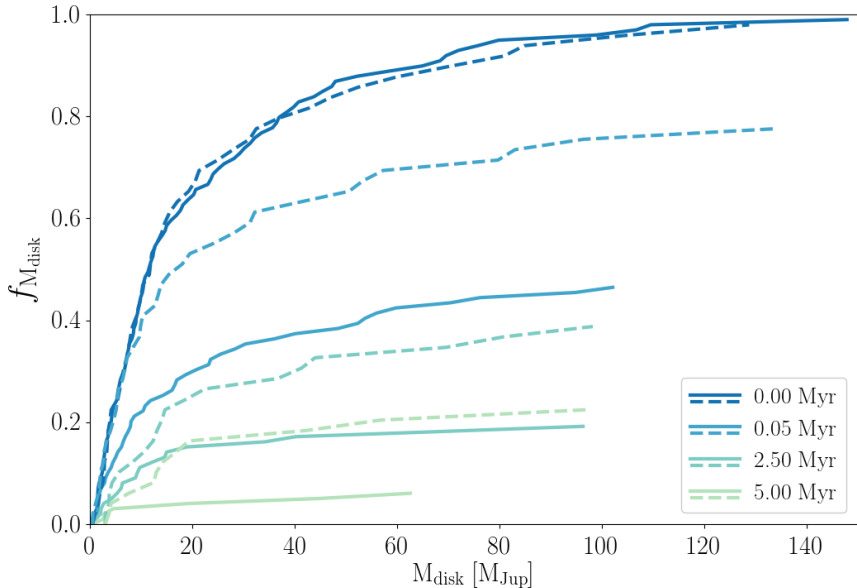


Figure 3.8: Cumulative distribution of disc masses at different simulation times. The solid lines correspond to the ρ_{100} region and the dashed lines correspond to the ρ_{50} region. Each curve shows the total number of discs in all simulations.

of a circumstellar disc. We expand on the consequences of this for our results in section 4.2.4

3.3.2. Disc lifetimes

The lifetime of circumstellar discs in young cluster regions is an important criterion to determine how photoevaporation affects planet formation. In Figure 3.9 we show disc fractions at different times of cluster evolution (black lines), together with observed disc fractions from Ribas et al. (2014) and Richert et al. (2018). The orange line shows the mean of the observations, calculated using a moving bin spanning 10 observation points. The calculation of the mean starts by binning the first 10 points, and then sliding horizontally through the observations one point at a time such that 10 points are always considered.

The relaxation time is defined as:

$$t_{\text{relax}} = 0.138 \frac{N}{\log(\gamma N)} t_{\text{dyn}} \quad (3.10)$$

(Spitzer 1988), where N is the number of stars, $\gamma = 0.4$, and the dynamical time is:

$$t_{\text{dyn}} = \sqrt{\frac{R^3}{GM}}, \quad (3.11)$$

where R is the radius of the cluster and M is its total mass. The relaxation time depends on the number of stars and the radius and mass of the stellar cluster. These are values that change through the dynamical evolution of a cluster, meaning that the relaxation time can grow and shrink at different time steps. These variations result in the jagged lines in Figure 3.9.

For the simulations shown in Figure 3.9 $t/t_{\text{relax}} = 0.5$ is reached at $t = 2.01 \pm 0.37$ Myr of evolution for ρ_{100} and at $t = 2.05 \pm 0.35$ Myr for ρ_{50} . Disc fractions in the ρ_{100} simulations drop to around 20% before 2 Myr of cluster evolution. In the regions with ρ_{50} the discs survive longer, but still most of the discs have disappeared by the end of the simulations.

Planet formation could still occur in discs that have been affected by photoevaporation as long as they are not completely dispersed. For gas giant cores and rocky planets to form, protoplanetary discs need to have a reservoir of dust mass $M_{\text{dust}} \gtrsim 10M_{\oplus}$ (Ansdell et al. 2018). In Figure 3.10 we show the fraction of discs with solid masses $M_{\text{disc}} > 10M_{\oplus}$ in time, for both simulated stellar densities. We use a 1:100 dust:gas mass ratio to turn the total disc mass into dust mass. For the ρ_{100} regions the number of discs that fulfil this mass requirement drops to around 20% at 1 Myr, with less than 10% of discs of said mass still present at the end of the simulations. For the less dense regions, at the end of the simulations around 20% of discs with masses $M_{\text{disc}} > 10M_{\oplus}$ survive.

In order to make a parallel with the Solar System, in Figure 3.11 we show the number of discs in time with radii higher than 50 au, for both density regions. The drop in disc sizes is slower than the drop in disc masses as seen in Figure 3.10 and in the ρ_{50} case the fraction of discs with radius > 50 au increases in the first time steps. This is related to the fact that, while some low mass discs get destroyed, others discs are still expanding due to viscous evolution. Some of these $R_{\text{disc}} > 50$ au discs could still have masses or surface densities that are too low to form a planetary system.

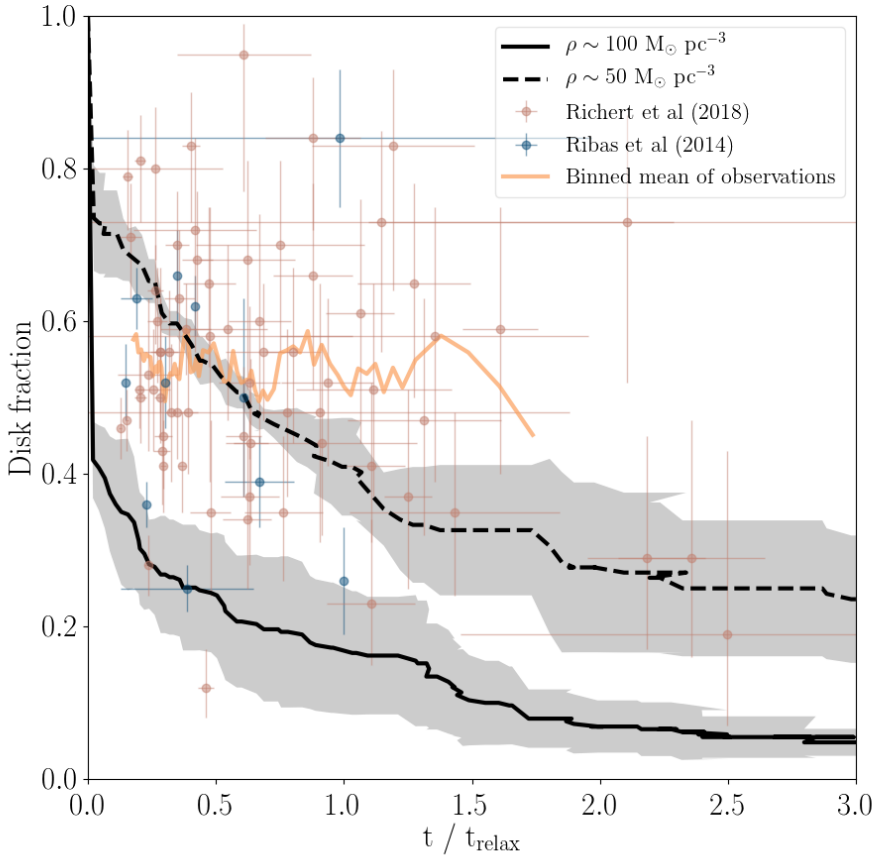


Figure 3.9: Fraction of stars with discs as a function of time. The solid black line shows the results for ρ_{100} and the dashed black line for ρ_{50} . The grey shaded areas indicate the standard deviation of the simulations. Observed disc fractions in star forming regions of different ages are shown for comparison. The orange line shows the mean of the observations, calculated using a moving bin spanning 10 observation points.

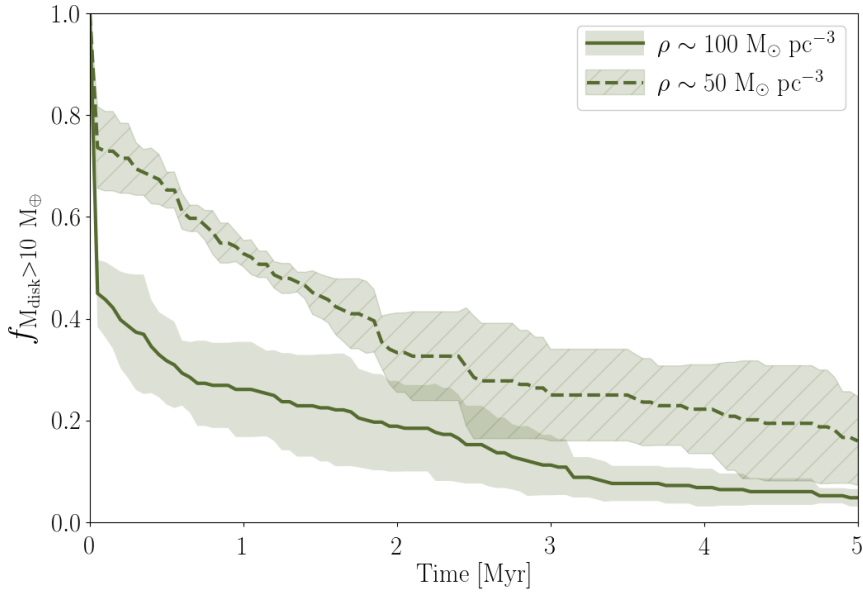


Figure 3.10: Fraction of discs with masses $M_{disc} > 10 M_{\oplus}$ in time, for regions of different stellar densities. The shaded areas indicate the standard deviation of the simulations.

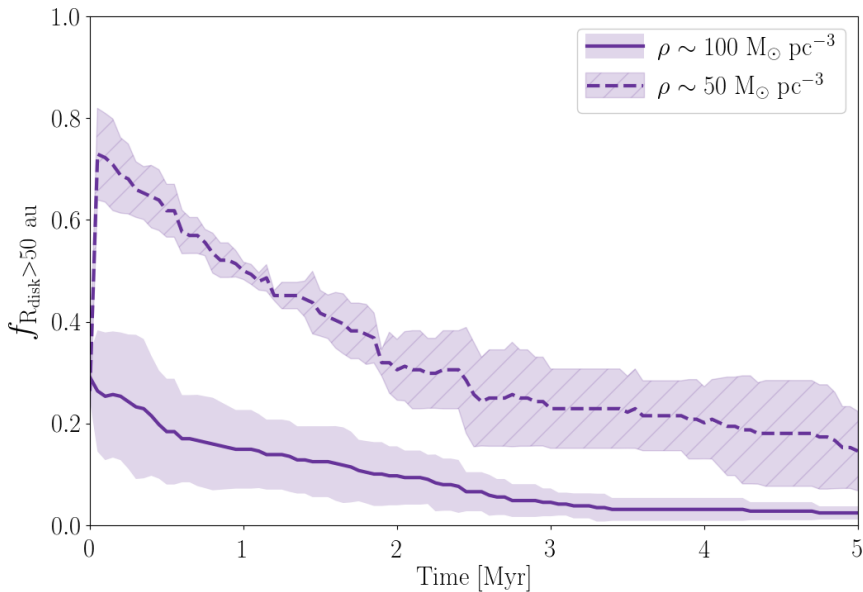


Figure 3.11: Fraction of discs with radius $R_{disk} > 50 au$ in time, for regions of different stellar densities. The shaded areas indicate the standard deviation of the simulations.

3.4. Discussion

3.4.1. Disc survival and consequences for planet formation

The results of the simulations carried out in this work characterize external photoevaporation as an important mechanism for disc dispersion. In comparison, the effect of dynamical truncations is negligible as a means for disc destruction.

The mean radiation received by the stars in our simulations fluctuates around $\sim 500 \text{ G}_0$ for the ρ_{100} region and around $\sim 50 \text{ G}_0$ for the ρ_{50} region. The FUV flux in the ONC is estimated to be $\sim 3 \times 10^4 \text{ G}_0$ [O'dell & Wen 1994]. Kim et al. (2016) estimate $\sim 3,000 \text{ G}_0$ around a B star in NGC 1977, a region close to the ONC. According to this and to our results, most of the discs in such a dense region would be destroyed before reaching 1 Myr of age. Figure 3.9 also agrees with results by Facchini et al. (2016) and Haworth et al. (2017), which show that photoevaporation mass loss can be important even for regions with $\sim 30 \text{ G}_0$ and $\sim 4 \text{ G}_0$, respectively. In particular, our results for the ρ_{50} region show that even very low FUV fields can be effective in dispersing circumstellar discs over time. Winter et al. (2020b) find similar dispersion timescales, with a median of 2.3 Myr in the solar neighbourhood and 0.5 Myr in the central regions of the Milky Way, for stars down to $0.8M_\odot$. Comparable results are obtained by Nicholson et al. (2019), who find the half life of protoplanetary discs to be around 2 – 3 Myr in clusters of various initial conditions.

Protoplanetary discs need to have a reservoir of dust mass $M_{dust} \gtrsim 10M_\oplus$ to be able to form the rocky cores of giant gas planets (Ansdell et al. 2018). Manara et al. (2018) show that such cores need to be already in place at ages $\sim 1 - 3$ Myr for this type of planets to form. Figure 3.10 is in agreement with these conclusions. In our simulations, by 1 Myr around 20% of the discs have masses $\gtrsim 10M_\oplus$. This number drops to $\sim 10\%$ by 3 Myr. According to our results rocky planets and gas giant cores must form very early on, otherwise the protoplanetary discs are not massive enough to provide the necessary amount of solids. This is in agreement with observational time constraints for planet formation and with the so-called “missing-mass” problem: solids mass measurements in protoplanetary discs are lower than the observed amount of heavy elements in extrasolar planetary systems around the same type of stars (see e.g. Manara et al. 2018, Najita & Kenyon 2014, Williams 2012, Greaves & Rice 2010, for discussions on this topic). Two scenarios have been proposed to explain this discrepancy in disc and exoplanet masses. The first one suggests that planet cores emerge within the first Myr of disc evolution, or even during the embedded phase while the disc is still being formed (e.g. Williams 2012, Greaves & Rice 2010). The second scenario proposes that discs can work as conveyor belts, transporting material from the surrounding interstellar medium towards the central star (e.g. Throop & Bally 2008, Kuffmeier et al. 2017).

Disc dispersal is not homogeneous across stellar types. There are observational indications that disc dispersion timescales depend on the mass of the host star, and that less massive ($\sim 0.1 - 1.2 M_\odot$) stars keep their discs for longer than massive stars (Carpenter et al. 2006, 2009, Luhman & Mamajek 2012). We do not see this effect in our simulations, where the most massive stars keep their discs for longer simply because they initially have the most massive discs. The same effect is observed in Winter et al. (2020b), who used an analytic approach to estimate protoplanetary disc dispersal time scales by external photoevaporation. The discrepancy between observations and theoretical results suggests that internal processes not considered in this work can also play an important role in disc dispersal. Radial drift of dust, fragmentation of large grains, and planetesimal formation are observed mechanisms that can affect both disc lifetimes and observed disc sizes. Viscous evolution alone is another internal process that can contribute to disc dispersal. A more complete model of disc evolution is needed to include the interplay between internal and external dispersion processes.

Initial disc masses are currently highly uncertain. Our chosen value of $M_d(t = 0) = 0.1M_*$ is arbitrary, but discs of higher masses could still be stably supported (Haworth et al. 2018a; Nixon et al. 2018).

Once a planetary system has formed, its survival inside a star cluster is not guaranteed. Of the 4071 exoplanets confirmed to date, only 30 have been found inside star clusters. Cai et al. (2019) performed simulations of planetary systems in dense, young massive star clusters. They found that the survival rate is $< 50\%$ for planetary systems with eccentricities $e \sim 0.05$ and semi-major axes < 20 au over 100 Myr of evolution. van Elteren et al. (2019) find that, in regions such as the Trapezium cluster, $\sim 30\%$ of planetary systems are affected by the influence of other stars. Their fractal initial conditions provide local regions of higher densities, which are more favourable for dynamical encounters than our initial conditions. When making parallels with currently observed exoplanet systems, it is important not only to consider the environment effects on the early protoplanetary discs, but also on the planets themselves once they are already formed.

Observations suggest that planets are able to circumvent all of these adversary processes and still form in highly unlikely regions. Evidence of star formation and even proplyd-like objects have been observed around Sgr A* (Yusef-Zadeh et al. 2015, 2017). Free-floating planets have been observed in the galactic center, and efficiency analyses of these detections suggest that there are many more yet to be observed (e.g. Ryu et al. 2020; Navarro et al. 2020).

3.4.2. Influence of initial conditions

The effect of switching on photoevaporation when our simulations start have dramatic consequences for the initial circumstellar discs. Mass loss due to photoevaporation occurs very quickly once the stars are immersed in the FUV field. Around 60% and 20% of the discs are dispersed within the initial 50.000 yr in the ρ_{100} and ρ_{50} regions, respectively. The mean mass of the host stars whose discs dispersed in the initial 50.000 yr is $0.17 \pm 0.03M_\odot$ for the ρ_{100} region and $0.14 \pm 0.04M_\odot$ for the ρ_{50} region. In Figure 3.12 we show the disc fractions in time, separately for stars with masses $M_* < 0.5M_\odot$ and $M_* \geq 0.5M_\odot$. It can be seen that, for the stars of masses $M_* < 0.5M_\odot$, the disc fractions drop much more dramatically during the first thousand years of cluster evolution.

In reality, if circumstellar discs do form around such low mass stars, they could be sheltered from photoevaporation by interstellar gas and dust, which can linger for several million years after star formation (Portegies Zwart et al. 2010). Models of the Cygnus OB2 region by Winter et al. (2019a) demonstrate that the extinction of FUV photons through the gas dampens the mass loss of the discs, increasing their lifetimes. They show that Cygnus OB2 probably underwent a primordial gas expulsion process that ended ~ 0.5 Myr ago. This is based on the fact that 0.5 Myr of exposure to FUV fields reproduces the observed disc fractions in the region. Given that the estimated age of Cygnus OB2 is 3 – 5 Myr (Wright et al. 2010) the primordial gas in the region insulated the discs from external photoevaporation for several Myr. A similar point is made by Clarke (2007), who propose that the FUV field of the star θ_1 Orionis C must have been “switched on” no more than 1 – 2 Myr ago to explain the disc size distribution observed around it. This switching on could have been caused by the star clearing out the primordial gas it was embedded in, thus reducing extinction around it and making its effective radiation field stronger (Ali & Harries 2019). The presence of gas in young star clusters could then protect the protoplanetary discs and make the disc fraction drop more smoothly than what is shown in Figure 3.9.

The observations shown in Figure 3.9 span clusters of many different ages and densities. Our simulation results show that one order of magnitude difference in initial cluster

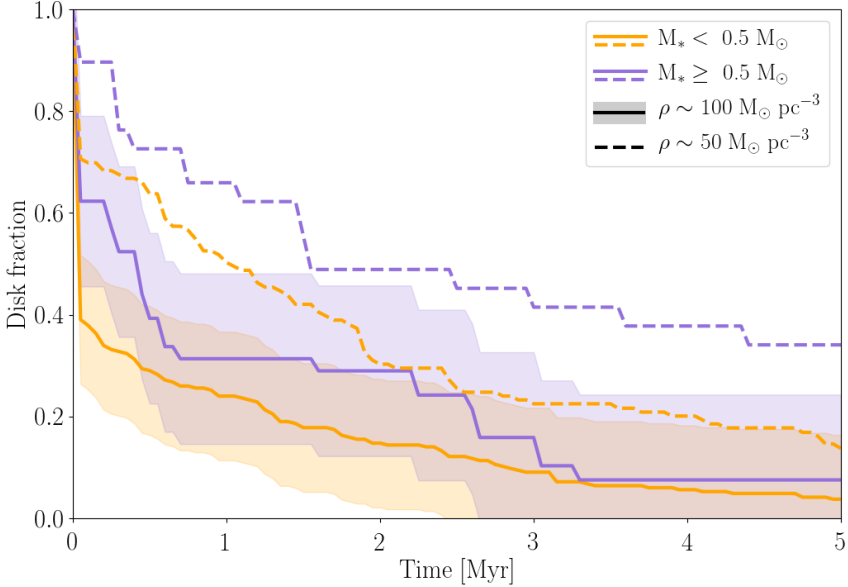


Figure 3.12: Disc lifetimes for stars $M_* < 0.5M_\odot$ (orange) and $M_* \geq 0.5M_\odot$ (purple). The shaded areas indicate the standard deviation of the simulations. For clarity, only the standard deviation for ρ_{100} is shown, but the one for ρ_{50} is of similar magnitude.

density can yield an important difference in the number of surviving discs. A one order of magnitude spread in cluster density translates to a three order of magnitude difference in cluster radius. The extent of stellar densities in regions where circumstellar discs have been detected does not only reflect the environment of these regions, but also the variety in initial cluster densities.

The initial spatial distribution of the stars in the simulations also plays an important role during the early stages of disc evolution. The stars in our simulations were initially distributed in a Plummer sphere with a specified radius and in virial equilibrium. An approach with fractal or filamentary (e.g. Winter et al. 2019a) initial conditions could change the overall disc survival rates. If a massive star is born in a clump of a fractal distribution, for example, stars in other clumps without massive stars could be minorly affected by radiation and have higher chances of surviving and, eventually, making planets. Higher density regions also increase the relevance of dynamical truncations. This effect of initial conditions could also be counteracted by dynamical mass segregation, in which massive stars move towards the center of the cluster. This would increase the effect of photoevaporation in the central regions of the cluster.

3.4.3. Model caveats

There are several physical processes not considered in this work which could affect the results presented here. One big caveat of our model is the lack of separation between dust and gas components in circumstellar discs. These separate disc components evolve differently and are affected in distinctive ways by outside mechanisms such as the ones implemented in this work. Gas discs has been observed to be larger than dust discs by a factor of ~ 2 (Ansdel

et al. 2018). Whether this is caused by different evolution for gas and dust or observational optical depth effects is still up for debate (see e.g. Birnstiel & Andrews 2013; Facchini et al. 2017; Trapman et al. 2019 for discussions on the topic). The dust in protoplanetary discs is subject to radial drifting and radially dependent grain growth, which can make it resilient to photoevaporation. This can have direct implications on the photoevaporation mass loss rates (Facchini et al. 2016; Haworth et al. 2018a) and consequences on planet formation. The conclusions regarding planet formation timescales derived in this work only consider the life expectancy of the discs, but considering different dust and gas disc components will likely affect these results.

While photoevaporation is considered to be primarily damaging for discs when coming from external sources, under certain regimes the photons coming from the host star can also contribute to disc dispersal. Gorti et al. (2009) and Gorti & Hollenbach (2009) show that FUV photons from the host star can drive photoevaporation mass loss at disc radius $\sim 1 - 10$ au and $\gtrsim 30$ au. Owen et al. (2010) and Font et al. (2004) show that internal photoevaporation can also remove loosely bound material from the outer regions, however the largest mass loss was from the inner ~ 20 au region. Fatuzzo & Adams (2008) and Hollenbach et al. (2000) find that external photoevaporation dominates for disc regions > 10 au. The approach used in this work is valid for the disc truncation approximation, however, a more complete analysis would have to consider the combined action and interplay of external and internal photoevaporation.

Mass loss due to photoevaporation was modelled by calculating a truncation radius and removing all the mass outside it, while the inner region of the disc remained unperturbed. In reality, external FUV radiation can heat the whole surface of the disc, and mass loss can occur not just as a radial flow but also as a vertical flow from all over the disc (Adams et al. 2004). Given that the mass in the outer regions of a disc is more loosely bound to its host star, the truncation approach is a good first order approximation for mass loss. Furthermore, the FRIED grid used to estimate the photoevaporation mass loss was built using a 1-dimensional disc model. New simulations by Haworth & Clarke (2019) show that, when considering a 2-dimensional disc model, mass loss rates can increase up to a factor 3.7 for a solar mass star. The photoevaporation mass losses obtained in this work should then be considered as lower limits, but are still a good estimate of the effects of bright stars in the vicinity of circumstellar discs.

In the present work we did not include binary stars or any multiples. The presence of multiple stellar systems can have direct consequences on the dynamical evolution of the cluster and on the effects of photoevaporation over the discs. Discs around binary stars have been observed in the star forming regions ρ Ophiuchus (Cox et al. 2017) and Taurus-Auriga (Harris et al. 2012; Akeson & Jensen 2014; Akeson et al. 2019). Observations suggest that these discs are more compact and less bright than the ones around isolated stars. Discs around binary stars might also have shorter lifetimes, due to effects of the companion on the viscous timescale of the disc and also because of photoevaporation inside the system (Shadmehri et al. 2018; Rosotti & Clarke 2018).

Another process that can have important consequences in the evolution of circumstellar discs are supernovae explosions. Close & Pittard (2017) showed that nearby (0.3 pc) supernova explosions can cause mass loss rates of up to $1 \times 10^{-5} M_{\odot} \text{yr}^{-1}$ which can be sustained for about 200 yr. Only discs that are faced with the flow face-on manage to survive, but still lose 50% of their mass in the process. Portegies Zwart et al. (2018) show that a supernova explosion at a distance between 0.15 and 0.4 pc could create a misalignment of $\sim 5^\circ$ between the star and its disc, which is consistent with the inclination of the plane of the Solar System. Such an event would also truncate a disc at around the edge of the Kuiper belt

(42 – 55 au). Similar effects can be caused by other outcomes of stellar evolution, such as winds (Pelupessy & Portegies Zwart 2012).

3.5. Conclusions

We perform simulations of star clusters with stellar densities $\rho \sim 100 M_{\odot} pc^{-3}$ and $\rho \sim 50 M_{\odot} pc^{-3}$. The stars with masses $M_* \leq 1.9 M_{\odot}$ are surrounded by circumstellar discs. Stars with masses $M_* > 1.9 M_{\odot}$ are considered sufficiently massive stars to emit UV radiation, causing the discs around nearby stars to evaporate. The discs are subject to viscous growth, dynamical encounters, and external photoevaporation. The simulations span 5 Myr of cluster evolution. The main results of this work are:

1. In clusters with density $\rho \sim 100 M_{\odot} pc^{-3}$ around 80% of discs are destroyed by external photoevaporation within 2 Myr. The mean background FUV field is $\sim 500 G_0$.
2. In clusters with density $\rho \sim 50 M_{\odot} pc^{-3}$ around 50% of discs are destroyed by external photoevaporation within 2 Myr. The mean background FUV field is $\sim 50 G_0$. This shows that even very low FUV fields can be effective at destroying discs over long periods of time.
3. Mass loss caused by dynamical encounters is negligible compared to mass loss caused by external photoevaporation. Disc truncations that result from dynamical encounters are not an important process in setting observed disc size and mass distributions.
4. At 1 Myr, $\sim 20\%$ of discs in the $\rho \sim 100 M_{\odot} pc^{-3}$ region and $\sim 50\%$ of discs $\rho \sim 50 M_{\odot} pc^{-3}$ region have masses $M_{disc} \geq 10 M_{\oplus}$, the theoretical limit for gas giant core formation.
5. Our results support previous estimations that planet formation must start in timescales $< 0.1 - 1$ Myr (e.g. Najita & Kenyon 2014; Manara et al. 2018).
6. The obtained disc fractions in the different density regions, together with the quick dispersion of the discs in all the simulations, suggest that initial conditions are very important in the development of models of early protoplanetary disc evolution.

Acknowledgements

We would like to thank the anonymous referee for their thoughtful comments that helped improve this paper. We would also like to thank Andrew Winter, Sierk van Terwisga, and the protoplanetary disc group at Leiden Observatory for helpful discussions and comments. F.C.-R. would like to thank Valeriu Codreanu from SURFsara for his invaluable technical assistance. The simulations performed in this work were carried out in the Cartesius supercomputer, part of the Dutch national supercomputing facility SURFsara. This paper makes use of the packages numpy (Van Der Walt et al. 2011), scipy (Virtanen et al. 2019), matplotlib (Hunter 2007), and makecite (Price-Whelan et al. 2018).

3.A. Resolution of the discs

We use a resolution of 50 cells for the discs which gives us a good trade-off between computing time and acceptable results. In isolated disc evolution this causes an overestimation of disc radius by $\sim 10\%$ on average over 1 Myr of disc evolution, compared with higher

resolutions (Figure 3.13). Since all the discs in the simulation are affected by photoevaporation from the start, no discs evolve as in the isolated case. Disc masses are overestimated by less than $\sim 5\%$ compared to higher resolution runs (Figure 3.14). This results, in turn, in a slight underestimation of the effects that mass removal, whether through photoevaporation or dynamical encounters, has on the survival times of the discs. Given that we define a disc as dispersed when it has lost $\sim 90\%$ of its initial mass, the slight mass overestimate obtained with the 50 cells resolution does not reflect in a quicker evaporation of the discs.

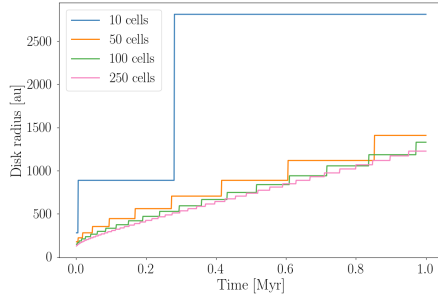


Figure 3.13: Disc radius in time for different resolutions, for a disc evolving in isolation for 1 Myr.

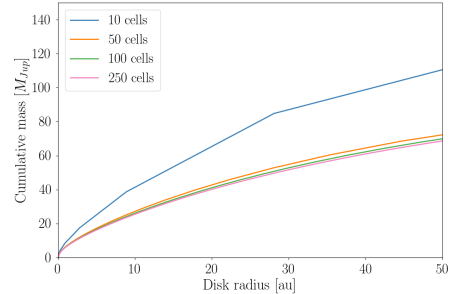


Figure 3.14: Cumulative disc mass for different resolutions, for a disc evolving in isolation for 1 Myr.

* * *

4

Effects of stellar density on the photoevaporation of circumstellar discs

F. Concha-Ramírez; M. J. C. Wilhelm;
S. Portegies Zwart; S. E. van Terwisga, A. Hacar
Monthly Notices of the Royal Astronomical Society
Volume 501, Issue 2, p.1782-1790 (2021)

CIRCUMSTELLAR discs are the precursors of planetary systems and develop shortly after their host star has formed. In their early stages these discs are immersed in an environment rich in gas and neighbouring stars, which can be hostile for their survival. There are several environmental processes that affect the evolution of circumstellar discs, and external photoevaporation is arguably one of the most important ones. Theoretical and observational evidence point to circumstellar discs losing mass quickly when in the vicinity of massive, bright stars. In this work we simulate circumstellar discs in clustered environments in a range of stellar densities, where the photoevaporation mass-loss process is resolved simultaneously with the stellar dynamics, stellar evolution, and the viscous evolution of the discs. Our results indicate that external photoevaporation is efficient in depleting disc masses and that the degree of its effect is related to stellar density. We find that a local stellar density lower than $100 \text{ stars pc}^{-2}$ is necessary for discs massive enough to form planets to survive for 2.0 Myr. There is an order of magnitude difference in the disc masses in regions of projected density $100 \text{ stars pc}^{-2}$ versus $10^4 \text{ stars pc}^{-2}$. We compare our results to observations of the Lupus clouds, the Orion Nebula Cluster, the Orion Molecular Cloud-2, Taurus, and NGC 2024, and find that the trends observed between region density and disc masses are similar to those in our simulations.



4.1. Introduction

Circumstellar discs are the reservoirs of gas and dust that surround young stars and have the potential to become planetary systems. Their evolution will determine the time and material available to form planets. Studying the evolution of circumstellar discs can then help us understand planet formation and the diversity of observed planetary systems.

These circumstellar discs develop almost immediately after star formation, as a direct consequence of the collapse of a molecular cloud and angular momentum conservation (Williams & Cieza 2011). Their surroundings are rich in gas and neighbouring stars, which can be hostile to the discs and affect their evolution in different ways. In environments with high stellar densities, dynamical encounters with nearby stars can truncate the discs (e.g. Pfalzner et al. 2006; Vincke et al. 2015; Portegies Zwart 2016; Bhandare & Pfalzner 2019). Face-on accretion of gas onto the circumstellar discs can cause them to shrink and increase their surface densities (e.g. Wijnen et al. 2016, 2017a). Feedback from processes related to stellar evolution, such as stellar winds and supernovae explosions, can also truncate, tilt, or completely destroy the discs (Pelupessy & Portegies Zwart 2012; Close & Pittard 2017; Portegies Zwart et al. 2018). The presence of bright, massive stars in the vicinity of circumstellar discs can heat their surface enough to evaporate mass from them. This process, known as external photoevaporation, is arguably one of the most important environmental mechanisms in depleting mass from young circumstellar discs, and its effects seem to greatly outperform that of other means for disc truncation (e.g. Hollenbach et al. 2000; Adams et al. 2004; Guarcello et al. 2016; Facchini et al. 2016; Winter et al. 2018b; Haworth & Clarke 2019; Winter et al. 2020b; Haworth & Owen 2020).

The effects of external photoevaporation have been identified in observational surveys of young stellar objects in star-forming regions. Proplyds –cometary tail-like structures formed by ionized, evaporating discs– have been observed in particular in dense regions of the Orion nebula (O’Neill & Wen 1994; O’Neill 1998; Vicente & Alves 2005; Eisner & Carpenter 2006; Mann et al. 2014; Kim et al. 2016). Surveys of protoplanetary discs in star-forming regions show that discs closer to bright stars are less massive than their counterparts in sparser regions (Fang et al. 2012; Mann & Williams 2009; Mann et al. 2014; Ansdell et al. 2017; van Terwisga et al. 2020), suggesting that discs in the vicinity of these stars are strongly affected by their environment. Disc fractions (the number of young stellar objects around which dust is detected, over the total number of objects) and disc mass distributions in younger and less dense star-forming regions, such as Lupus and Taurus, are statistically indistinguishable from each other in terms of disc mass distributions. The average disc mass in these regions is higher than in the Orion Nebula Cluster (ONC) (Ansdell et al. 2016; Eisner et al. 2008, 2018; van Terwisga et al. 2019), which is a much denser environment.

The extent of the effects of radiation in depleting disc mass depends on the proximity to bright stars. As such, the effects of external photoevaporation are important in clustered environments, and different theoretical models have been developed to study the process in that context. Scally & Clarke (2001) model the dynamics of a cluster with 4,000 stars, with discs of radii 100 au which remain constant throughout the simulation. The mass loss due to photoevaporation is calculated in post processing, by keeping track of the radiation to which each star is exposed during the simulation. Their results show that external photoevaporation is important in depleting disc mass in regions similar to the centre of the ONC. A different approach is taken by Adams et al. (2006) and Fatuzzo & Adams (2008), who model the dynamics of star clusters of different sizes and derive the background FUV radiation for each simulation. They then estimate the photoevaporation mass loss rates of the discs depending on the average background radiation that they have been exposed to. Adams et al.

(2006) model star clusters with 100, 300, and 1,000 stars and find that external photoevaporation is only important for disc radii larger than 30 au, due to the low average background UV exposure. Furthermore, models of single, externally illuminated discs show that the supersonic flows caused by far-ultraviolet (FUV) photons heating the disc surface can explain the observed proplyd shapes (e.g. Richling & Yorke (1997); Johnstone et al. (1998); Störzer & Hollenbach (1999); Adams et al. (2004)).

In more recent work, Winter et al. (2018b) and Winter et al. (2020a) use a statistical approach to model background FUV radiation fields in regions of different stellar number density. Winter et al. (2020a) find that 90% of circumstellar discs are destroyed by external photoevaporation within 1.0 Myr in a region comparable to the Central Molecular Zone of the Milky Way, and that the effects of photoevaporation are particularly destructive for discs around low mass stars ($M_* < 0.3M_\odot$). For regions similar to the solar neighbourhood (surface density $\Sigma_0 = 12 M_\odot \text{ pc}^{-2}$) they find a mean dispersal timescale of ~ 3.0 Myr. Similar results are obtained by Nicholson et al. (2019), who calculate mass loss rates in N-body simulations using the same prescriptions as Scally & Clarke (2001) and find that, in regions with high degree of substructure (density $\sim 100 M_\odot \text{ pc}^{-3}$), 50% of the discs with initial radii ≥ 100 au are destroyed by external photoevaporation within 1 Myr. In regions of lower densities ($\sim 10 M_\odot \text{ pc}^{-3}$), half of the discs are destroyed within 2 Myr.

In Concha-Ramírez et al. (2019b) (hereafter Paper I) we presented a new numerical implementation which allows for self-contained simulations of external photoevaporation in clustered environments. Photoevaporation process is solved simultaneously with the stellar dynamics (including disc encounters and truncations), stellar evolution, and viscous spreading of the circumstellar discs. This causes disc masses, sizes, and column densities to vary in time, and the mass loss rate of the discs is calculated accordingly. The results of the simulations in Paper I show that external photoevaporation is efficient in destroying circumstellar discs on a relatively short timescale. For regions of stellar densities $\sim 100 M_\odot \text{ pc}^{-3}$, around 80% of discs have evaporated within 2.0 Myr. Between 25% and 60% of the discs, depending on region density, are destroyed within the first 0.1 Myr. We argue that the rapid decrease in disc mass is dominated by external photoevaporation, rather than dynamical truncations, and that the former mechanism constrains the time available for planet formation.

Observational and theoretical evidence suggest that the local stellar density is a key factor in the survival of circumstellar discs and in their eventual observed mass distributions. Understanding disc mass and size distributions in young star clusters is therefore paramount for understanding planet formation and evolution. Here we use the model developed in Paper I to determine for which range of stellar densities the effects of photoevaporation are most efficient. We perform simulations of circumstellar discs embedded in star clusters and explore a parameter space of stellar densities spanning five orders of magnitude. The clusters are evolved for 2.0 Myr and we investigate the final mass distributions of the disc population. We compare our simulation results to observed dust masses of young stellar objects in the Lupus clouds (Ansdell et al. (2016, 2018)), the Orion Nebula Cluster (Mann et al. (2014); Eisner et al. (2018)), the Orion Molecular Cloud-2 (van Terwisga et al. (2019)), the Taurus region (Andrews et al. (2013)), and NGC 2024 (Getman et al. (2014); van Terwisga et al. (2020)).

4.2. Model

We use the Astrophysical Multipurpose Software Environment, AMUSE¹ (Portegies Zwart et al. (2009, 2013)), to bring together codes for viscous disc evolution, stellar dynamics, and

¹<http://amusecode.github.io>

stellar evolution, along with an implementation of external photoevaporation. The setup and models used for the simulations in this paper are the same as in Paper I. In the present work we perform simulations spanning a larger range of stellar densities.

Here we present a summary of the implementation used for the simulations. For a detailed explanation of the model the reader should refer to Paper I. All the code developed for the simulations, data analyses, and figures of this paper is available online².

4.2.1. Stars and circumstellar discs

We separate the stars in the simulations into two populations: stars with masses $M_* \leq 1.9 M_\odot$, and stars with masses $M_* > 1.9 M_\odot$. The reason for this mass limit is related to the photoevaporation mass loss calculation and further explained in section 4.2.2. This mass separation is for photoevaporation purposes only and does not influence the dynamical evolution of the stars. All stars with masses $M_* \leq 1.9 M_\odot$ are surrounded by a circumstellar disc, while stars with higher masses have no discs and are considered only as generating ionizing radiation. Massive stars are subject to stellar evolution, implemented using the code SeBa (Portegies Zwart & Verbunt 1996; Toonen et al. 2012) through its AMUSE interface. Stars with discs do not undergo stellar evolution in the simulations. The dynamical evolution of the clusters is implemented using the 4th-order N-body code ph4, incorporated in AMUSE.

Circumstellar discs are implemented using the Viscous Accretion disc Evolution Resource (VADER) developed by Krumholz & Forbes (2015). VADER models mass and angular momentum transport on a thin, axisymmetric disc. This allows us to take into consideration the viscous spreading of the discs. Each VADER disc in our simulations is composed of a grid of 100 logarithmically spaced cells between 0.05 and 2.000 au. The discs have a turbulence parameter of $\alpha = 5 \times 10^{-3}$.

The initial disc column density follows the standard disc profile by Lynden-Bell & Pringle (1974), with characteristic radius $r_c \approx r_d$ (Anderson et al. 2013). To properly calculate the photoevaporation mass loss rate we need to keep track of the outer disc edge (see section 4.2.2) which we define as the cell closest to a low column density value, Σ_{edge} (Clarke 2007; Haworth et al. 2018a). We set the column density outside r_d to a negligible value $\Sigma_{\text{edge}} = 10^{-12} \text{ g cm}^{-2}$. The initial surface density then takes the form:

$$\Sigma(r, t=0) = \begin{cases} \frac{m_d}{2\pi r_d(1-e^{-1})} \frac{\exp(-r/r_d)}{r} & \text{for } r \leq r_d, \\ 10^{-12} \text{ g cm}^{-2} & \text{for } r > r_d, \end{cases} \quad (4.1)$$

where r_d and m_d are the initial radius and mass of the disc, respectively.

4.2.2. External photoevaporation

External photoevaporation is dominated by far-ultraviolet (FUV) photons (Armitage 2000; Adams et al. 2004; Gorti & Hollenbach 2009). To model the FUV radiation from the massive stars we pre-compute a relation between stellar mass and FUV luminosity using the UVBLUE spectral library (Rodriguez-Merino et al. 2005). The obtained FUV luminosity fit is shown in Figure 2 of Paper I. During the simulations we use this fit to obtain the FUV luminosity of each massive star at every time step.

Mass loss due to external photoevaporation is calculated for each disc using the Far-ultraviolet Radiation Induced Evaporation of Discs (FRIED) grid (Haworth et al. 2018b). The

²<https://doi.org/10.5281/zenodo.3897171>

FRIED grid provides a set of pre-calculated, external photoevaporation mass loss rates for discs immersed in radiation fields of varying intensity, from $10 G_0$ to $10^4 G_0$. The grid spans discs of mass $\sim 10^{-4} M_{\text{Jup}}$ to $10^2 M_{\text{Jup}}$, radius from 1 au to 400 au, and host star mass from $0.05 M_{\odot}$ to $1.9 M_{\odot}$. To stay within the limits of the grid, we give all stars with masses $M_* \leq 1.9 M_{\odot}$ a circumstellar disc, and all stars with masses $M_* > 1.9 M_{\odot}$ are considered as only generating radiation.

We calculate the mass loss of every disc as follows. For each disc we begin by calculating its distance to every star of mass $M_* > 1.9 M_{\odot}$ and determining the total radiation that the disc receives from those stars. We do not consider extinction in this calculation. We then use this total radiation and the disc parameters to interpolate a mass loss rate \dot{M} from the FRIED grid. This \dot{M} is then used to calculate the total mass lost by the disc in the current time step. Assuming a constant mass loss rate over the time step, the mass is removed from the outer regions of the disc: we advance over the disc cells starting from the outside removing mass from each, until the corresponding amount of mass has been removed. Through this process, mass loss due to photoevaporation results in a decrease of disc mass and disc radius.

In some cases a massive star gets close enough to a disc to enter a photoevaporation regime dominated by extreme ultraviolet (EUV) radiation. In this regime the mass loss is calculated as [Johnstone et al. (1998)]:

$$\dot{M}_{\text{EUV}} = 2.0 \times 10^{-9} \frac{(1+x)^2}{x} \epsilon r_{d,14} M_{\odot} \text{ yr}^{-1} \quad (4.2)$$

with $x \approx 1.5$ and $\epsilon \approx 3$.

We consider a disc dispersed when its mass drops below $0.03 M_{\oplus}$, based on the non-detection mass limits from [Ansdel et al. (2016)], or when its mean column density is lower than 1 g cm^{-2} [Pascucci et al. (2016)] (see also Section 4.2.4).

4.2.3. Initial conditions

Star clusters

We simulate clusters with 10^3 stars and initial virial radii of 0.1, 0.3, 0.5, 1.0, 2.5, and 5.0 pc. Stars are initially distributed in a Plummer sphere (Plummer (1911)). Stellar masses are drawn from a random Kroupa mass distribution (Kroupa (2001)) with upper limit $100 M_{\odot}$. All models start in virial equilibrium (virial ratio $Q = 0.5$). No primordial mass segregation, binaries, or higher multiplicity systems are considered.

In Table 4.1 we present the models used for this work. The mean number of stars with discs in each simulation is 974.7 ± 1.7 . The mean mass of the stars with discs is $0.23^{+1.66}_{-0.22} M_{\odot}$. The mean number of stars generating UV radiation is 25.3 ± 1.7 . The third column of Table 4.1 shows the mass ranges spanned by these stars.

We evolve each cluster for 2.0 Myr. We run each model 6 times, with a different random seed for the mass function and the initial stellar positions and velocities.

Circumstellar discs

Observations of resolved circumstellar discs suggest they are generally compact, with radii around 20 to 50 au (Trapman et al. (2020); Tobin et al. (2020)). The initial radii of the discs in our simulations are given by:

$$r_d(t=0) = R' \left(\frac{M_*}{M_{\odot}} \right)^{0.5}, \quad (4.3)$$

| Model name | R_{vir} [pc] | $\bar{M}_{M_* > 1.9M_\odot}$ [M_\odot] | \bar{N}_{*B} | \bar{N}_{*O} |
|------------|-----------------------|--|----------------|----------------|
| R0.1 | 0.1 | $6.61^{+57.18}_{-7.57}$ | 23.5 ± 1.1 | 2.2 ± 1.1 |
| R0.3 | 0.3 | $6.62^{+81.98}_{-7.07}$ | 22.5 ± 2.8 | 2.5 ± 0.5 |
| R0.5 | 0.5 | $5.22^{+53.54}_{-4.41}$ | 25.1 ± 2.5 | 1.8 ± 1.1 |
| R1.0 | 1.0 | $5.61^{+41.72}_{-5.56}$ | 22.0 ± 3.0 | 1.8 ± 0.1 |
| R2.5 | 2.5 | $5.94^{+46.09}_{-5.06}$ | 23.8 ± 7.8 | 1.8 ± 1.2 |
| R5.0 | 5.0 | $6.37^{+76.43}_{-5.24}$ | 25.2 ± 4.3 | 2.5 ± 1.5 |

Table 4.1: Simulation models. First column: model name. Second column: initial virial radius, in parsec. Third column: mean mass of radiating stars ($M_* > 1.9M_\odot$), in M_\odot . Fourth column: mean number of B type stars. Fifth column: mean number of O type stars. All means are calculated over 6 runs for each model.

where R' is a constant. We choose $R' = 30$ au, which yields an initial disc radii distribution between ~ 5 au and ~ 40 au. Initial discs masses are defined as 10% of the mass of their host star.

4.2.4. Model caveats

Our model is designed as a controlled experiment to investigate the physical processes going on inside star-forming regions, in particular with regards to external photoevaporation. There are quite a number of assumptions in our simulations which we justify based on previous theoretical work and observations. Below we discuss some of these processes and parameters and the implications they might have.

Star-forming regions are not only rich in stars but also in gas, which can linger for several million years (Portegies Zwart et al. 2010). Intracluster gas could influence our results in two main ways: first, the presence of gas and its subsequent expulsion in time affect the virial equilibrium and thus the dynamics of the star clusters. Second, gas can absorb some of the FUV radiation coming from bright stars, effectively protecting the discs from external photoevaporation and allowing them to live for longer (Winter et al. 2019b; Ali & Harries 2019; van Terwisga et al. 2020), therefore giving more time for the planet formation process to occur. The presence of gas can also explain the ‘proplyd lifetime problem’ observed in the ONC, in which discs not massive enough to survive in the environment of $\theta^1 C$ Ori are still observed in the region (Winter et al. 2019b).

The FRIED grid was constructed using a 1-dimensional disc model, but later simulations by Haworth & Clarke (2019) show that mass loss rates can increase up to a factor of 3.7 when considering 2-dimensional discs. It is likely then that the mass losses used in this work are only a lower limit for the effects of external photoevaporation.

Internal photoevaporation, the process in which X-Ray and UV photons coming from the host star itself lead to mass loss, is not considered in these simulations. Internal photoevaporation can drive mass loss in the inner regions of the discs ($\sim 1 - 10$ au and 30 au, Gorti et al. 2009; Gorti & Hollenbach 2009) and even in outer regions under certain conditions (Owen et al. 2010; Font et al. 2004). However, external photoevaporation is arguably the dominant process in regions > 10 au (Hollenbach et al. 2000; Fatuzzo & Adams 2008). Our approximation of external photoevaporation removing mass from the outer regions of the disc only is

also idealized, since while internal photoevaporation seems to clear the disc at specific radii, FUV photons coming from external sources can heat and evaporate mass from the whole disc surface (Adams et al. 2004).

Our conditions for disc dispersal might be overestimating the number of destroyed discs, particularly for relatively high mass stars. In some cases, a disc of density 1 g cm^{-2} or lower can still be detectable with modern instruments. As the mean mass of stars with discs in our simulations is 0.23 M_\odot (corresponding to an initial disc mass of $24 \text{ M}_{\text{Jup}}$), and as most of the massive discs in our simulations survive until the end (see section 4.3.1), we consider this possible underestimation of surviving discs to be within the uncertainty of our simulations and to not affect our results.

Our prescription of the EUV mass loss rate (Eq. 5.4) is taken from Johnstone et al. (1998) and corresponds to a thick photodissociation region (PDR). In practice, in EUV dominated fluxes the PDR is expected to be thin. This can change the value of the EUV mass loss rate \dot{M}_{EUV} calculated in each time step. However, since our focus is on FUV photoevaporation, and since discs are only in the EUV regimes for a short time in our simulation, this hardly affects our mass loss rate calculations.

Regarding disc masses, it is generally accepted that a 100:1 gas-to-dust mass ratio defines the composition of circumstellar discs. However, several authors have pointed out that this value might change across discs and in time (Williams & Best 2014; Manara et al. 2020). This can lead to observed disc dust masses being greatly underestimated (Manara et al. 2018). New models of externally irradiated, evaporating discs by Haworth et al. (2018a) show that considering grain growth can lead to less dust being lost through external photoevaporation, and thus to the dust:gas ratio increasing in time. A more careful implementation of the separate dust and gas components in a disc can help to overcome this problem.

The distribution of stars in a Plummer sphere is an idealized geometry. Star-forming regions have complex configurations and can present fractal structures, filaments, and other regions of increased surface density (e.g. Scalo 1990; Elmegreen & Falgarone 1996; Elmegreen et al. 2000; Bate 2010; Hacar et al. 2013; Chevance et al. 2020; Krause et al. 2020). The simulations carried out for this work represent only local densities, but for improved analyses of disc survival in star-forming regions it is important to consider different spatial distributions.

4.3. Results

To illustrate the evolution of our model in time for individual discs, in Figure 4.1 we show the evolution of several stars and their corresponding circumstellar discs. These particular tracks are taken from one of the realisations of model R1.0 (see Table 4.1). We show seven stars with discs as they move through the cluster. Black crosses mark the position of each star at the beginning of the simulation, and the label next to each shows the mass of the star. The sizes of the coloured circles in the stellar tracks are proportional to the disc radii, and their colour indicates the total disc mass. Red crosses, where present, show the moment when the disc is dispersed. The black thin lines that follow a red cross indicate the continuation of the orbit of the star, which keeps moving through the cluster after its disc has been evaporated. The trajectories of some massive, radiating stars are shown in thin blue lines. The solid and dashed circles in the background show the core radius and half mass radius of the cluster, respectively, at $t = 0.0 \text{ Myr}$. A disc around a 0.37 M_\odot star survives all through the simulation, however, the variations of its radius in time due to photoevaporation and viscous expansion can be seen. A 0.14 M_\odot star initially near the centre keeps its disc until around halfway through the simulation. A very low mass star, 0.06 M_\odot , loses its disc very quickly even if located in the periphery of the cluster. While our simulations are three-dimensional, in this

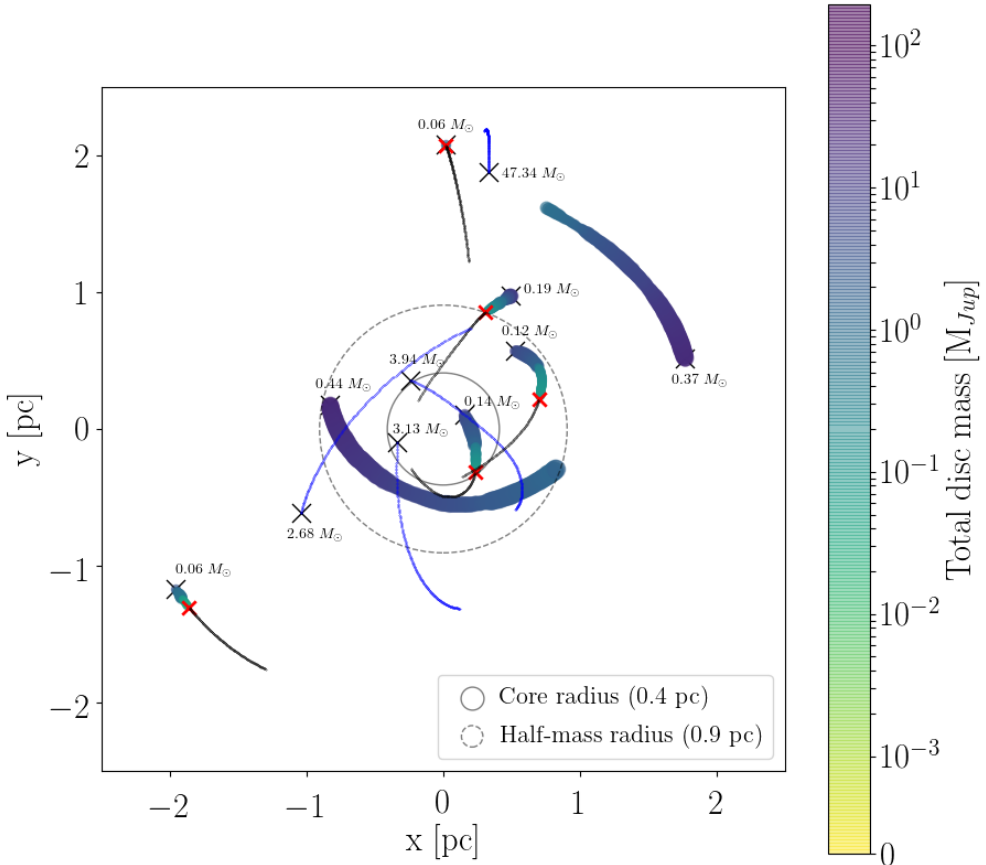


Figure 4.1: Example of cluster evolution for a realisation of the R1.0 model. Black crosses mark the position of the stars at the beginning of the simulation, and the label next to them shows the stellar mass. The sizes of the large, coloured points are proportional to the disc radii, and their colour indicates the total disc mass. The red crosses, when present, show the moment when a disc is dispersed. The thin black lines that follow a red cross indicate the continuing orbit of the star, which keeps moving through the region after its disc has been evaporated. The trajectories of some massive, radiating stars are shown in thin blue lines.

| Model name | Mean disc lifetime [Myr] | Discs half-life [Myr] |
|------------|--------------------------|-----------------------|
| R0.1 | 0.38 ± 0.47 | 0.20 ± 0.01 |
| R0.3 | 0.38 ± 0.47 | 0.22 ± 0.03 |
| R0.5 | 0.47 ± 0.51 | 0.39 ± 0.16 |
| R1.0 | 0.52 ± 0.55 | 0.59 ± 0.11 |
| R2.5 | 0.59 ± 0.56 | 0.97 ± 0.25 |
| R5.0 | 0.65 ± 0.55 | 1.42 ± 0.33 |

Table 4.2: Disc lifetimes and half-life for the different models. First column: model name. Second column: mean disc lifetimes for each model, in Myr. Third column: disc half-life in Myr, calculated as the moment when 50% of the discs in a simulation have been destroyed. The values are averaged over 6 runs for each model, and the errors represent the variations between runs.

illustrative figure we show a two-dimensional projection of the location of the stars.

4.3.1. Disc fractions and lifetimes

We define the disc fraction at time t as the number of discs at t over the initial number of discs in each cluster. In Figure 4.2 we show disc fractions separated in terms of the mass of their host stars: low mass stars ($M_* \leq 0.5M_\odot$) in the top panel and high mass stars ($0.5M_\odot < M_* \leq 1.9M_\odot$) in the bottom panel. The disc fraction for high mass stars stays constant through time for the R1.0, R2.5, and R5.0 models. These discs lose mass but not enough to be completely evaporated, except for a slight decrease near the end for the R1.0 model. In the R0.1, R0.3, and R0.5 models, however, starting around 1.0 Myr even massive discs get destroyed. Final disc fractions decrease with increasing stellar number density. The R0.1 and R0.3 models show a very similar evolution, meaning that the density of the R0.3 model is a higher limit for the effects of external photoevaporation in destroying discs in such simulations.

A large drop in the number of stars with discs before 0.2 Myr is observed in models R0.1 and R0.3. Similar behaviour was obtained in the simulations performed in Paper I. This drop is related to discs around very low mass stars being dispersed rapidly once the simulation begins and external photoevaporation is ‘switched on’. This drop can be seen in all the curves, but it becomes less pronounced for lower densities.

In Table 4.2 we present the mean disc lifetimes and disc half-life for each model, averaged over 6 runs. Disc lifetimes are calculated as a mean of the times when a disc is completely dispersed in the simulations, following the dispersion criteria explained in section 4.2.2. It is important to mention that this mean is calculated only considering the discs that get dispersed within the 2.0 Myr spanned by the simulation, and the discs that survive would likely increase these values. Considering the resulting disc fractions, however, the obtained disc lifetimes are a good approximation. The disc half-life corresponds to the moment when half of the discs in a simulation run have been dispersed. Both the disc lifetimes and the half-life increase with decreasing stellar density.

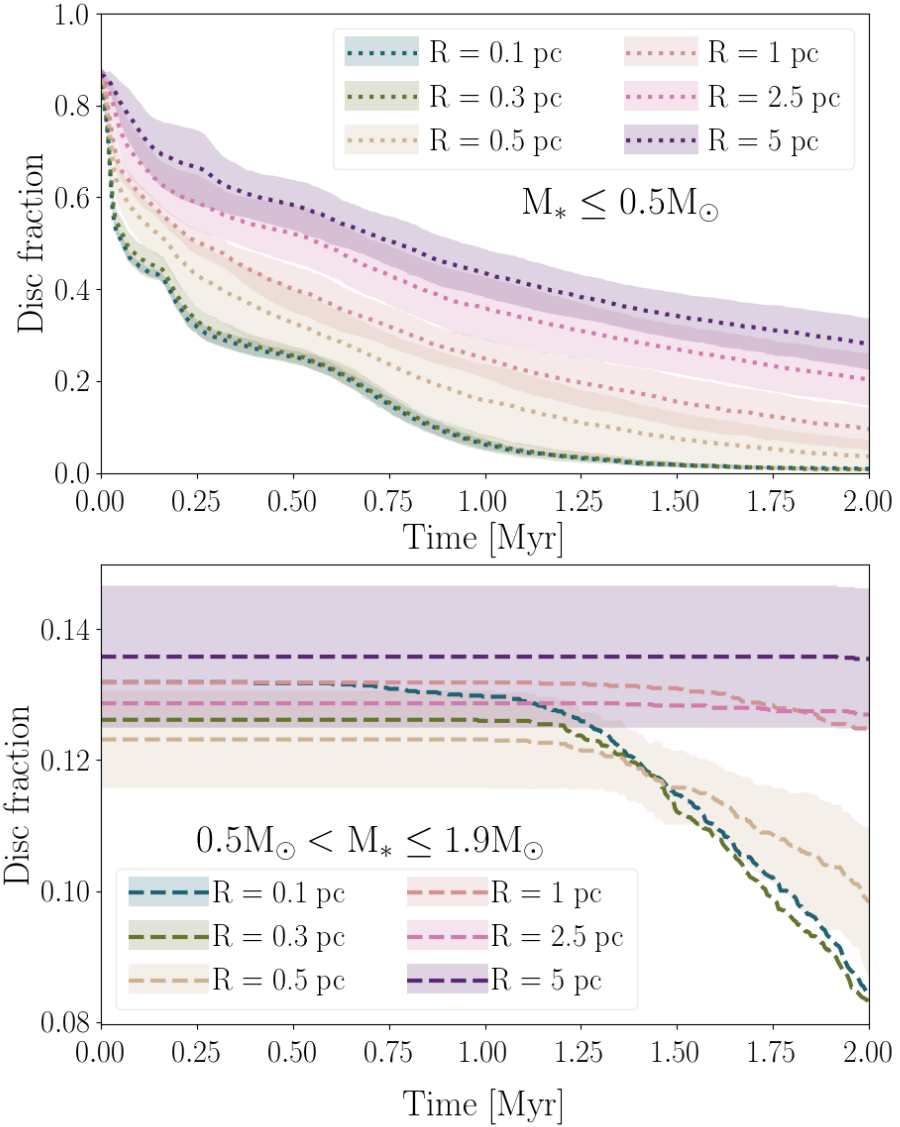


Figure 4.2: Disc fractions in time separated by stellar mass. The top panel shows disc fractions for low mass stars ($M_* \leq 0.5M_\odot$) and the bottom panel for high mass stars ($0.5M_\odot < M_* \leq 1.9M_\odot$). The lines show the mean for 6 runs of each model, and the shaded areas represent the standard deviation. For clarity, in the bottom panel we plot the standard deviation only for the R0.5 and R5.0 models, but the rest of the models have deviations of similar magnitude.

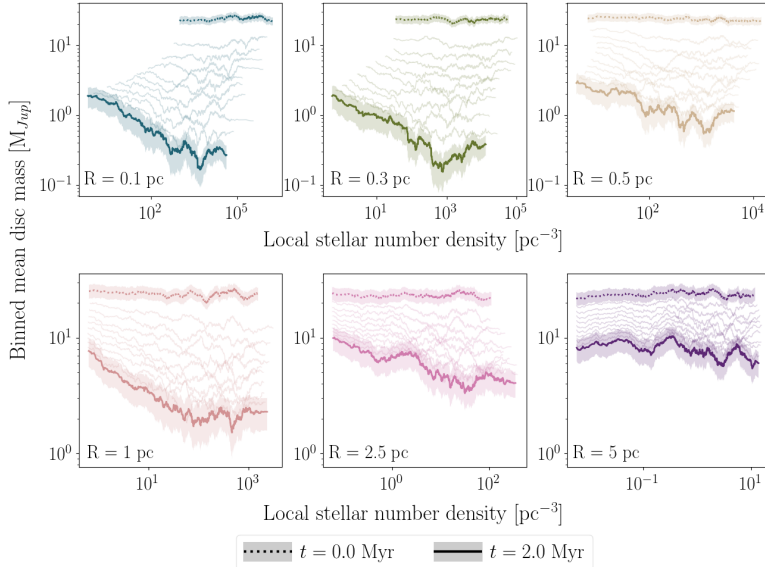


Figure 4.3: Binned mean disc mass versus local stellar number density. The mean mass is calculated using a moving bin spanning 100 stars. The local density is calculated for each star as explained in section 4.3.2. The dotted lines thick represent the binned mean disc mass at $t = 0.0$ Myr and the solid thick lines at $t = 2.0$ Myr. The shaded areas show the standard error. The thin lines represent the binned mean at 0.2 Myr intervals.

4.3.2. Disc masses

In Figure 4.3 we show the evolution of the mean disc mass in time versus the local stellar number density. The local stellar number density is calculated for each star using the method described by Casertano & Hut (1985) with the five nearest neighbours. The binned mean disc mass is calculated using a sliding bin spanning 100 stars.

The thick dotted lines in Figure 4.3 show the mean disc mass at $t = 0.0$ Myr, and the thick solid lines at $t = 2.0$ Myr. The shaded areas around these lines represent the standard error. The thin lines in between show the evolution of the curve in 0.2 Myr intervals. The expansion of the clusters in time is reflected by the $t = 2.0$ Myr curves spanning larger density ranges than the $t = 0.0$ Myr curves. This effect is less pronounced in the R1.0, R2.5, and R5.0 models because they expand in a longer time scale. The slope of the final mean disc mass distribution increases with decreasing stellar density. This is related to the core density in each region, which is also decreasing: the curves in the R5.0 model are several orders of magnitude lower, in terms of density, than the R0.1 model. The R0.1 model has a distribution of disc masses such that the most massive discs are found further away from the centre, with differences of about one order of magnitude between the discs located in the centre and in the outskirts of the cluster. In the R5.0 model, the mass difference between discs in different locations is much smaller, and the disc masses are of the same order of magnitude through all the density range.

In Figure 4.4 we show the mean dust mass of the discs versus the projected local stellar density. We use a 1:100 dust:gas mass ratio to determine the dust mass of our discs. We calculate the density in the same way as in Figure 4.3, but projecting the distances between stars to two dimensions. This allows us to compare disc dust masses in our simulations to

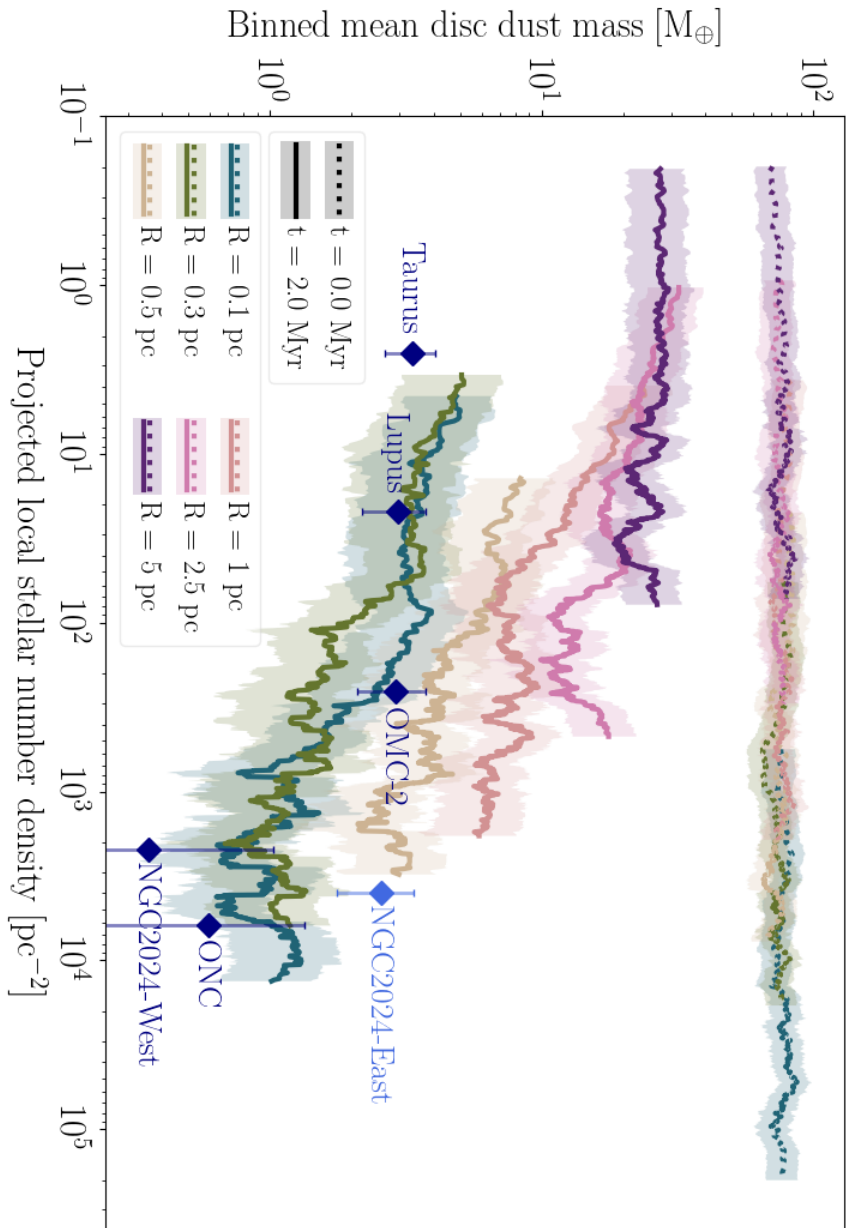


Figure 4.4: Binned mean disc mass versus local stellar number density, projected in two dimensions. The mean mass is calculated using a moving bin spanning 100 stars. The local density is calculated for each star as explained in section 4.3.2 but projecting the distances between stars into two dimensions. The dotted lines thick represent the binned mean disc mass at $t = 0.0 \text{ Myr}$ and the solid thick lines at $t = 2.0 \text{ Myr}$. The shaded areas show the standard error. Diamonds show average disc dust masses and local stellar densities for several observed regions. The different color used for NGC 2024 symbolises the different age of the region.

observed disc populations. The blue diamonds show points of observed average disc dust mass versus local density of young stellar objects for the Lupus clouds (Ansdell et al. 2016, 2018), the Orion Nebula Cluster (ONC, Mann et al. 2014; Eisner et al. 2018), the Orion Molecular Cloud-2 (OMC-2, van Terwisga et al. 2019), Taurus (Andrews et al. 2013), and NGC 2024 East and West (Getman et al. 2014; van Terwisga et al. 2020), as labelled.

Figure 4.4 shows a break in disc masses around a local density of $100 \text{ stars pc}^{-2}$. The slope of the disc mass distribution changes around that point for all models, except R5.0. In models R2.5 and R1.0 we see the slope of the distributions increasing as we move towards higher densities. For the R0.1, R0.3, and R0.5 models, we see disc mass distributions stay relatively constant for densities lower than $100 \text{ stars pc}^{-2}$, and for higher densities we see a negative slope. The difference in masses for discs in regions of density between $100 \text{ stars pc}^{-2}$ and $10^4 \text{ stars pc}^{-2}$ is about one order of magnitude. A similar effect can be seen in the observational points, except for NGC 2024 East. This behaviour suggests that $100 \text{ stars pc}^{-2}$ is a critical density for determining disc masses.

The average disc dust masses of the observations are calculated by fitting a log-normal distribution on the masses. Although disc masses span a large dynamic range, a log-normal distribution is a good description of these populations (Williams et al. 2019). The local density for each point is calculated using the five nearest neighbours method. Lupus data is an average for all the clouds, using the complete list of Class II sources in Ansdell et al. (2016) and Ansdell et al. (2018). It is important to note that the Lupus III cloud dominates the signal for that particular region, because it has the largest population of Class II sources. For the OMC-2 the data comes from van Terwisga et al. (2019), who use the source catalogue from Megeath et al. (2012) assuming completeness. ONC data comes from Megeath et al. (2016), including completeness corrections.

In the OMC-2 and ONC regions, observations sample two different density regimes in the same cloud, relatively close together in space. Therefore, the conditions in our models most closely resemble the properties of the discs that were sampled by the observations, and we can interpret them as different density bins along a single model. It is immediately apparent that both the gradient of average disc mass with density as well as the average disc masses themselves resemble the models closely. Given the considerable uncertainties in extracting disc masses from millimeter-continuum observations (see, for instance, the discussion in Eisner et al. (2018)) the similarity in the gradients suggests that our models are successful at capturing the general behaviour of external photoevaporation.

In NGC 2024, Getman et al. (2014) find evidence for an age gradient of young stars, which van Terwisga et al. (2020) suggest as an explanation for the large difference in mean disc masses in NGC 2024 East and NGC 2024 West. In NGC 2024, the western part is the older and resembles the ONC in age and conditions, while the eastern disc population has a lower average age. We represent this difference in the figure by making NGC 2024 East in a different shade. Comparing these models to the observations, we see that the NGC 2024 West data lie closely to those of the ONC, while the data for the eastern subpopulation occupy a region of average disc mass and local stellar density space which is more consistent with a younger, compact population of stars.

Lupus and Taurus discs, on the other hand, sample a much more heterogeneous part of parameter space in terms of initial densities. Our models do not closely resemble the conditions under which the stars in these samples formed (see, for instance, Roccatagliata et al. (2020)). However, the result that when the average stellar number density is low enough (below $\sim 100 \text{ stars pc}^{-2}$) the average disc masses are similar at similar ages does seem to apply to these star-forming regions, even though this is a part of parameter space we do not explore.

4.4. Discussion

In the simulations performed for this work, external photoevaporation is effective in destroying the majority number of discs within 2.0 Myr of evolution. The initial stellar density of each region affects the fraction of surviving discs, as well as their final mass distributions. In all models, except for R5.0, half of the discs are destroyed before 1.0 Myr of cluster evolution. A break in the disc mass distributions is seen around 100 stars pc⁻², in particular for the R0.1 and R0.3 models, with masses dropping about one order of magnitude between 100 stars pc⁻² and 10⁴ stars pc⁻². Several surveys have shown that disc mass decreases in the vicinity of bright stars, and in regions with higher stellar number density (e.g. Fang et al. 2012; Mann & Williams 2009; Mann et al. 2014; Ansdell et al. 2017; van Terwisga et al. 2020). In Figure 4.4 we show our simulation results and compare them with mean disc masses of various observed regions. It is important to note that, due to the nature of estimating disc masses from observations, the mean disc masses from our simulations and from observed regions differ systematically. In observations, mean disc masses are estimated by fitting a log-normal distribution to the measured dust masses (e.g. Williams et al. 2019). By calculating the same value for our simulations simply using the mean disc mass, the simulation curves are biased toward high mass discs. Still, the behaviour observed in the simulated disc masses follows the trend of the observations: disc masses decrease as stellar density increases.

The trend in the disc mass distribution for local stellar densities 100 stars pc⁻² to 10⁴ stars pc⁻² suggests that, in our models, discs in regions in that density range are less likely to survive long enough or to have enough mass to form planetary systems. The planet formation process should already be underway before 1.0 Myr (Figure 4.2) for discs to have the minimum reservoir of 10M_⊕ in solids proposed by Ansdell et al. (2016) as necessary to form rocky planets or the cores of gas giants. From Figure 4.4 it can be seen that, in our simulations, all discs in the R5.0, R2.5, and R1.0 models that are in areas of projected local density lower than 100 stars pc⁻² have masses in excess of 10 M_⊕. The mean disc dust mass in all other models is below this threshold by 2.0 Myr.

Most of the surviving discs in our simulations are around massive stars (0.5 M_⊙ to 1.9 M_⊙, see Figure 4.2). A big factor in this is simply the construction of our models, where initial disc mass is proportional to stellar mass. Figure 4.2 however, shows that drops of around 50% in fractions of discs around high mass stars are still present in high density regions.

At the end of the simulations, the most massive discs are located in areas where the local stellar density is below 100 stars pc⁻³. This implies that large, massive discs observed today either formed in low density regions or migrated to the outskirts of their birth locations fairly quickly. Discs born in the periphery of such regions have a much larger chance of surviving, and we could argue that the disc distributions seen in these low density regions are similar to primordial disc distributions as they are pretty much unperturbed by external photoevaporation.

4.5. Conclusions

We perform simulations of star clusters with circumstellar discs. We implement the stellar dynamics, stellar evolution, viscous evolution of the discs, and external photoevaporation process to evolve simultaneously. We model our clusters as Plummer spheres with 10³ stars and initial virial radii of 0.1, 0.3, 0.5, 1.0, 2.5, and 5.0 pc to span a range of different number densities. Stars with masses M_{*} ≤ 1.9M_⊕ are initially surrounded by a circumstellar disc,

and stars with masses $M_* > 1.9M_\odot$ do not have discs and are considered as only emitting UV radiation. Each cluster is evolved for 2.0 Myr. We can summarise our findings as follows:

1. External photoevaporation is efficient in destroying circumstellar discs quickly in all simulation models.
2. Mean disc lifetimes range from 0.38 ± 0.47 Myr in the denser models ($R_{\text{cluster}} = [0.1, 0.3, 0.5]$ pc), to 0.65 ± 0.55 Myr for the sparser models ($R_{\text{cluster}} = [1.0, 2.5, 5.0]$ pc).
3. Disc half-life, the time that it takes for half of the discs to be destroyed in a simulation run, ranges from 0.20 ± 0.01 Myr in the denser models to 1.42 ± 0.33 Myr in the sparser models.
4. Disc lifetimes, disc half-lives, disc fractions, and disc masses decrease as the stellar density of the models increase.
5. For the final disc masses in the denser regions ($R_{\text{cluster}} = [0.1, 0.3, 0.5]$ pc) a projected local number density of 100 stars pc^{-2} introduces a break in the distributions. There are only small variations in the masses of discs around stars in areas of lower densities. As the density increases beyond 100 stars pc^{-2} , the denser regions present a drop of almost an order of magnitude in disc masses.
6. The trends obtained in our simulations between disc mass and local stellar density are in agreement with dust mass measurements of discs in different observed regions: we compare our simulation results to masses of dusty young stellar objects in the Lupus clouds, the Orion Nebula Cluster, the Orion Molecular Cloud-2, Taurus, and NGC 2024.

Acknowledgements

We would like to thank the anonymous referee for their constructive comments, which greatly helped improve this paper. F.C.-R. would like to thank the Star formation and protoplanetary disc group at Leiden Observatory for helpful discussions and insights. This work was carried out on the Dutch national e-infrastructure with the support of SURF Cooperative. This work was performed using resources provided by the Academic Leiden Interdisciplinary Cluster Environment (ALICE). This paper makes use of the packages `numpy` (Van Der Walt et al. 2011), `scipy` (Virtanen et al. 2019), `matplotlib` (Hunter 2007), and `makecite` (Price-Whelan et al. 2018).

Data availability

The data underlying this article are available at <https://doi.org/10.5281/zenodo.3897171>.

* * *

5

Evolution of circumstellar discs in young star forming regions

F. Concha-Ramírez; S. Portegies Zwart;
M. J. C. Wilhelm

Monthly Notices of the Royal Astronomical Society
In review

THE EVOLUTION of circumstellar discs is highly influenced by their surroundings, in particular by external photoevaporation due to nearby stars and dynamical truncations. The impact of these processes on disc populations depends on the dynamical evolution of the star-forming region. Here we implement a simple model of molecular cloud collapse and star formation to obtain primordial positions and velocities of young stars and follow their evolution in time, including that of their circumstellar discs. Our disc model takes into account viscous evolution, internal and external photoevaporation, dust evolution, and dynamical truncations. The disc evolution is resolved simultaneously with the star cluster dynamics and stellar evolution. Our results show that an extended period of star formation allows for massive discs formed later in the simulations to survive for several million years. This could explain massive discs surviving in regions of high UV radiation.

*

5.1. Introduction

Circumstellar discs are a natural consequence of the star formation process, and emerge within the first 10^4 yr after star formation (Williams & Cieza 2011). The star formation environment, rich in gas and newly-formed stars, can greatly affect the evolution of the discs. The imprints that this environment will leave on the young discs have important repercussions on their potential to form planets and on the configurations of the planetary systems that eventually do develop.

There are several ways in which the environment can influence the evolution of circumstellar discs. Close encounters between circumstellar discs and stellar fly-bys can affect the size, mass, and surface density of the discs. Close encounters can remove mass from the outskirts of the discs, decreasing both their mass and radius (e.g. Clarke & Pringle 1991, 1993; Pfalzner et al. 2005b; Breslau et al. 2014; Vincke et al. 2015; Vincke & Pfalzner 2016; Portegies Zwart 2016; Vincke & Pfalzner 2018; Cuello et al. 2019; Winter et al. 2018a; Conchá-Ramírez et al. 2019a). Several numerical implementations of this process have shown that close encounters can lead to a hardening of the discs surface density (Rosotti et al. 2014), the formation of spiral arms and other structures (Pfalzner 2003; Pfalzner et al. 2005a), accretion bursts onto the host star (Pfalzner et al. 2008), and exchange of mass between discs (Pfalzner et al. 2005b; Jílková et al. 2016). Observational evidence for the effects of stellar fly-bys has been presented in several studies. Cabrit et al. (2006) study the ~ 600 au trailing “tail” in the disc of RW Aur A and suggest that it might have been caused by a recent fly-by. Reche et al. (2009) suggest that the spiral arms observed in the disc of the triple star system HD 141569 might be the result of a fly-by. Observations by Rodriguez et al. (2018) reveal newly-detected tidal streams in RW Aur A and they propose that these might be the result of many subsequent close encounters. Winter et al. (2018c) simulate the disc around DO Tau, which presents a tidal tail, and argue that this shape could have been caused by a close encounter with the nearby triple system HV Tau. There is also evidence that the young disc of the solar system was affected by such an encounter. The sharp edge of the solar system at ~ 30 au could be a sign that a passing star truncated its early disc (Breslau et al. 2014; Punzo et al. 2014). The highly eccentric and inclined orbits of the *Sednitos*, a group of 13 detected planetoids in the outskirts of the solar system, suggest they might have been captured from the disc of a passing nearby star (Jílková et al. 2015).

Another mechanism that can alter the evolution of circumstellar discs is photoevaporation. Photoevaporation is the process in which high energy photons heat the disc surface, causing them to evaporate. The source of these photons can be the host star (internal photoevaporation) or bright stars in the vicinity (external photoevaporation). Photoevaporation is driven by far ultraviolet (FUV), extreme ultraviolet (EUV), and X-ray photons (Johnstone et al. 1998; Adams et al. 2004). The effects of internal and external photoevaporation on circumstellar discs are rather distinct. Internal photoevaporation can clear areas of the disc at specific disc radii, causing the opening of gaps (Gorti et al. 2009; Gorti & Hollenbach 2009; Owen et al. 2010; Font et al. 2004; Fatuzzo & Adams 2008; Hollenbach et al. 2000). External photoevaporation can remove mass from all over the disc surface, but the outer regions of the discs are more vulnerable because the material is less strongly bound to the host star (Johnstone et al. 1998; Adams et al. 2004).

Observational evidence of external photoevaporation was first obtained through the imaging of evaporating discs in the Orion nebula (O’Neill & Wen 1994; O’Neill 1998). These objects, now known as ‘proplyds’, are circumstellar discs immersed in the radiation fields of nearby stars. Their cometary tail-like structure reveals the ongoing mass loss. Subsequent observations of the region showed that circumstellar disc masses decrease when close to mas-

sive stars. This effect has been observed in several regions such as the Trapezium cluster (e.g. Vicente & Alves 2005; Eisner & Carpenter 2006; Mann et al. 2014), the Orion Nebula Cluster (e.g. Mann & Williams 2010; Eisner et al. 2018), Cygnus OB2 (Guarcello et al. 2016), NGC 1977 (Kim et al. 2016), NGC 2244 (Balog et al. 2007), Pismis 24 (Fang et al. 2012), NGC 2024 (van Terwisga et al. 2020), σ Orionis (Ansdell et al. 2017), and λ Orionis (Ansdell et al. 2020). Younger and low-mass star-forming regions such as Lupus, Taurus, Ophiuchus, and the Orion Molecular Cloud 2 tend to have higher average disc masses than denser regions such as the Orion Nebula Cluster (Eisner et al. 2008; Ansdell et al. 2016; Eisner et al. 2018; van Terwisga et al. 2019). van Terwisga et al. (2020) present the discovery of two distinct disc populations, in terms of mass, in the NGC 2024 region. The discs to the east of the region are embedded in a dense molecular ridge and are more massive than the discs outside the ridge, which are also closer to two OB type stars. They propose that the difference in masses is caused by the eastern population being protected from the radiation of nearby massive star IRS 1.

Several models have demonstrated external photoevaporation is efficient in depleting disc masses on timescales much shorter than their estimated lifetimes of ~ 10 Myr (e.g. Scally & Clarke 2001; Adams et al. 2006; Fatuzzo & Adams 2008; Haworth et al. 2016), even in low radiation fields (Facchini et al. 2016; Kim et al. 2016; Haworth et al. 2017). Because external photoevaporation is caused by massive stars in the vicinity of the discs, the extent of its effects depends on the density of the stellar region and the number of massive stars in the surroundings. Even in high density regions ($N_* \gtrsim 10^4 \text{ pc}^{-3}$) the disc mass-loss rates caused by external photoevaporation are orders of magnitude higher than those caused by dynamical truncations (Winter et al. 2018b, 2019b; Concha-Ramírez et al. 2019b). Concha-Ramírez et al. (2021) show that, in regions of local stellar densities $N_* > 100 \text{ pc}^{-3}$, external photoevaporation can evaporate up to 90% of circumstellar discs within 2.0 Myr. In low density regions ($\sim 10 M_\odot \text{ pc}^{-3}$), only $\sim 60\%$ of discs are evaporated within the same timescale. Winter et al. (2020b) model a region comparable to the central molecular zone of the Milky Way (surface density $\Sigma_0 = 10^3 M_\odot \text{ pc}^{-2}$) and find that external photoevaporation destroys 90% of circumstellar discs within 1.0 Myr. In regions of lower density ($\Sigma_0 = 12 M_\odot \text{ pc}^{-2}$) they find a mean disc dispersion timescale of 3.0 Myr. Similar results are obtained by Nicholson et al. (2019) who find that external photoevaporation destroys 50% of discs within 1.0 Myr in regions of density $\sim 100 M_\odot \text{ pc}^{-3}$, and within 2.0 Myr in regions of density $\sim 10 M_\odot \text{ pc}^{-3}$.

While observational and numerical evidence indicate that disc masses decrease with increasing stellar density, massive discs are still observed in high density regions. In particular, there are discs in the ONC whose masses are much higher than other discs in the proximity of the massive star θ^1 Ori C. If the discs are coeval with θ^1 Ori C they should have already been dispersed by external photoevaporation, unless they were extraordinarily massive to begin with ($M_{\text{disc}} \gtrsim 1 M_\odot$). Alternatively, θ^1 Ori C would have to be considerably younger than the ONC average ($\lesssim 0.1$ Myr) for these discs to have survived. This is known as the ‘proplyd lifetime problem’. Störzer & Hollenbach (1999) propose that these discs are currently passing by the centre of the region, but have spent most of their lifetimes far enough from it to be protected from the radiation. Scally & Clarke (2001) model external photoevaporation on a cluster similar to the ONC and find that the necessary orbits proposed by Störzer & Hollenbach (1999) are not dynamically plausible in such a region. Winter et al. (2019b) revisit the problem and propose a solution to describe why these discs exist. The solution consists of a combination of factors: different eras of star formation allow for massive discs to be around stars that are younger than the average of the ONC population; stars forming in subvirial states with respect to the gas potential allows young stars to migrate to the central region of the ONC; and interstellar gas protects the discs from the radiation, allowing them to live

longer than expected.

The star-formation history and primordial stellar distributions in young star-forming regions are key to understanding the effects that the environment will have on the disc populations. The star formation process results in regions with different morphologies, with clumps and filaments likely to be present. This structure is far from the spherical, idealized initial conditions commonly used in models. The collapse of the giant molecular clouds (GMCs) from which stars form is affected by turbulent flows (Falgarone et al. 1991, Falgarone & Phillips 1991) which result in filamentary, clumpy, and fractal gas substructure in the cloud (e.g. Scalo 1990; Larson 1995; Elmegreen et al. 2000; Hacar et al. 2018). The mass of these clumps ranges from around one solar mass to several thousand solar masses, and linear sizes from less than half a parsec to tens of parsecs (e.g. Lada & Lada 2003; Williams et al. 2000). They can form individual stars, small multiple systems, or bigger associations and clusters. The initial distribution of the stars will be a direct result of the local densities of the gas in the molecular cloud. Given that circumstellar discs emerge during the protostellar phase (Williams & Cieza 2011), the star formation process will define the environment in which the discs are immersed in their early stages.

To get a broader understanding of the environmental effects on circumstellar discs, it is important to take a step back in time and study how the star formation process influences stellar densities. In this work we present a model for circumstellar discs inside young star-forming regions. We adopt a relatively simple model for the star formation process, starting from the collapse of a giant molecular cloud to obtain masses, positions, and velocities of newly formed stars. These form the input for our star cluster evolution code. During the evolution we take into account the viscous evolution of the discs, dynamical truncations, external and internal photoevaporation, and dust evolution. We evolve the discs simultaneously with the stellar dynamics and stellar evolution.

5.2. Model

We model several different astrophysical processes which operate simultaneously and at very distinct scales: the collapse of a molecular cloud, star formation, stellar dynamics, and viscous circumstellar discs which are affected by dynamical truncations and photoevaporation. We bring these processes together using the Astrophysical Multipurpose Software Environment, AMUSE (Portegies Zwart et al. 2013; Pelupessy et al. 2013). The results presented in this work are obtained through two different simulation stages: first, we perform a simple model of the collapse of a molecular cloud and the subsequent star formation process. This returns a spatial, velocity, and mass distribution of stars to be used in the second simulation stage, in which we follow the evolution of the circumstellar discs in the star-forming regions. This second stage encompasses the stellar dynamics, stellar evolution, viscous evolution of the discs, and photoevaporation. All the code developed for this work is available online¹.

5.2.1. Molecular cloud collapse and star formation

The first stage of the simulations deals with a simple model of the star formation process. We simulate the collapse of a molecular cloud using the smoothed particle hydrodynamics (SPH) code F i (Pelupessy et al. 2004). We model the star formation process through the use of sink particles, which are created from regions of the cloud where the local gas density is higher than a threshold. We set this threshold at $1M_{\odot}/\epsilon^3$, where $\epsilon = 0.05$ pc is the softening

¹<https://doi.org/10.5281/zenodo.4436316>

of the simulation. Once a sink particle forms it continues accreting gas from the molecular cloud. Each of these sink particles can form several stars.

Since we look to preserve a power-law stellar mass function similar to the one observed in the galaxy, the stars in our simulations cannot be formed without introducing a predetermined star formation efficiency (SFE). We set a SFE of 0.3 (Lada & Lada 2003). We implement this SFE by keeping track of the mass in sinks, since this is the mass that will eventually be turned into stars. When the total sinks mass reaches 30% of the mass of the cloud, the SPH code is stopped. We keep track of the existing sinks in a separate dynamics code to guarantee that they continue to move after the SPH code is stopped. The star formation process continues until all the mass in the sinks has turned into stars.

The star formation process begins once sink particles have accreted enough mass to sample stars from a random initial mass function (IMF). We base the star formation mechanism on Wall et al. (2019). We begin by sampling a random stellar mass m from a Kroupa IMF (Kroupa 2001) of 10,000 stars, with lower limit $0.08 M_{\odot}$ and upper limit $150 M_{\odot}$ (Wall et al. 2019). Then we check if there is a sink massive enough to form a star of mass m . If there is one, we subtract the mass m from the sink and create a star particle. If $m \leq 1.9M_{\odot}$ the star will have a circumstellar disc (see section 5.2.2), and we subtract the mass of the star and the initial mass of the disc from the sink. The position of the newly formed star is determined by taking the position of the sink and adding a random offset in each spatial dimension. This offset is calculated within the sink diameter. The velocity of the new star is set to the velocity of its birth sink.

After a sink has formed a star, we set a delay time which must pass before it creates a new star. We implement this step to counteract the fact that our sampling will be biased toward forming low mass stars, by allowing sinks to become more massive before forming another star. This delay is implemented as an exponentially decaying timescale:

$$t_{\text{delay}} = t_{\text{ff}} \exp\left(\frac{-0.1 t}{1 \text{ Myr}}\right) \quad (5.1)$$

where t_{ff} is the free-fall time scale of the corresponding sink and t is the current model time.

During the molecular cloud collapse simulation we keep track of the mass, position, velocity, and birth time of the newly formed stars. This data will then be given as input for the second part of the simulations, which involve the disc evolution and stellar dynamics. The dynamical evolution of the stars is calculated using the 4th-order Hermite integrator ph4, which is evolved simultaneously with the SPH integrator in a leap-frog scheme using the Bridge (Fujii et al. 2007) coupling method in AMUSE (see Portegies Zwart et al. 2020, for implementation details).

5.2.2. Stellar dynamics and circumstellar discs

The second simulation stage begins at the time when the first star has formed. For each star, we evolve its disc and calculate its external photoevaporation mass loss rate as explained in sections 5.2.2 and 5.2.2 respectively. The star formation process ends when all the mass in sinks has been formed into stars. Then, the leftover gas is expelled and we only deal with the stellar dynamics and processes explained in the following sections. This second stage of the simulations evolve for 2 Myr after the last star has formed. Below we describe how each of the processes is modelled.

Circumstellar discs

We model circumstellar discs using the Viscous Accretion disc Evolution Resource (VADER, Krumholz & Forbes 2015). VADER models the viscous transport of mass and angular momentum on a thin, axisymmetric disc. We use the standard disc profile of Lynden-Bell & Pringle (1974) to establish the initial column density of the discs as:

$$\Sigma(r, t = 0) \approx \frac{m_d}{2\pi r_d (1 - e^{-1})} \frac{\exp(-r/r_d)}{r} \quad (5.2)$$

where r_d is the initial disc radius, m_d is the initial disc mass, and Σ_0 is a normalisation constant. We consider the characteristic radius to be $r_c \approx r_d$ (Anderson et al. 2013).

For the external photoevaporation process we keep track of the outer edge of the disc. We define the disc radius as the radius which encloses 99% of the disc mass (Anderson et al. 2013). The mass loss due to external photoevaporation (section 5.2.2), as well as dynamical truncations (section 5.2.2), causes the disc to develop a steep density profile at the outer edge. The location of the edge is insensitive to the value of Σ_{edge} , given that it is sufficiently low (Clarke 2007). We set the column density outside r_d to a negligible value $\Sigma_{\text{edge}} = 10^{-12} \text{ g cm}^{-2}$.

Each of the VADER discs in the simulations consists of a grid of 100 logarithmically spaced cells, ranging from 0.05 au to 2.000 au. All the discs have a constant turbulence parameter of $\alpha = 5 \times 10^{-3}$.

External photoevaporation

We calculate the mass loss due to external photoevaporation using the Far-ultraviolet Radiation Induced Evaporation of Discs (FRIED) grid (Haworth et al. 2018). This grid provides a pre-calculated set of mass loss rates for discs immersed in UV radiation fields of varying strengths, from 10 G_0 to 10^4 G_0 , where G_0 is the FUV field measured in Habing units, $1.6 \times 10^{-3} \text{ erg s}^{-1} \text{ cm}^{-2}$ (Habing 1968). The grid spans discs of mass $\sim 10^{-4} \text{ M}_{\text{Jup}}$ to $10^2 \text{ M}_{\text{Jup}}$, radius from 1 au to 400 au, and host star mass from 0.05 M_{\odot} to 1.9 M_{\odot} .

To stay inside the boundaries of the FRIED grid we consider only stars of mass $M_* \leq 1.9 \text{ M}_{\odot}$ as having a circumstellar disc. More massive stars are considered to generate radiation. This mass distinction is for external photoevaporation calculations only; for the stellar dynamics evolution there is no separation between these two stellar groups.

Far-ultraviolet (FUV) photons dominate in the external photoevaporation process (Armitage 2000; Adams et al. 2004; Gorti & Hollenbach 2009). We calculate the FUV radiation from the massive stars by pre-computing a relation between stellar mass and FUV luminosity using the UVBLUE spectral library (Rodriguez-Merino et al. 2005). The obtained fit is presented in Figure 2 of Concha-Ramírez et al. (2019b). We use that fit to determine the FUV radiation emitted by each massive star at every simulation time step.

We model the external photoevaporation process as follows. At every time step we calculate the distance from every disc to every star of mass $M_* > 1.9 \text{ M}_{\odot}$ and determine the total radiation received by each disc. We do not consider extinction due to interstellar material. We interpolate from the FRIED grid using the calculated total radiation and the disc parameters to find a photoevaporation driven mass loss rate for each disc. Assuming the mass loss rate \dot{M} to be constant during the current time step, we use it to calculate the total mass loss. This mass is then removed from the outer regions of the disc. We move through the disc cells starting from the outermost one, removing mass from each, until the required amount of mass has been removed. External photoevaporation then results in a decrease of disc mass and disc radius.

Under certain circumstances, external photoevaporation can be dominated by extreme ultraviolet (EUV) photons. This happens when a disc is closer to a radiating star than a minimum distance derived by Johnstone et al. (1998) as:

$$d_{min} \simeq 5 \times 10^{17} \left(\frac{\varepsilon^2}{f_r \Phi_{49}} \right)^{-1/2} r_{d_{14}}^{1/2} \text{ cm} \quad (5.3)$$

where f_r is the fraction of EUV photons absorbed in the ionizing flow, $\Phi_{49} = \frac{\Phi_4}{10^{49}} \text{ s}^{-1}$ is the EUV luminosity of the source, ε is a dimensionless normalizing parameter, $\left(\frac{\varepsilon^2}{f_r \Phi_{49}} \right)^{1/2} \approx 4$, and $r_{d_{14}} = \frac{r_d}{10^{14} \text{ cm}}$ with r_d the disc radius.

When the distance d between a disc and a massive star is $d < d_{min}$, the disc enters the EUV-dominated photoevaporation regime. The mass loss in this case is calculated as:

$$\dot{M}_{EUV} = 2.0 \times 10^{-9} \frac{(1+x)^2}{x} \varepsilon r_{d_{14}} M_\odot \text{ yr}^{-1} \quad (5.4)$$

with $x \approx 1.5$ and $\varepsilon \approx 3$ (Johnstone et al. 1998).

A disc is dispersed when it has lost 99% of its initial gas mass (Ansdell et al. 2016) or when its mean column density drops below 1 g/cm^2 (Pascucci et al. 2016). After a disc is dispersed, its host star continues to evolve normally in the stellar dynamics code.

Internal photoevaporation

Internal photoevaporation is driven by X-ray radiation (Owen et al. 2010, 2012). We calculate the X-ray luminosity of the stars with discs using the fit obtained by Flaccomio et al. (2012) for T-Tauri stars as a function of stellar mass:

$$\log \left(\frac{L_X}{\text{erg s}^{-1}} \right) = 1.7 \log \left(\frac{M_*}{1 M_\odot} \right) + 30 \quad (5.5)$$

where M_* is the mass of the host star.

Picogna et al. (2019) calculate X-ray mass loss profiles and mass loss rates for a star of mass $0.7 M_\odot$. Owen et al. (2012) developed scaling relations that allow to calculate these values for stars with masses $M_* \leq 1.5 M_\odot$. We combine the results of Picogna et al. (2019) with the scaling relations of Owen et al. (2012) to span a larger range of stellar masses. The internal photoevaporation mass loss rate is then given by:

$$\dot{M}_X = 10^\Delta \left(\frac{M_*}{0.7 M_\odot} \right)^{-0.068} M_\odot \text{ yr}^{-1}, \quad (5.6)$$

where

$$\Delta = -2.7326 \exp \left[\frac{(\ln(\log(L_X)) - 3.3307)^2}{2.9868 \times 10^{-3}} \right] - 7.2580 \quad (5.7)$$

is the X-ray mass loss rate derived by Picogna et al. (2019).

The mass loss profile takes the form:

$$\begin{aligned} \dot{\Sigma}_w(x) = \ln(10) & \left(\frac{6a \ln(x)^5}{x \ln(10)^b} + \frac{5b \ln(x)^4}{x \ln(10)^5} + \frac{4c \ln(x)^3}{x \ln(10)^4} + \frac{3d \ln(x)^2}{x \ln(10)^3} \right. \\ & \left. + \frac{2e \ln(x)}{x \ln(10)^2} + \frac{f}{x \ln(10)} \right) \frac{\dot{M}_w(x)}{2\pi x} M_\odot \text{ au}^{-2} \text{ yr}^{-1}, \end{aligned} \quad (5.8)$$

where

$$\dot{M}_w(x) = \dot{M}_X 10^{a \log x^6 + b \log x^5 + c \log x^4 + d \log x^3 + e \log x^2 + f \log x + g} \quad (5.9)$$

with $a = -0.5885$, $b = 4.3130$, $c = -12.1214$, $d = 16.3587$, $e = -11.4721$, $f = 5.7248$, and $g = -2.8562$ (Picogna et al. 2019); and

$$x = 0.85 \left(\frac{r}{\text{au}} \right) \left(\frac{M_*}{1M_\odot} \right)^{-1} \quad (5.10)$$

is the scaling from Owen et al. (2012), where M_* is the mass of the host star.

The internal photoevaporation process removes mass from the disc following the profile defined in Eq. 5.8. In the case where a grid cell contains less mass than is prescribed to be removed, this excess is removed in the nearest outer cell. As the cells are traversed inside-out, this takes the form of inside-out disc clearing.

Disc dust evolution

Circumstellar discs are composed of gas and dust. Initially, a 100:1 gas:dust ratio is assumed for the composition of the discs. This value is derived from the consideration that the ratio is inherited from the interstellar medium (Bohlin et al. 1978). Grain growth might result in much lower gas:dust ratios (Williams & Best 2014), and the ratio is likely to change during the lifetime of a disc (Manara et al. 2020). Models of dust evolution and radial drift (Birnstiel et al. 2010; Rosotti et al. 2019) show that the dust:gas ratio decreases in time. In the present work we introduce a simple prescription for the dust evolution inside circumstellar discs.

We follow the prescription of Haworth et al. (2018a) to calculate the mass loss rate of dust entrapped in the photoevaporation wind. This mass loss rate is described as:

$$\dot{M}_{dw} = \delta \dot{M}_{gas}^{3/2} \left(\frac{\nu_{th}}{4\pi F G M_* \rho_g a_{min}} \right)^{1/2} \exp \left(\frac{-\delta(GM)^{1/2} t}{2R_d^{3/2}} \right), \quad (5.11)$$

where δ is the initial dust:gas ratio (10^{-2}), \dot{M}_{gas} is the gas mass loss rate (determined as explained in sections 5.2.2 and 5.2.2), $\nu_{th} = \sqrt{8k_b T / \pi \mu / m_H}$ is the mean thermal speed of the gas particles, F is the solid angle subtended by the disc at the outer edge, ρ_g is the grain mass density (1 g/cm^3 , Facchini et al. 2016), and a_{min} is the minimum grain size at the disc radius R_d . We assume $a_{min} = 0.01 \mu\text{m}$ (Haworth et al. 2018a; Facchini et al. 2016).

This model takes into account what fraction of the dust is entrained in the photoevaporation wind, and how it decreases over time due to dust growth. Mass is removed from a single, scalar reservoir. The radial structure is implicitly assumed to follow the gas structure, multiplied by the dust-to-gas ratio $\delta \sim 0.01$, and doesn't account for the dust fraction enhancement due to the evaporation-resistant dust population.

Dynamical truncations

We calculate a semi-analytical truncation radius based on Adams (2010), who propose that the new radius of a disc after a truncating encounter is $R' \approx b/3$ where b is the pericentre distance of the encounter. We combine this with the mass dependence of Breslau et al. (2014) to define a truncation radius:

$$R' = \frac{r_{enc}}{3} \left(\frac{m_1}{m_2} \right)^{0.32}, \quad (5.12)$$

where m_1 and m_2 are the masses of the encountering stars. We follow (Portegies Zwart 2016) in defining an initial collisional radius of $r_{col} = 0.02$ pc for all stars. This value is updated to $r_{col} = 0.5r_{enc}$ after every encounter, to make sure that each encounter is only detected once within the time step. Not all encounters result in disc truncation. If the calculated truncation radius R' is larger than the current radius of an encountering disc, the disc is not affected by the encounter. If a disc is truncated in an encounter, we set the new radius of a disc to R' by making the column density $\Sigma_{\text{edge}} = 10^{-12}$ g cm⁻² for every disc cell outside R' . The truncated disc then continues to expand viscously.

Dynamical encounters not only change the disc sizes and strip mass from the outskirts, but can also lead to changes in the mass distribution of the discs and mass exchange can occur between the encountering discs (Pfalzner et al. 2005b; Rosotti et al. 2014; Jílková et al. 2015; Portegies Zwart 2016). Because of our implementation of the discs (section 5.2.2) we do not consider mass exchange or any other changes to the mass distribution during dynamical encounters, other than truncation. When a disc is truncated in our model, all the mass outside its new radius R' is simply lost.

5.2.3. Initial conditions

Molecular cloud

Our simulations start with an spherical cloud model of mass 10^4 M_⊙ and initial radius 3 pc. We use 32,000 SPH particles, which results in a resolution of 0.3 M_⊕ per particle. The softening in the simulations is 0.05 pc. We use a power-law velocity spectrum to model large scale turbulence (Bate et al. 2003). Each realization of a molecular cloud has a different random seed, so the substructure that originates is different in every run of the simulation. We run 6 realizations of the molecular cloud collapse simulations. There realizations differ only in the random seed used to determine the position and velocities of the SPH particles.

Circumstellar discs

We choose the initial disc radii as:

$$r_d(t=0) = R' \left(\frac{M_*}{M_\odot} \right)^{0.5}, \quad (5.13)$$

where R' is a constant. We choose $R' = 30$ au, which results in initial disc radii between ~ 5 au and ~ 40 au. This is in agreement with observations that suggest that young circumstellar discs are generally quite compact (radii around 20 to 50 au, (Trapman et al. 2020; Tobin et al. 2020)). We set the initial radius of each disc on the grid through the procedure explained in section 5.2.2.

The initial mass of the discs is:

$$M_d(t=0) = 0.1M_*. \quad (5.14)$$

This yields initial disc masses ranging from ~ 8 M_{Jup} to ~ 200 M_{Jup}.

5.3. Results

5.3.1. Star formation and cluster evolution

In Figure 5.2 we show the number of stars in time for each simulation run. In Table 5.1 we present the final number of stars in each run. The mean number of stars created in six

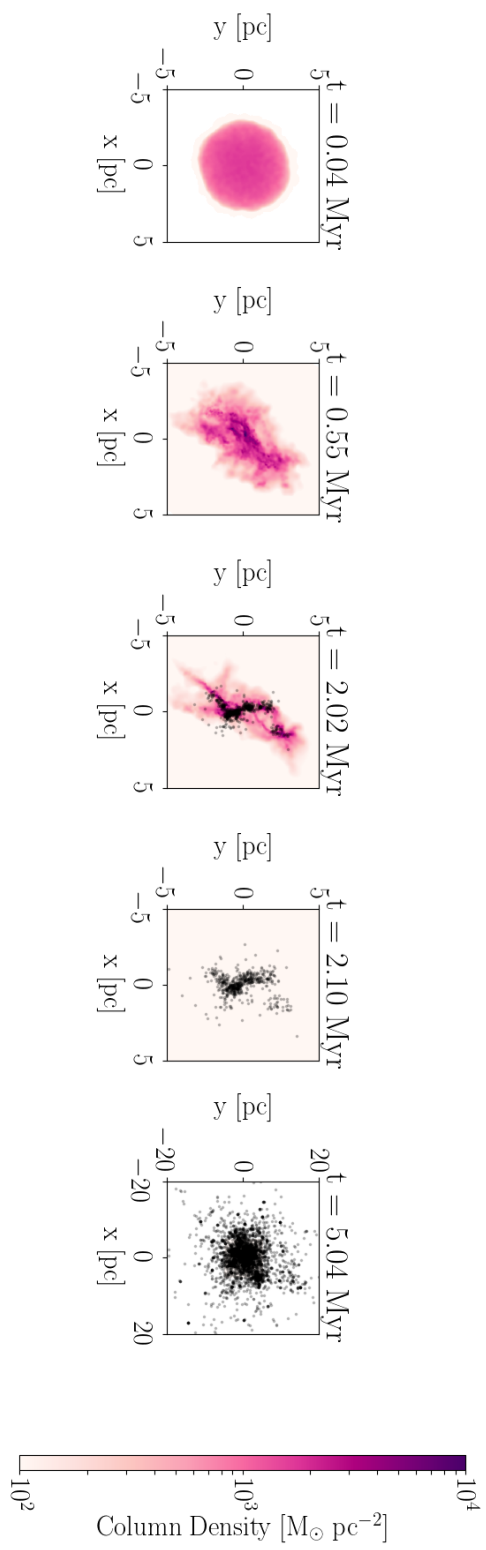


Figure 5.1: Evolution of the molecular cloud collapse and star formation process in run #4. The center panel shows the moment before gas expulsion, and the rightmost panel shows the region close to the end of the simulation.

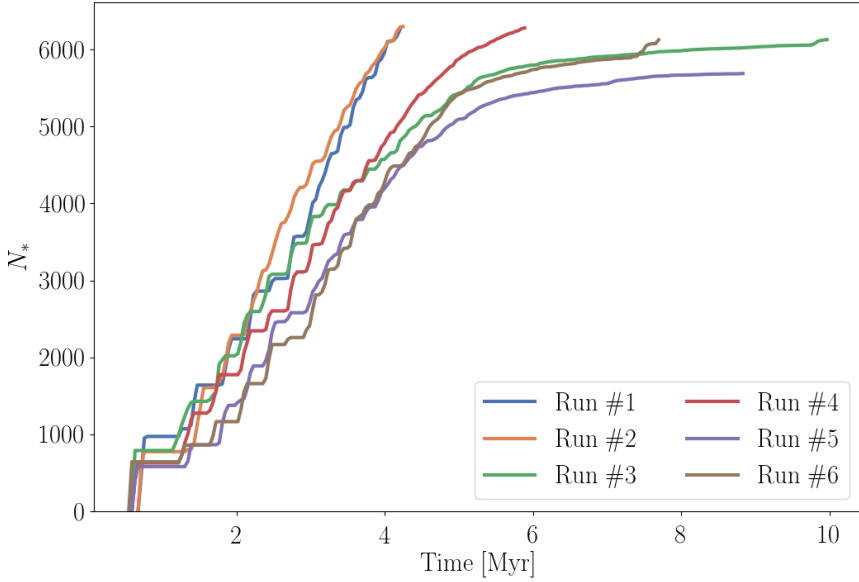


Figure 5.2: Number of stars in time for each simulation run.

runs is 6146 ± 214 . In Figure 5.1 we show the evolution of the molecular cloud collapse and star formation process in one of our simulation runs, for illustrative purposes.

In Figure 5.3 we show the evolution of the virial radius in time for each of our simulations. We also show the virial radius as a function of time of a Plummer sphere with 6,000 stars and initial virial radius 3 pc for comparison. The solid lines show the virial radius while star formation is still ongoing, whereas the dotted lines follow the radius after all stars have formed and gas has been removed from the clusters. It can be seen that all the regions expand gradually at a rate of 1 to 2 pc/Myr, but as soon as the gas is expelled their radii grow very quickly in a short time frame to settle on a gradual growth.

To quantify the spatial distribution of the stars resulting from the molecular cloud collapse simulations, we look at the Q parameter of the minimum spanning tree (Cartwright & Whitworth 2004) and the fractal dimension in each region at the end of the star formation process. The Q parameter is calculated as:

$$Q = \frac{\bar{m}}{\bar{s}}, \quad (5.15)$$

where \bar{m} is the mean length of the minimum spanning tree and \bar{s} is the mean separation between the stars. Regions with $Q > 0.8$ are smooth and centrally concentrated, while values of $Q < 0.8$ correspond to regions with substructure.

In Figure 5.4 we show the Q parameter in time for each of our simulations, along with values for several observed regions. The Q parameter of the simulations is calculated from a 2D projection of the stellar distances, and considers only stars with masses $M_* > 0.5 M_\odot$. In Table 5.2 we summarize the values for Q and the estimated ages for each region, along with the corresponding references. The simulation results span a range of $Q \sim 0.6$ to $Q \sim 1.5$. This means that in certain runs some substructure is still present, while others result in smoother regions. This result can greatly vary depending on stellar membership. Regions

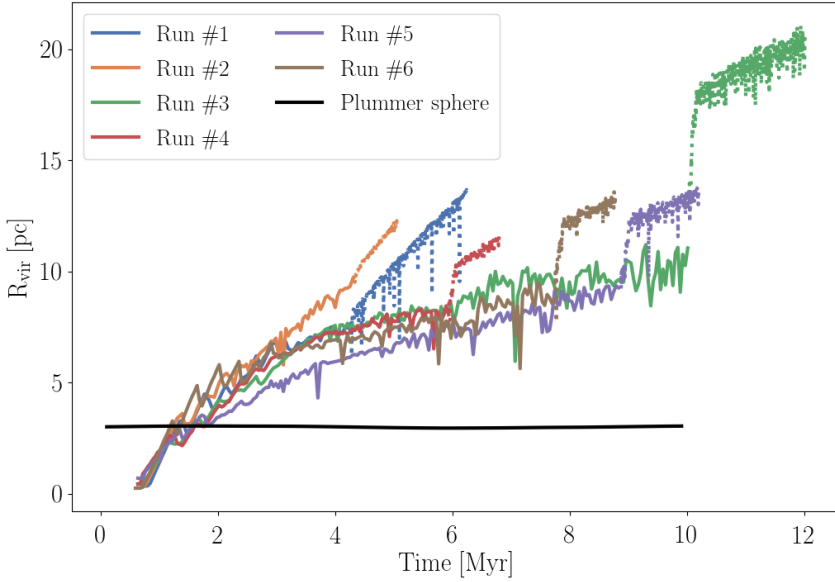


Figure 5.3: Virial radius of the simulations in time. The solid lines correspond to the virial radius while star formation is still ongoing, and the dotted lines after it has ended. The black line shows the virial radius in time of a Plummer sphere with 6,000 stars and initial virial radius 3 pc for comparison.

with lower Q , such as Corona Australis (Parker 2014), Cygnus OB2 (Wright et al. 2014), and Taurus (Cartwright & Whitworth 2004) are highly substructured. In observations of star-forming regions, Q might vary depending on membership uncertainty (Parker & Meyer 2012). This leads to some regions having more than one value of Q , such as Corona Australis, Chamaeleon, the ONC, Ophiuchus, and Upper Scorpio.

As can be seen in Figure 5.4, the final shapes of the clusters generated by our simulations are smoother than those of observed clusters. This might be caused by the fact that we do not take into account stellar winds and feedback from stellar processes, which might be important for the emergence of substructure (e.g. Mac Low & Klessen 2004; Hansen et al. 2012; Offner & Arce 2015). We expand on this discussion in Section 5.4.

Another way to quantify the structure of a star-forming region is by measuring its fractal

Table 5.1: Run number, final number of stars (N_*), time of the end of star formation ($t_{\text{end}}^{\text{SF}}$), Q parameter, and fractal dimension (F_d) for our simulation results.

| Region | N_* | $t_{\text{end}}^{\text{SF}}$ [Myr] | Q_{end} | F_d |
|--------|-------|------------------------------------|------------------|-------|
| Run #1 | 6289 | 4.25 | 0.82 | 1.6 |
| Run #2 | 6315 | 4.29 | 0.78 | 1.5 |
| Run #3 | 6162 | 10.01 | 0.71 | 1.7 |
| Run #4 | 6283 | 5.93 | 0.75 | 1.5 |
| Run #5 | 5691 | 8.87 | 0.74 | 1.4 |
| Run #6 | 6137 | 7.74 | 0.66 | 1.6 |

Table 5.2: Region name, number of stars (N_*), age, Q parameter, and fractal dimension (F_d) for our simulation results and observed regions. References: (a) Parker [2014]; (b) Neuhäuser & Forbrich [2008]; (c) Luhman et al. [2010]; (d) Luhman et al. [2016]; (e) Hillenbrand & Hartmann [1998]; (f) Cartwright & Whitworth [2004]; (g) Hartmann [2002]; (h) Kraus & Hillenbrand [2008]; (i) Simon [1997]; (j) Bontemps et al. [2001]; (k) Simon [1997]; (l) Wright et al. [2010]; (m) Wright et al. [2014]; (n) Carpenter et al. [2006]; (o) Luhman & Mamajek [2012]; (p) Sacco et al. [2017]; (q) Galli et al. [2020]; (r) Luhman & Esplin [2020]; (s) Luhman [2018].

| Region | N_* | Age [Myr] | Q | F_d |
|------------------------|--------------------|---------------------|---|--|
| Corona Australis (CrA) | $\sim 313^{(q)}$ | $\sim 1.0^{(a)}$ | $0.32^{(b)}, 0.38^{(a)}$ | - |
| NGC 1333 | $\sim 200^{(c)}$ | $\sim 1.0^{(c)}$ | $0.89^{(d)}$ | - |
| ONC | $\sim 1,000^{(e)}$ | $\sim 1.0^{(e)}$ | $0.87^{(e)}, 0.94^{(a)}$ | - |
| Taurus | $\sim 438^{(s)}$ | $\sim 1.0^{(f)}$ | $0.47^{(f)}$ | $1.5^{(f)}, 1.02 \pm 0.04^{(g)}, 1.049 \pm 0.007^{(h)}, 1.5 \pm 0.2^{(i)}$ |
| Trapezium | $\sim 1,000^{(e)}$ | $\sim 1.0^{(e)}$ | - | $1.5 \pm 0.2^{(i)}$ |
| Ophiuchus | $199^{(f)}$ | $1.6 \pm 1.4^{(j)}$ | $0.85^{(f)}, 0.58^{(a)}$ | $1.5 \pm 0.2^{(i)}$ |
| Chamaeleon I | $120^{(p)}$ | $2.5 \pm 0.5^{(k)}$ | $0.67^{(f)}, 0.71^{(a)}, 0.80 \pm 0.08^{(p)}$ | $2.25^{(f)}$ |
| Cygnus OB2 | $\sim 2,700^{(l)}$ | $4.0 \pm 1.0^{(l)}$ | $0.45 \pm 0.05^{(m)}$ | - |
| IC 348 | $\sim 500^{(c)}$ | $4.0 \pm 2.0^{(c)}$ | $0.98^{(d)}$ | - |
| Upper Scorpio | $\sim 1761^{(r)}$ | $8.0 \pm 3.0^{(n)}$ | $0.88^{(h)}, 0.75^{(a)}$ | $0.69 \pm 0.09^{(h)}$ |

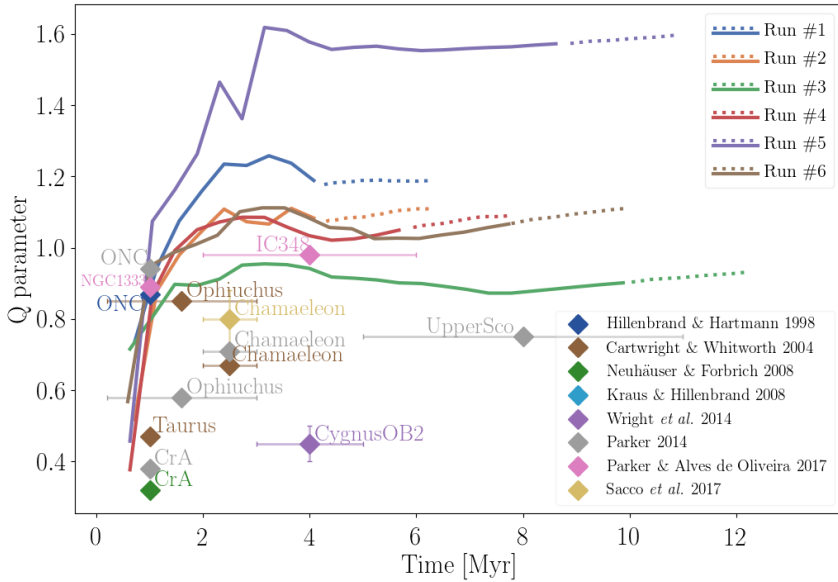


Figure 5.4: Q parameter of our simulations in time, and values for observed star-forming regions. The Q parameter in our simulations considers only stars with masses $M_* > 0.5 M_\odot$. The solid lines represent the times where star formation is still ongoing, and the dotted lines after all stars have been formed.

dimension, F_d . In Figure 5.5 we show the evolution of the fractal dimension in time for each simulation run, along with a Plummer sphere of 6,000 stars and initial virial radius 3 pc for comparison. The solid lines show the fractal dimension while star formation is still ongoing. The dotted lines show the evolution after the star formation process has ended. Once a region reaches a stable value of F_d , it remains the same up to the end of the simulation. We also show measured values of the fractal dimension for several observed regions. As with the Q parameter, when measuring the fractal dimension from observations the values might vary depending on membership, leading to regions with more than one value of F_d . In Table 5.2 we present the values of F_d for all observed regions.

From Figures 5.3, 5.4, and 5.5 it can be seen that after the gas in the regions is expelled, the

5.3.2. Disc masses

In Figure 5.6 we show the disc mass versus local number density for all simulation runs. The left panel shows the discs at the end of the star formation process. The right panel shows the discs at the end of the simulations, 2 Myr after star formation has finished. The color of each disc represents the time at which it was born. We calculate the local stellar density using the method by Casertano & Hut (1985) with the five nearest neighbours. While star formation is still ongoing, stars and discs form in regions spanning the whole range of stellar density. In particular, given our implementation of the star formation process with sink particles, many stars tend to form in regions of high stellar densities. Once the star formation process ends and the gas is expelled, the clusters expand to regain virial equilibrium. This brings about an overall decrease in local number density. As stars are no longer being formed,

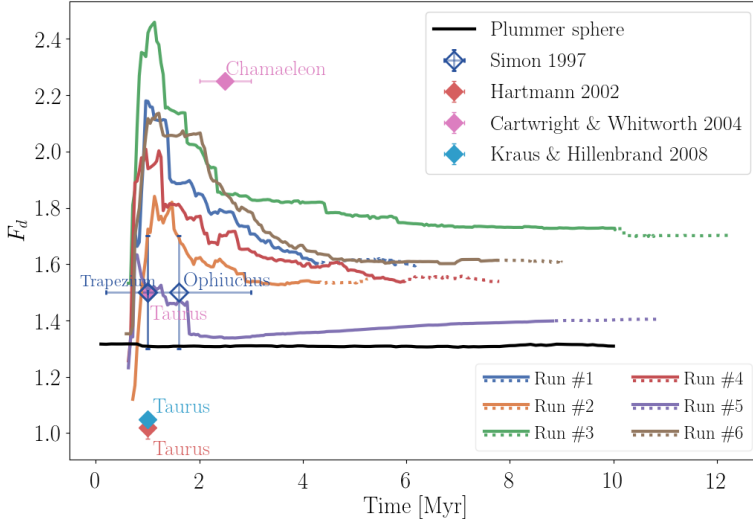


Figure 5.5: Fractal dimension of the simulations in time. The solid lines correspond to the fractal dimension while star formation is still ongoing, and the dotted lines after it has ended. The black line shows the fractal dimension in time of a Plummer sphere with 6,000 stars and initial virial radius 3 pc for comparison.

the areas of high stellar density become less populated, since discs are losing mass due to photoevaporation. By the end of the simulations, almost no discs are present in regions of local density $\gtrsim 10^5$ stars pc $^{-3}$. Even in low density regions, the maximum disc mass decreases from ~ 200 M $_{Jup}$ to ~ 100 M $_{Jup}$. Massive, large discs are present only in regions of low stellar density. The vertical ridges seen in the left panel of Figure 5.6 are a numerical effect on the measurement of disc mass and do not affect the overall results.

In Figure 5.7 we show the mean mass in time for the discs in each run. The solid lines show the times while star formation is still ongoing, and the dotted lines once the last star has formed. While star formation is still happening, there is variability in the mean disc mass given the fact that some discs are exposed to external photoevaporation and some new discs are being formed. However, once star formation stops, the decrease in disc mass is sharp.

In Figure 5.8 we present the binned mean gas and dust masses of the discs versus the projected local stellar number density, at the end of the simulations. The local stellar density is calculated in the same way as for Figure 5.6 but with the distances between stars projected to two dimensions. The binned mean is calculated using a rolling bin spanning 100 stars. The dust mass remains relatively constant across densities, whereas the gas mass shows a slight decrease with stellar density. This can be explained by the fact that some dust is lost in photoevaporation early on, but it soon becomes resilient to this effect. Gas, on the other hand, is consistently lost throughout the simulations.

In Figure 5.9 we show the cumulative distribution of disc dust masses at the end of star formation and at the end of the simulations. The lines show the mean values for all runs and the shaded areas show the standard deviation. By the end of star formation, all existing discs have dust masses $\gtrsim 50$ M $_{\oplus}$, up to ~ 500 M $_{\oplus}$. After 2 Myr of evolution, the distribution spans discs with dust masses from $\sim 10^{-1}$ M $_{\oplus}$ to ~ 400 M $_{\oplus}$. Around 80% of the final discs have dust masses higher than 10 M $_{\oplus}$, which is a lower limit mass for the formation of rocky

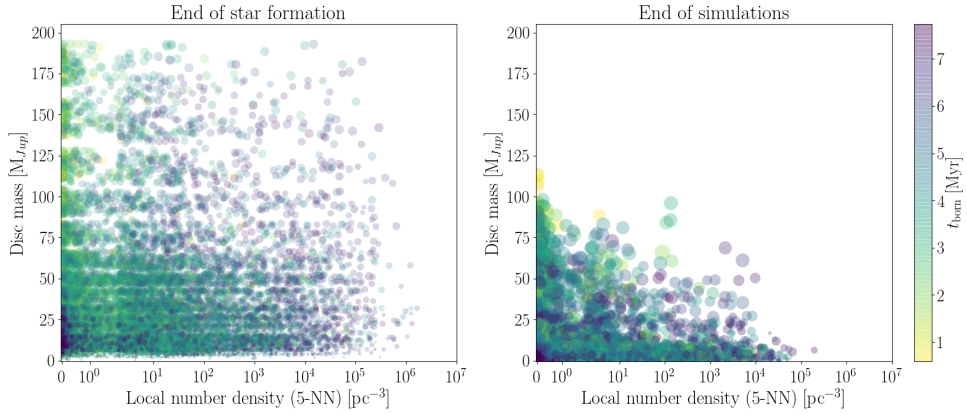


Figure 5.6: Disc mass versus local number density for all discs in all simulation runs. The left panel shows the discs at the end of the star formation process. The right panel shows the discs at the end of the simulations, 2 Myr after star formation has finished. The size of the points is proportional to the disc radius. The color shows the time at which each disc was born.

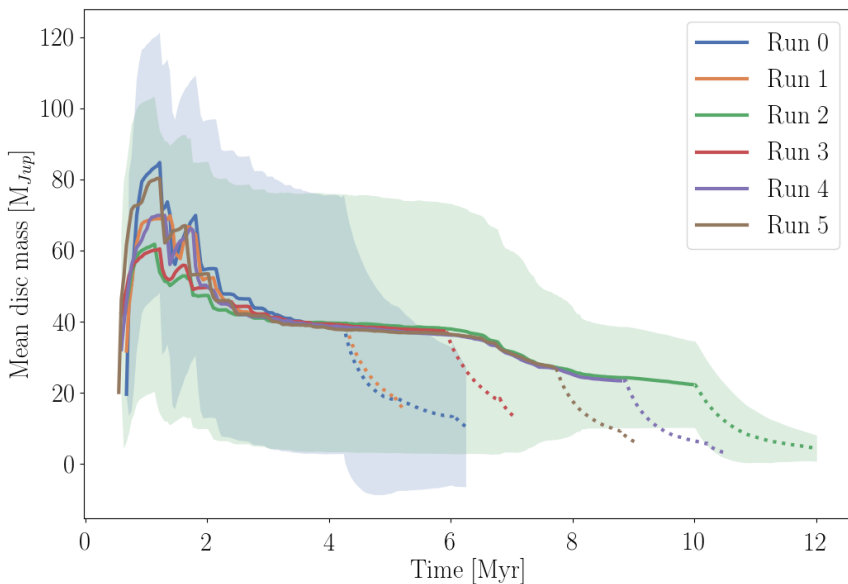


Figure 5.7: Mean disc mass in time for each simulation run. The solid lines correspond to ongoing star formation, and the dotted lines after it has ended. The standard deviation in two of the runs is shown as an example; the other runs have standard deviations of similar magnitude.

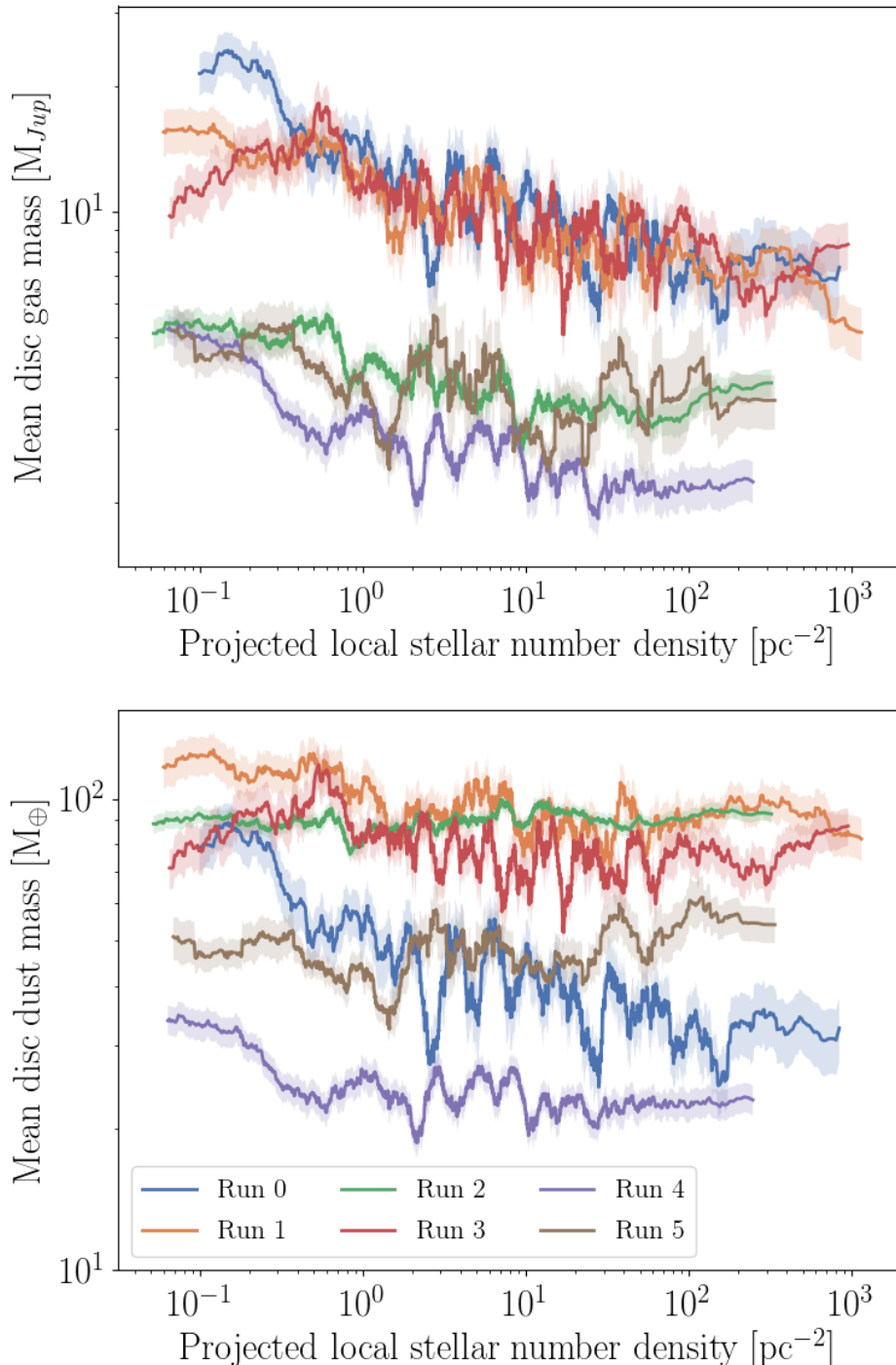


Figure 5.8: Binned mean gas mass (top panel, M_{Jup}) and dust mass (bottom panel, M_{\oplus}) at the end of the simulations versus projected local stellar density. The binned mean is calculated using a rolling bin spanning 100 stars. The local stellar number density is calculated as specified in section 5.3.2.

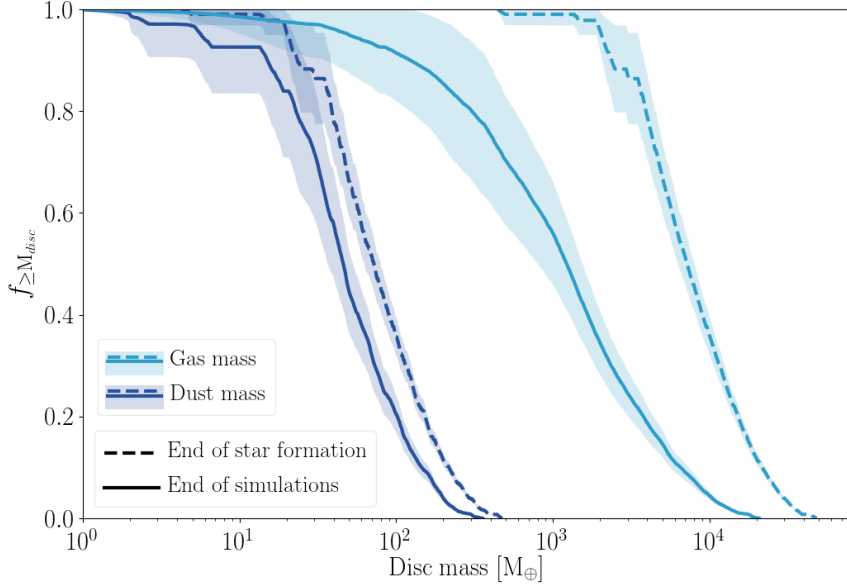


Figure 5.9: Cumulative distribution of disc dust and gas masses at the end of star formation (dashed lines) and at the end of the simulations (solid lines). The lines show the mean values for all runs and the shaded areas show the standard deviation.

planets and the cores of gas giants (Ansdel et al. 2016). The masses obtained in the present simulations are higher than those in Concha-Ramírez et al. (2021). This suggests that the extended period of star formation might play a role in allowing massive discs to survive for longer. We expand on this discussion in Section 5.4.

In Figure 5.10 we show the evolution of the mean dust-to-gas disc mass ratio, or $\delta = M_{dust}/M_{gas}$ in time, aggregated for all simulation runs. By definition, the discs in the simulations are initialized with a value of $\delta = 10^{-2}$. As gas mass is lost from the discs due to photoevaporation, this ratio tends to increase in time. By the end of the simulations the mean value is $\delta \approx 3 \times 10^{-2}$. The dust quickly becomes resistant to photoevaporation, but gas continues being removed from the discs.

5.4. Discussion

In previous work (Concha-Ramírez et al. 2019b, 2021) we performed simulations of star clusters where stars with masses $M_* \leq 1.9 M_{\odot}$ have circumstellar discs. These discs were subject to viscous evolution and external photoevaporation. We assumed the dust mass to be 1% of the total disc mass, and that only gas mass is removed through photoevaporation. In those previous simulations we found that discs get depleted of mass quickly enough so that $\sim 60\%$ to 90% of them (depending on the stellar density of the region) are completely dispersed within 2 Myr of evolution. The initial spatial distribution of the stars were Plummer spheres, and all stars were formed at the same time and evolved for the 2 Myr that the simulations lasted.

In the present work we improve our previous model in two main ways. First, we imple-

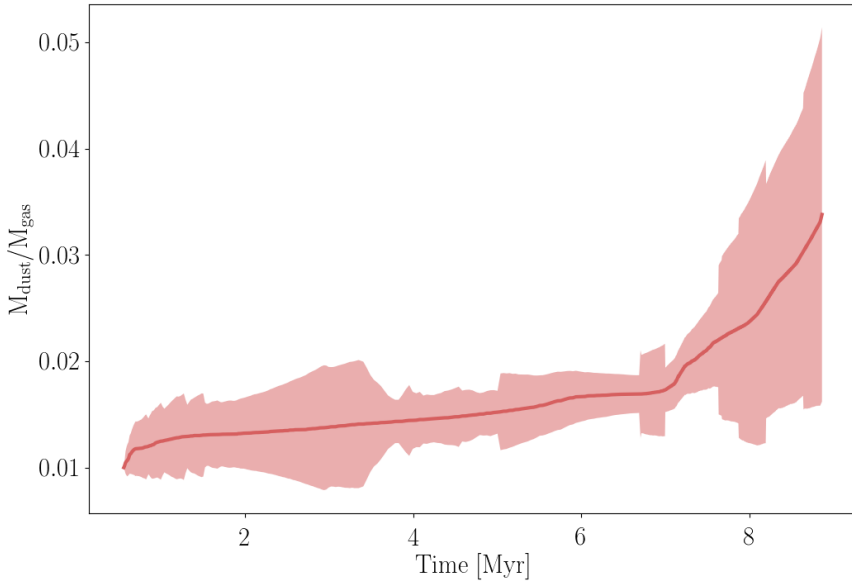


Figure 5.10: Mean $M_{\text{dust}}/M_{\text{gas}}$ versus time.

ment a simple model of molecular cloud collapse and star formation. This results in the stars not having spherical initial distributions, and in new stars being added to the simulation in time throughout an extended star formation process. Second, we implement a simple model for the evolution of the dust in the discs (Haworth et al. 2018a), in order to follow its progression directly and not simply approximate it to 1% of the total mass. We also implement internal photoevaporation as an additional means to remove gas mass from the discs.

During the first few million years of evolution the star formation process is ongoing and, as discs lose mass due to photoevaporation, the new discs that are constantly being formed keep the mean mass of the overall population relatively unaffected (Figure 5.7). As soon as this constant replenishing of stars and discs stops, the mean mass of the discs quickly drops. This is consistent with the results from Concha-Ramírez et al. (2019b) and Concha-Ramírez et al. (2021). However, disc masses at the end of the simulations (see Figure 5.8 and the bottom panel of Figure 5.6) are higher than in our previous simulations. In particular, unlike in our previous calculations, the dust masses in this work do not diminish as strongly with increasing stellar density.

This discrepancy can be explained by an interplay of different processes. The dust model that we implement is such that some dust is initially trapped in the photoevaporation wind. As the discs continue to evolve, the dust becomes resistant to photoevaporation and it is mostly gas mass that is lost from the discs. After a few hundred thousand years of evolution, the amount of dust mass becomes independent of the radiation received by the discs. The gas mass does decrease with increasing stellar density (see top panel of Figure 5.8) and in time (Figure 5.7). Ansdell et al. (2016) propose that a rapid depletion of gas mass in discs can lead to the observed characteristics of exoplanet populations. Traditional theories of planet formation suggest that $\sim 10M_{\oplus}$ cores should be able to rapidly accrete gaseous envelopes, and reach masses of $\sim 1M_{Jup}$ within ~ 0.1 Myr when gas is still available in the disc. How-

ever, observational surveys show that “super-Earths”, or intermediate-mass rocky planets, are about an order of magnitude more common than gas giants (e.g. Petigura et al. 2013). Ansdell et al. (2016) suggest that, if typical $\sim 10M_{\oplus}$ cores form in discs which are already depleted of gas, this would result in the observed discrepancy in the number of planetary types. The evolution of dust and gas disc masses in our simulations suggests a similar context for planet formation. On the other hand, Sellek et al. (2020) propose that photoevaporation of light dust grains can lead to a more efficient radial drift on large grains, meaning that the dust-to-gas ratio is not greatly increased. While our current model improves previous implementations of this ratio, further modelling of the dust evolution is needed to get a better picture of how it affects the material available for planet formation.

Another mechanism which affects our results is the long-lived star formation process. In our previous work all the stars and discs were formed at the start of the simulations and evolved for the same amount of time. In our current simulations, some discs are destroyed while new stars with discs are forming constantly. By the end of the simulations, the stars span ages from ~ 2 Myr (the simulations evolve for 2 Myr after star formation has ended, so the last stars to form are slightly older than this) to ~ 12 Myr, if we consider the first stars formed in our longest-running realization as the eldest ones. In Concha-Ramírez et al. (2019b) we show that around 60% of discs are destroyed by photoevaporation within the first 100,000 years of evolution in a region of stellar density ~ 100 stars pc $^{-3}$. Similar rapid effects of photoevaporation are found in Concha-Ramírez et al. (2021). While discs are also destroyed quickly in the present simulations, the fact that discs are constantly being added to the region helps keep the disc number and disc masses higher. Massive, radiating stars also do not form all at the same time, and because of the way we implement the star formation process (see Section 5.2.1), they tend to form later in our simulations than low mass stars. This also gives discs more time to evolve, and the older discs will be immersed in lower radiation fields during most of their life than the younger discs.

The gas present in the clusters during the star formation process also affects the final masses of the discs in our simulations. While we do not take into account the dampening effects of the gas on radiation, the gas in our simulations does have important consequences for the dynamics of the regions. As can be seen in Figure 5.3, after star formation ends and the gas is expelled, the clusters quickly expand to regain virial equilibrium. This expansion leads to a decrease in the local stellar densities and an increase in the distance between stars, both of which reduce the amount of radiation received by the discs. Considering the absorption of radiation by the gas results in a protective effect for the discs, with the gas actively shielding them from external photoevaporation. The presence of gas is an important point determined by Winter et al. (2019a) to reproduce the disc population of Cygnus OB2, and to explain the so-called ‘proplyd lifetime problem’ discussed below. Observational surveys also suggest the presence of gas being protective for the discs (e.g. van Terwisga et al. 2020). Our model shows that the effects of the gas over the dynamics of the regions could also have an important effect in the final disc fractions and disc mass distributions.

Our present results suggest that the strong trends seen in Concha-Ramírez et al. (2019b) and Concha-Ramírez et al. (2021) of disc masses diminishing in time due to external photoevaporation might be a temporary effect. The low mass disc distributions can be “washed-out” in time if the star formation process lasts for an extended period of time. Massive discs that are born late in the star formation process, that is, shortly before the gas in our simulations is expelled, will be protected by the effects of external photoevaporation by the expansion of the clusters as they regain virial equilibrium. In our simulations, the moment when a disc is born is crucial for determining its long term survival and planet-forming potential, even more so than its initial mass.

The ‘proplyd lifetime problem’ is the name given to the fact that circumstellar discs are observed in regions where external radiation should have evaporated them already, in particular in the ONC. Discs observed within 0.3 pc of the massive star $\theta^1 C$ Ori are exposed to strong radiation fields ($\sim 10^4 G_0$, e.g. O’dell & Wen 1994). The fact that there are still discs observed in the vicinity of the star suggest that either the discs were initially extremely massive ($\gtrsim 1 M_\odot$), or that $\theta^1 C$ Ori is younger than 0.1 Myr. Given that such massive discs are gravitationally unstable, and that the stellar age distribution in the ONC is ~ 1 Myr (e.g. Da Rio et al. 2010, 2012), there must be other factors at play for these discs to have survived. Störzer & Hollenbach (1999) suggest that these discs are observed at a particular moment: they are passing close to the center of the ONC, but they have spent the majority of their lives in regions of lower background radiation fields. Scally & Clarke (2001) model the inner area of the ONC and propose that the type of orbits necessary for the hypothesis of Störzer & Hollenbach (1999) to be feasible are not dynamically possible in such regions. However, a short-lived trajectory through high stellar density regions might not be the only way to explain the presence of massive discs in the center of the ONC. Winter et al. (2019b) propose that the solution to this problem is a combination of several mechanisms, one of them being extended periods of star formation. While the survival of discs in star forming regions with strong radiation background depends on a series of different factors, our results show that star formation that is sustained in time could be an explanation for massive discs being detected in the vicinity of massive stars.

The spatial distribution of star-forming regions also plays an important role on disc mass distributions. In previous work we performed simulations starting from a spherical star cluster. In this work we model the collapse of a molecular cloud to improve on these initial conditions. The resulting clusters, however, are on average smoother than observed star-forming regions (see Figure 5.4). Stellar feedback, in particular stellar winds and jets from protostars, can have an important effect on the morphology of star-forming regions (e.g. Mac Low & Klessen 2004; Hansen et al. 2012; Offner & Arce 2015). There is also observational and numerical evidence that the filaments and fibres observed in star-forming regions are shaped by magnetic fields (e.g. Heyer et al. 2016; Tritsis & Tassis 2016; Chen et al. 2017; Ballesteros-Paredes et al. 2020). Considering these mechanisms could increase the amount of substructure in the clusters and affect the final distributions of disc masses.

5.5. Summary and conclusions

We perform simulations of molecular cloud collapse and star formation. We begin with molecular clouds of mass $10^4 M_\odot$ and a star formation efficiency of 30%. The star formation process ends when the star formation efficiency has been reached. The leftover gas is then removed instantaneously and the simulations continue. Stars with masses $M_* \leq 1.9 M_\odot$ have circumstellar discs, and massive stars ($M_* > 1.9 M_\odot$) emit UV radiation. The discs are subject to internal photoevaporation, external photoevaporation, dynamical truncations, and viscous evolution. We also implement a model for the evolution of dust inside the discs. We run the simulations for 2 Myr after the last star has formed. We conclude that:

1. Extended periods of star formation allow for relatively massive ($M_{\text{gas}} \sim 100 M_{Jup}$, $M_{\text{dust}} \sim 100 M_\oplus$) discs to survive the effects of photoevaporation for at least 2 Myr.
2. The discs that make it to the end of our simulations are the ones that were born later (after ~ 4 Myr) in the star formation process.
3. While photoevaporation removes gas from the discs, dust quickly becomes resistant to

- photoevaporation and the $M_{\text{dust}}/M_{\text{gas}}$ ratio increases with time. This might allow discs to keep enough mass to form rocky planets, even when depleted of gas.
4. The presence of gas plays an important role in the survival of circumstellar discs, not just because it can absorb radiation from massive stars but also because it affects the dynamics of the regions.
 5. Extended periods of star formation can allow for massive discs to be detected in areas with strong radiation fields.

Our results show that, while photoevaporation is an important process for the depletion of disc masses, other factors such as the morphology of the star-forming regions and the length of the star formation process can allow for circumstellar discs to survive for long periods of time, and to remain massive enough to form planets. This could help explain the great variety of disc mass distributions observed in star-forming regions of different ages and configurations, and could also be a factor in solving the ‘proplyd-lifetime problem’, where massive discs are observed in regions of high stellar density and background radiation.

Acknowledgements

F.C.-R. would like to thank Steven Rieder and the Star formation and protoplanetary disc group at Leiden Observatory for helpful discussions and insights. This work was carried out on the Dutch national e-infrastructure with the support of SURF Cooperative. This work was performed using resources provided by the Academic Leiden Interdisciplinary Cluster Environment (ALICE).

Data availability

The data underlying this article are available at <https://doi.org/10.5281/zenodo.4436316>

Software

The present works makes use of the following software: AMUSE (Portegies Zwart et al. 2013; Pelupessy et al. 2013), Fi (Pelupessy et al. 2004), ph4, Bridge (Fujii et al. 2007; Portegies Zwart et al. 2020), VADER (Krumholz & Forbes 2015), numpy (Van Der Walt et al. 2011), scipy (Virtanen et al. 2019), matplotlib (Hunter 2007), and makecite (Price-Whelan et al. 2018).

Energy consumption

The simulations presented in this work took ~ 10 days to run and used 10 cores each. Accounting for only the 6 runs shown on this paper (not considering the many test runs), this amounts to 14,400 CPU hours. Considering 12 Wh for a CPU, this results in ~ 173 kWh. Using the conversion factor 0.283 kWh/kg (Portegies Zwart 2020), this results in ~ 611 kg of CO₂. Estimating the number of tests to be of the same order of magnitude of the final runs, the total CO₂ output of the computations performed for this paper are ~ 1 tonne.

* * *

Bibliography

- Adams F. C., 2010, *ARA&A*, 48, 47
- Adams F. C., Myers P. C., 2001, *ApJ*, 553, 744
- Adams F. C., Hollenbach D., Laughlin G., Gorti U., 2004, *ApJ*, 611, 360
- Adams F. C., Proszkow E. M., Fatuzzo M., Myers P. C., 2006, *ApJ*, 641, 504
- Akeson R. L., Jensen E. L. N., 2014, *ApJ*, 784, 62
- Akeson R. L., Jensen E. L. N., Carpenter J., Ricci L., Laos S., Nogueira N. F., Suen-Lewis E. M., 2019, *ApJ*, 872, 158
- Alcalá J. M., et al., 2014, *A&A*, 561, A2
- Ali A. A., Harries T. J., 2019, *MNRAS*, 487, 4890
- Anderson K. R., Adams F. C., Calvet N., 2013, *ApJ*, 774, 9
- Andrews S. M., Williams J. P., 2005, *ApJ*, 631, 1134
- Andrews S. M., Wilner D. J., Hughes A. M., Qi C., Dullemond C. P., 2010, *ApJ*, 723, 1241
- Andrews S. M., Rosenfeld K. A., Kraus A. L., Wilner D. J., 2013, *ApJ*, 771, 129
- Andrews S. M., et al., 2016, *ApJ*, 820, L40
- Ansdell M., et al., 2016, *ApJ*, 828, 46
- Ansdell M., Williams J. P., Manara C. F., Miotello A., Facchini S., van der Marel N., Testi L., van Dishoeck E. F., 2017, *AJ*, 153, 240
- Ansdell M., et al., 2018, *ApJ*, 859, 21
- Ansdell M., et al., 2020, *AJ*, 160, 248
- Antoniucci S., García López R., Nisini B., Caratti o Garatti A., Giannini T., Lorenzetti D., 2014, *A&A*, 572, A62
- Appenzeller I., Tscharnutter W., 1975, *A&A*, 40, 397
- Armitage P. J., 2000, *A&A*, 362, 968
- Armitage P. J., 2011, *ARA&A*, 49, 195
- Armitage P. J., Livio M., Pringle J. E., 2001, *MNRAS*, 324, 705

- Bae J., Pinilla P., Birnstiel T., 2018, *ApJ*, 864, L26
- Baldry I. K., et al., 2002, *The Astrophysical Journal*, 569, 582
- Ballesteros-Paredes J., et al., 2020, *Space Science Reviews*, 216, 76
- Bally J., 2016, *ARA&A*, 54, 491
- Balog Z., Muzerolle J., Rieke G. H., Su K. Y. L., Young E. T., Megeath S. T., 2007, *ApJ*, 660, 1532
- Barenfeld S. A., Carpenter J. M., Ricci L., Isella A., 2016, *ApJ*, 827, 142
- Barenfeld S. A., Carpenter J. M., Sargent A. I., Isella A., Ricci L., 2017, *ApJ*, 851, 85
- Bate M. R., 1998, *ApJ*, 508, L95
- Bate M. R., 2010, *MNRAS*, 404, L79
- Bate M. R., 2011, *MNRAS*, 417, 2036
- Bate M. R., 2012, *MNRAS*, 419, 3115
- Bate M. R., Bonnell I. A., Bromm V., 2003, *MNRAS*, 339, 577
- Baugh C. M., et al., 2019, *MNRAS*, 483, 4922
- Baumgardt H., Kroupa P., 2007, *MNRAS*, 380, 1589
- Baumgardt H., Makino J., 2003, *MNRAS*, 340, 227
- Bergin E. A., Williams J. P., 2018, arXiv e-prints, p. arXiv:1807.09631
- Bhandare A., Pfalzner S., 2019, *Computational Astrophysics and Cosmology*, 6, 3
- Bhandare A., Breslau A., Pfalzner S., 2016, *A&A*, 594, A53
- Birnstiel T., Andrews S. M., 2013, *ApJ*, 780, 153
- Birnstiel T., Dullemond C. P., Brauer F., 2010, *A&A*, 513, A79
- Bodenheimer P., Burkert A., Klein R. I., Boss A. P., 2000, *Protostars and Planets IV*, p. 675
- Bohlin R. C., Savage B. D., Drake J. F., 1978, *ApJ*, 224, 132
- Bonnell I., Kroupa P., 1998, arXiv Astrophysics e-prints, pp arXiv:astro-ph/9802306
- Bontemps S., et al., 2001, *A&A*, 372, 173
- Boulanger F., Bronfman L., Dame T. M., Thaddeus P., 1998, *A&A*, 332, 273
- Boylan-Kolchin M., Springel V., White S. D. M., Jenkins A., Lemson G., 2009, *MNRAS*, 398, 1150
- Breslau A., Steinhäusen M., Vincke K., Pfalzner S., 2014, *A&A*, 565, A130
- Bressert E., et al., 2010, *MNRAS*, 409, L54
- Brown A. G. A., et al., 2018, *A&A*, 616, A1
- Caballero J. A., 2008, *MNRAS*, 383, 375

- Cabrit S., Pety J., Pesenti N., Dougados C., 2006, *A&A*, 452, 897
- Cai M. X., Kouwenhoven M. B. N., Portegies Zwart S. F., Spurzem R., 2017, *MNRAS*, 470, 4337
- Cai M. X., Portegies Zwart S., Kouwenhoven M. B. N., Spurzem R., 2019, *MNRAS*, 489, 4311
- Carmona A., et al., 2008, *A&A*, 477, 839
- Carpenter J. M., Mamajek E. E., Hillenbrand L. A., Meyer M. R., 2006, *ApJ*, 651, L49
- Carpenter J. M., Mamajek E. E., Hillenbrand L. A., Meyer M. R., 2009, *ApJ*, 705, 1646
- Cartwright A., Whitworth A. P., 2004, *MNRAS*, 348, 589
- Casertano S., Hut P., 1985, *ApJ*, 298, 80
- Chen C.-Y., Li Z.-Y., King P. K., Fissel L. M., 2017, *ApJ*, 847, 140
- Chevalier R. A., 2000, *ApJ*, 538, L151
- Chevance M., et al., 2020, *Space Science Reviews*, 216, 50
- Christiaens V., Casassus S., Perez S., van der Plas G., Ménard F., 2014, *ApJ*, 785, L12
- Clarke C. J., 2007, *MNRAS*, 376, 1350
- Clarke C. J., Pringle J. E., 1991, *MNRAS*, 249, 588
- Clarke C. J., Pringle J. E., 1993, *MNRAS*, 261, 190
- Clarke C. J., Bonnell I. A., Hillenbrand L. A., 2000, Protostars and Planets IV, p. 151
- Clarke C. J., Gendrin A., Sotomayor M., 2001, *MNRAS*, 328, 485
- Close J. L., Pittard J. M., 2017, *MNRAS*, 469, 1117
- Colless M., et al., 2001, *Monthly Notices of the Royal Astronomical Society*, 328, 1039
- Comerón F., 2008, in Reipurth B., ed., , Handbook of Star Forming Regions, Volume II: The Southern Sky. ASP Monograph Publications, USA
- Concha-Ramírez F., Vaher E., Portegies Zwart S., 2019a, *MNRAS*, 482, 732
- Concha-Ramírez F., Wilhelm M. J. C., Portegies Zwart S., Haworth T. J., 2019b, *MNRAS*, 490, 5678
- Concha-Ramírez F., Wilhelm M. J. C., Zwart S. P., van Terwisga S. E., Hacar A., 2021, *MNRAS*, 501, 1782
- Cox E. G., et al., 2017, *ApJ*, 851, 83
- Cuello N., et al., 2019, *MNRAS*, 483, 4114
- Da Rio N., Robberto M., Soderblom D. R., Panagia N., Hillenbrand L. A., Palla F., Stassun K. G., 2010, *ApJ*, 722, 1092
- Da Rio N., Robberto M., Hillenbrand L. A., Henning T., Stassun K. G., 2012, *ApJ*, 748, 14
- Dai F., Facchini S., Clarke C. J., Haworth T. J., 2015, *MNRAS*, 449, 1996

- Dinnbier F., Kroupa P., 2020, *A&A*, 640, A84
- Dobbs C. L., Liow K. Y., Rieder S., 2020, *MNRAS*, 496, L1
- Dong R., Liu S.-Y., Fung J., 2019, *ApJ*, 870, 72
- Dunham M. M., et al., 2015, *ApJS*, 220, 11
- Eisner J. A., Carpenter J. M., 2006, *ApJ*, 641, 1162
- Eisner J. A., Plambeck R. L., Carpenter J. M., Corder S. A., Qi C., Wilner D., 2008, *ApJ*, 683, 304
- Eisner J. A., et al., 2018, *ApJ*, 860, 77
- Elmegreen B. G., Efremov Y. N., 1997, *ApJ*, 480, 235
- Elmegreen B. G., Falgarone E., 1996, *ApJ*, 471, 816
- Elmegreen B. G., Scalo J., 2004, *ARA&A*, 42, 211
- Elmegreen B. G., Efremov Y., Pudritz R. E., Zinnecker H., 2000, Protostars and Planets IV, p. 179
- Ercolano B., Clarke C. J., Hall A. C., 2011, *MNRAS*, 410, 671
- Evans N. J. I., et al., 2009, *ApJS*, 181, 321
- Facchini S., Clarke C. J., Bisbas T. G., 2016, *MNRAS*, 457, 3593
- Facchini S., Birnstiel T., Bruderer S., Dishoeck E. F. v., 2017, *A&A*, 605, A16
- Falgarone E., Phillips T. G., 1991, Proceedings of the International Astronomical Union, 147, 119
- Falgarone E., Phillips T. G., Walker C. K., 1991, *ApJ*, 378, 186
- Fall S. M., Krumholz M. R., Matzner C. D., 2010, *ApJ*, 710, L142
- Fang M., et al., 2012, *A&A*, 539, A119
- Fatuzzo M., Adams F. C., 2008, *ApJ*, 675, 1361
- Faucher-Giguère C.-A., Kaspi V. M., 2006, *ApJ*, 643, 332
- Field G. B., Somerville W. B., Dressler K., 1966, *ARA&A*, 4, 207
- Field G. B., Blackman E. G., Keto E. R., 2008, *MNRAS*, 385, 181
- Flaccomio E., Micela G., Sciortino S., 2012, *A&A*, 548, A85
- Font A. S., McCarthy I. G., Johnstone D., Ballantyne D. R., 2004, *ApJ*, 607, 890
- Forbes D. A., et al., 2018, *Proceedings of the Royal Society A: Mathematical, Physical and Engineering Sciences*, 474, 20170616
- Francis L., van der Marel N., 2020, *ApJ*, 892, 111
- Fujii M. S., Portegies Zwart S., 2011, *Science*, 334, 1380

- Fujii M. S., Portegies Zwart S., 2015, *MNRAS*, 449, 726
- Fujii M. S., Portegies Zwart S., 2016, *ApJ*, 817, 4
- Fujii M., Iwasawa M., Funato Y., Makino J., 2007, *Publications of the Astronomical Society of Japan*, 59, 1095
- Galli P. A. B., Bouy H., Olivares J., Miret-Roig N., Sarro L. M., Barrado D., Berihuete A., Brandner W., 2020, *A&A*, 634, A98
- Getman K. V., Feigelson E. D., Kuhn M. A., 2014, *ApJ*, 787, 109
- Gieles M., Portegies Zwart S. F., 2011, *MNRAS*, 410, L6
- Gnedin O. Y., Ostriker J. P., Tremaine S., 2014, *ApJ*, 785, 71
- Goldsmith P. F., Bergin E. A., Lis D. C., 1997, *ApJ*, 491, 615
- Goodwin S. P., 1997, *MNRAS*, 284, 785
- Goodwin S. P., Whitworth A. P., 2004, *A&A*, 413, 929
- Gorti U., Hollenbach D., 2009, *ApJ*, 690, 1539
- Gorti U., Dullemond C. P., Hollenbach D., 2009, *ApJ*, 705, 1237–1251
- Gorti U., Hollenbach D., Dullemond C. P., 2015, *ApJ*, 804, 29
- Gorti U., Liseau R., Sandor Z., Clarke C., 2016, *Space Science Reviews*, 205, 125
- Gounelle M., Meibom A., 2008, *ApJ*, 680, 781
- Greaves J. S., Rice W. K. M., 2010, *MNRAS*, 407, 1981
- Grudi M. Y., Hopkins P. F., Faucher-Gigure C.-A., Quataert E., Murray N., Kerea D., 2018, *MNRAS*, 475, 3511
- Guarcello M. G., Prisinzano L., Micela G., Damiani F., Peres G., Sciortino S., 2007, *A&A*, 462, 245
- Guarcello M. G., Micela G., Damiani F., Peres G., Prisinzano L., Sciortino S., 2009, *A&A*, 496, 453
- Guarcello M. G., Damiani F., Micela G., Peres G., Prisinzano L., Sciortino S., 2010, *A&A*, 521, A18
- Guarcello M. G., et al., 2016, arXiv:1605.01773 [astro-ph]
- Gunn J. E., Gott J. Richard I., 1972, *ApJ*, 176, 1
- Gutermuth R. A., et al., 2008, *ApJ*, 674, 336
- Habing H. J., 1968, *Bulletin of the Astronomical Institutes of the Netherlands*, 19, 421
- Hacar A., Tafalla M., Kauffmann J., Kovacs A., 2013, *A&A*, 554, A55
- Hacar A., Tafalla M., Forbrich J., Alves J., Meingast S., Grossschedl J., Teixeira P. S., 2018, *A&A*, 610, A77

- Haisch K. E. J., Lada E. A., Lada C. J., 2001, *ApJ*, 553, L153
- Hall S. M., 1997, *MNRAS*, 287, 148
- Hall S. M., Clarke C. J., Pringle J. E., 1996, *MNRAS*, 278, 303
- Halley E., 1715, Philosophical Transactions of the Royal Society of London Series I, 29, 390
- Hansen C. E., Klein R. I., McKee C. F., Fisher R. T., 2012, *ApJ*, 747, 22
- Harris R. J., Andrews S. M., Wilner D. J., Kraus A. L., 2012, *ApJ*, 751, 115
- Hartmann L., 2002, *ApJ*, 578, 914
- Hartmann L., Calvet N., Gullbring E., D'Alessio P., 1998, *ApJ*, 495, 385
- Hartmann L., Herczeg G., Calvet N., 2016, *ARA&A*, 54, 135
- Haworth T. J., Clarke C. J., 2019, *MNRAS*, 485, 3895
- Haworth T. J., Owen J. E., 2020, *MNRAS*, 492, 5030
- Haworth T. J., Boubert D., Facchini S., Bisbas T. G., Clarke C. J., 2016, *MNRAS*, 463, 3616
- Haworth T. J., Facchini S., Clarke C. J., Cleeves L. I., 2017, *MNRAS*, 468, L108
- Haworth T. J., Facchini S., Clarke C. J., Mohanty S., 2018a, *MNRAS*, 475, 5460
- Haworth T. J., Clarke C. J., Rahman W., Winter A. J., Facchini S., 2018b, *MNRAS*, 481, 452
- Hernández J., et al., 2007, *ApJ*, 671, 1784
- Hernquist L., Katz N., Weinberg D. H., Miralda-Escudé J., 1996, *ApJ*, 457, L51
- Heyer M., Goldsmith P. F., Yıldız U. A., Snell R. L., Falgarone E., Pineda J. L., 2016, *MNRAS*, 461, 3918
- Hillenbrand L. A., 1997, *AJ*, 113, 1733
- Hillenbrand L. A., 2008, *Physica Scripta*, T130, 014024
- Hillenbrand L. A., Hartmann L. W., 1998, *ApJ*, 492, 540
- Hollenbach D., Johnstone D., Lizano S., Shu F., 1994, *ApJ*, 428, 654
- Hollenbach D. J., Yorke H. W., Johnstone D., 2000, Protostars and Planets IV, p. 401
- Hoyle F., 1953, *ApJ*, 118, 513
- Huang J., et al., 2020, *ApJ*, 891, 48
- Hueso R., Guillot T., 2005, *A&A*, 442, 703
- Hunter C., 1964, *ApJ*, 139, 570
- Hunter C., 1977, *ApJ*, 218, 834
- Hunter J. D., 2007, *Computing in Science & Engineering*, 9, 90
- Hurley J. R., Pols O. R., Tout C. A., 2000, *MNRAS*, 315, 543

- Isella A., Carpenter J. M., Sargent A. I., 2009, *ApJ*, 701, 260
- Isella A., Pérez L. M., Carpenter J. M., 2012, *ApJ*, 747, 136
- Jeans J. H., 1902, *Philosophical Transactions of the Royal Society of London Series A*, 199, 1
- Jílková L., Portegies Zwart S., Pijloo T., Hammer M., 2015, *MNRAS*, 453, 3157
- Jílková L., Hamers A. S., Hammer M., Portegies Zwart S., 2016, *MNRAS*, 457, 4218
- Johnstone D., Hollenbach D., Bally J., 1998, *ApJ*, 499, 758
- Kant I., 1755, Zeitz, Bei W. Webel, 1798. Neue aufl.
- Kim J. S., Clarke C. J., Fang M., Facchini S., 2016, *ApJ*, 826, L15
- King I. R., 1966, *AJ*, 71, 64
- King R. R., Goodwin S. P., Parker R. J., Patience J., 2012, *MNRAS*, 427, 2636
- Klessen R. S., Burkert A., 2000, *ApJS*, 128, 287
- Klessen R. S., Burkert A., Bate M. R., 1998, *ApJ*, 501, L205
- Klessen R. S., Heitsch F., Mac Low M.-M., 2000, *ApJ*, 535, 887
- Klypin A., Trujillo-Gomez S., Primack J., 2011, *ApJ*, 740, 102
- Korycansky D. G., Papaloizou J. C. B., 1995, *MNRAS*, 274, 85
- Kratter K., Lodato G., 2016, *ARA&A*, 54, 271
- Kraus A. L., Hillenbrand L. A., 2008, *ApJ*, 686, L111
- Kraus S., et al., 2020, *Science*, 369, 1233
- Krause M. G. H., et al., 2020, *Space Science Reviews*, 216, 64
- Kroupa P., 2001, *MNRAS*, 322, 231
- Kruijssen J. M. D., 2009, *A&A*, 507, 1409
- Kruijssen J. M. D., 2014, *Classical and Quantum Gravity*, 31, 244006
- Kruijssen J. M. D., Maschberger T., Moeckel N., Clarke C. J., Bastian N., Bonnell I. A., 2012, *MNRAS*, 419, 841
- Krumholz M. R., Forbes J. C., 2015, *Astronomy and Computing*, 11, 1
- Krumholz M. R., McKee C. F., 2020, *MNRAS*, 494, 624
- Kuffmeier M., Haugbole T., Nordlund A., 2017, *ApJ*, 846, 7
- Kuffmeier M., Goicovic F. G., Dullemond C. P., 2020, *A&A*, 633, A3
- Lada C. J., Lada E. A., 1991, The formation and evolution of star clusters, 13, 3
- Lada E. A., Lada C. J., 1995, *ApJ*, 109, 1682
- Lada C. J., Lada E. A., 2003, *ARA&A*, 41, 57

- Lada C. J., Margulis M., Dearborn D., 1984, *ApJ*, 285, 141
- Lada E. A., Strom K. M., Myers P. C., 1993, *Protostars and Planets III*, pp 245–277
- Lada C. J., et al., 2006, *AJ*, 131, 1574
- Lamers H. J. G. L. M., Baumgardt H., Gieles M., 2010, *MNRAS*, 409, 305
- Laplace P. S., 1796, *Exposition du système du monde*
- Larson R. B., 1969, *MNRAS*, 145, 271
- Larson R. B., 1985, *MNRAS*, 214, 379
- Larson R. B., 1995, *MNRAS*, 272, 213
- Larson R. B., 2003, *Reports on Progress in Physics*, 66, 1651
- Lee C.-F., Li Z.-Y., Hirano N., Shang H., Ho P. T. P., Zhang Q., 2018, *ApJ*, 863, 94
- Longmore S. N., et al., 2014, *Protostars and Planets VI*, pp 291–314
- Lucas W. E., Rybak M., Bonnell I. A., Gieles M., 2018, *MNRAS*, 474, 3582
- Lüghausen F., Parmentier G., Pflamm-Altenburg J., Kroupa P., 2012, *MNRAS*, 423, 1985
- Luhman K. L., 2007, *ApJS*, 173, 104
- Luhman K. L., 2018, *AJ*, 156, 271
- Luhman K. L., Esplin T. L., 2020, *AJ*, 160, 44
- Luhman K. L., Mamajek E. E., 2012, *ApJ*, 758, 31
- Luhman K. L., Allen P. R., Espaillat C., Hartmann L., Calvet N., 2010, *ApJS*, 186, 111
- Luhman K. L., Esplin T. L., Loutrel N. P., 2016, *ApJ*, 827, 52
- Lynden-Bell D., Pringle J. E., 1974, *MNRAS*, 168, 603
- Mac Low M.-M., Klessen R. S., 2004, *Reviews of Modern Physics*, 76, 125
- Madrid J. P., Leigh N. W. C., Hurley J. R., Giersz M., 2017, *MNRAS*, 470, 1729
- Malmberg D., Davies M. B., Heggie D. C., 2011, *MNRAS*, 411, 859
- Mamajek E. E., 2009, *EXOPLANETS AND DISKS: THEIR FORMATION AND DIVERSITY: Proceedings of the International Conference*, 1158, 3
- Manara C. F., Robberto M., Da Rio N., Lodato G., Hillenbrand L. A., Stassun K. G., Soderblom D. R., 2012, *ApJ*, 755, 154
- Manara C. F., et al., 2016, *A&A*, 591, L3
- Manara C. F., et al., 2017, *A&A*, 604, A127
- Manara C. F., Morbidelli A., Guillot T., 2018, *A&A*, 618, L3
- Manara C. F., et al., 2020, *A&A*, 639, A58

- Mann R. K., Williams J. P., 2009, *ApJ*, 694, L36
- Mann R. K., Williams J. P., 2010, *ApJ*, 725, 430
- Mann R. K., et al., 2014, *ApJ*, 784, 82
- Marino S., et al., 2018, *MNRAS*, 479, 5423
- Marino S., Yelverton B., Booth M., Faramaz V., Kennedy G. M., Matrà L., Wyatt M. C., 2019, *MNRAS*, 484, 1257
- Masunaga H., Inutsuka S.-i., 2000, *ApJ*, 531, 350
- Matzner C. D., 2002, *ApJ*, 566, 302
- Matzner C. D., McKee C. F., 2000, *ApJ*, 545, 364
- Maucó K., et al., 2016, *ApJ*, 829, 38
- Mayor M., Queloz D., 1995, *Nature*, 378, 355
- Megeath S. T., et al., 2012, *ApJ*, 144, 192
- Megeath S. T., et al., 2016, *ApJ*, 151, 5
- Ménard F., et al., 2020, *A&A*, 639, L1
- Merín B., et al., 2008, *ApJS*, 177, 551
- Mestel L., 1965, Quarterly Journal of the Royal Astronomical Society, 6, 161
- Mestel L., Spitzer L. J., 1956, *MNRAS*, 116, 503
- Miotello A., et al., 2017, *A&A*, 599, A113
- Mitchell P. D., et al., 2018, *MNRAS*, 474, 492
- Moeckel N., Throop H. B., 2009, *ApJ*, 707, 268
- Mori M., Burkert A., 2000, *ApJ*, 538, 559
- Muench A. A., Lada E. A., Lada C. J., Alves J., 2002, *ApJ*, 573, 366
- Mulders G. D., Dominik C., 2012, *A&A*, 539, A9
- Mulders G. D., Pascucci I., Manara C. F., Testi L., Herczeg G. J., Henning T., Mohanty S., Lodato G., 2017, *ApJ*, 847, 31
- Murillo N. M., Lai S.-P., Bruderer S., Harsono D., van Dishoeck E. F., 2013, *A&A*, 560, A103
- Murray N., Rahman M., 2010, *ApJ*, 709, 424
- Najita J. R., Kenyon S. J., 2014, *MNRAS*, 445, 3315
- Najita J. R., Andrews S. M., Muzerolle J., 2015, *MNRAS*, 450, 3559
- Nakamura F., Li Z.-Y., 2012, *FIRST STARS IV*, 1480, 30
- Navarro M. G., Ramos R. C., Minniti D., Pullen J., Capuzzo-Dolcetta R., Lucas P. W., 2020, *ApJ*, 893, 65

- Neuhäuser R., Forbrich J., 2008, Handbook of Star Forming Regions, Volume II, p. 735
- Newton I., 1687, Newtoni principia philosophiae. Apud Guil. & Joh. Innys, Regiae Societatis typographos.
- Nicholson R. B., Parker R. J., Church R. P., Davies M. B., Fearon N. M., Walton S. R. J., 2019, *MNRAS*, 485, 4893
- Nixon C. J., King A. R., Pringle J. E., 2018, *MNRAS*, 477, 3273
- O'dell C. R., 1998, *AJ*, 115, 263
- O'dell C. R., Wen Z., 1994, *MNRAS*, 436, 194
- Offner S. S. R., Arce H. G., 2015, *ApJ*, 811, 146
- Offner S. S. R., Chaban J., 2017, *ApJ*, 847, 104
- Olczak C., Pfalzner S., Spurzem R., 2006, *ApJ*, 642, 1140
- Olczak C., Pfalzner S., Eckart A., 2008, *A&A*, 488, 191
- Olczak C., Pfalzner S., Eckart A., 2010, *A&A*, 509, A63
- Owen J. E., Ercolano B., Clarke C. J., Alexander R. D., 2010, *MNRAS*, 401, 1415
- Owen J. E., Clarke C. J., Ercolano B., 2012, *MNRAS*, 422, 1880
- Paczynski B., 1977, *ApJ*, 216, 822
- Parker R. J., 2014, *MNRAS*, 445, 4037
- Parker R. J., Alves de Oliveira C., 2017, *MNRAS*, 468, 4340
- Parker R. J., Meyer M. R., 2012, *MNRAS*, 427, 637
- Parker R. J., Church R. P., Davies M. B., Meyer M. R., 2014, *MNRAS*, 437, 946
- Parravano A., Hollenbach D. J., McKee C. F., 2003, *ApJ*, 584, 797
- Pascucci I., et al., 2016, *ApJ*, 831, 125
- Pelupessy F. I., Portegies Zwart S., 2012, *MNRAS*, 420, 1503
- Pelupessy F. I., van der Werf P. P., Icke V., 2004, *A&A*, 422, 55
- Pelupessy F. I., van Elteren A., de Vries N., McMillan S. L. W., Drost N., Portegies Zwart S. F., 2013, *A&A*, 557, A84
- Petigura E. A., Howard A. W., Marcy G. W., 2013, *Proceedings of the National Academy of Science*, 110, 19273
- Pfalzner S., 2003, *ApJ*, 592, 986
- Pfalzner S., Vogel P., Scharwächter J., Olczak C., 2005a, *A&A*, 437, 967
- Pfalzner S., Umbreit S., Henning T., 2005b, *ApJ*, 629, 526
- Pfalzner S., Olczak C., Eckart A., 2006, *A&A*, 454, 811

- Pfalzner S., Tackenberg J., Steinhausen M., 2008, *A&A*, 487, L45
- Pfalzner S., Bhandare A., Vincke K., Lacerda P., 2018, *ApJ*, 863, 45
- Picogna G., Ercolano B., Owen J. E., Weber M. L., 2019, *MNRAS*, 487, 691
- Pinte C., Dent W. R. F., Ménard F., Hales A., Hill T., Cortes P., de Gregorio-Monsalvo I., 2016, *ApJ*, 816, 25
- Plummer H. C., 1911, *MNRAS*, 71, 460
- Portegies Zwart S. F., 2016, *MNRAS*, 457, 313
- Portegies Zwart S., 2020, *Nature Astronomy*, 4, 819
- Portegies Zwart S. P., McMillan S., 2018, *Astrophysical Recipes: The Art of AMUSE*, 1st edn. AAS-IOP Astronomy, Institute of Physics Publishing, Great Britain
- Portegies Zwart S. F., Verbunt F., 1996, *A&A*, 309, 179
- Portegies Zwart S., et al., 2009, *New Astronomy*, 14, 369
- Portegies Zwart S. F., McMillan S. L. W., Gieles M., 2010, *ARA&A*, 48, 431
- Portegies Zwart S., McMillan S. L. W., van Elteren E., Pelupessy I., de Vries N., 2013, *Computer Physics Communications*, 183, 456
- Portegies Zwart S., Pelupessy I., van Elteren A., Wijnen T. P. G., Lugaro M., 2018, *A&A*, 616, A85
- Portegies Zwart S., Pelupessy I., Martínez-Barbosa C., van Elteren A., McMillan S., 2020, *Communications in Nonlinear Science and Numerical Simulations*, 85, 105240
- Preibisch T., Mamajek E., 2008, in Reipurth B., ed., , *Handbook of Star Forming Regions*, Volume II. ASP Monograph Publications, USA, p. 235
- Prentice A. J. R., 1978, *Moon and Planets*, 19, 341
- Price-Whelan A., Mechev A., jumeroag 2018, adrn/makecrite: v0.2, Zenodo, doi:10.5281/zenodo.1343299
- Pringle J. E., 1981, *ARA&A*, 19, 137
- Pringle J. E., 1989, *MNRAS*, 239, 361
- Punzo D., Capuzzo-Dolcetta R., Portegies Zwart S., 2014, *MNRAS*, 444, 2808
- Reche R., Beust H., Augereau J.-C., 2009, *A&A*, 493, 661
- Ribas A., Merín B., Bouy H., Maud L. T., 2014, *A&A*, 561, A54
- Richert A. J. W., Getman K. V., Feigelson E. D., Kuhn M. A., Broos P. S., Povich M. S., Bate M. R., Garmire G. P., 2018, *MNRAS*, 477, 5191
- Richling S., Yorke H. W., 1997, *A&A*, 327, 317
- Robberto M., Song J., Mora Carrillo G., Beckwith S. V. W., Makidon R. B., Panagia N., 2004, *ApJ*, 606, 952

- Roccatagliata V., Sacco G. G., Franciosini E., Randich S., 2018, *A&A*, 617, L4
- Roccatagliata V., Franciosini E., Sacco G. G., Randich S., Sicilia-Aguilar A., 2020, *A&A*
- Rodriguez-Merino L. H., Chavez M., Bertone E., Buzzoni A., 2005, *ApJ*, 626, 411
- Rodriguez J. E., et al., 2018, *ApJ*, 859, 150
- Rosotti G. P., Clarke C. J., 2018, *MNRAS*, 473, 5630
- Rosotti G. P., Dale J. E., de Juan Ovelar M., Hubber D. A., Kruijssen J. M. D., Ercolano B., Walch S., 2014, *MNRAS*, 441, 2094
- Rosotti G. P., Clarke C. J., Manara C. F., Facchini S., 2017, *MNRAS*, 468, 1631
- Rosotti G. P., Dale J. E., de Juan Ovelar M., Hubber D. A., Kruijssen J. M. D., Ercolano B., Walch S., 2018, *MNRAS*, 473, 3223
- Rosotti G. P., Tazzari M., Booth R. A., Testi L., Lodato G., Clarke C., 2019, *MNRAS*, 486, 4829
- Russell S. S., Hartmann L., Cuzzi J., Krot A. N., Gounelle M., Weidenschilling S., 2006, *Meteorites and the Early Solar System II*, pp 233–251
- Ryu Y.-H., et al., 2020, *AJ*, 159, 58
- Sacco G. G., et al., 2017, *A&A*, 601, A97
- Salyk C., Pontoppidan K., Corder S., Muñoz D., Zhang K., Blake G. A., 2014, *ApJ*, 792, 68
- Scally A., Clarke C., 2001, *MNRAS*, 325, 449
- Scalo J., 1990, *Physical Processes in Fragmentation and Star Formation*, 162, 151
- Scalo J., Elmegreen B. G., 2004, *ARA&A*, 42, 275
- Schaefer G. H., et al., 2016, *AJ*, 152, 213
- Schaye J., et al., 2015, *MNRAS*, 446, 521
- Schulz N. S., Huenemoerder D. P., Günther M., Testa P., Canizares C. R., 2015, *ApJ*, 810, 55
- Sellek A. D., Booth R. A., Clarke C. J., 2020, *MNRAS*, 492, 1279
- Shadmehri M., Ghoreyshi S. M., Alipour N., 2018, *ApJ*, 867, 41
- Shakura N. I., Sunyaev R. A., 1973, *A&A*, 24, 337
- Sherry W. H., Walter F. M., Wolk S. J., 2004, *AJ*, 128, 2316
- Sicilia-Aguilar A., Hartmann L. W., Fürész G., Henning T., Dullemond C., Brandner W., 2006, *AJ*, 132, 2135
- Sicilia-Aguilar A., Henning T., Hartmann L. W., 2010, *ApJ*, 710, 597
- Simon M., 1997, *ApJ*, 482, L81
- Smith B. A., Teriley R. J., 1984, *Science*, 226, 1421
- Spitzer Lyman J., 1940, *MNRAS*, 100, 396

- Spitzer Lyman J., 1968, Nebulae and Interstellar Matter, p. 1
- Spitzer L., 1988, Dynamical evolution of globular clusters. Princeton Series in Astrophysics, Princeton University Press, USA
- Springel V., Hernquist L., 2003, *MNRAS*, 339, 289
- Springel V., et al., 2005, *Nature*, 435, 629
- Spurzem R., Giersz M., Heggie D. C., Lin D. N. C., 2009, *ApJ*, 697, 458
- Steinhausen M., Pfalzner S., 2014, *A&A*, 565, A32
- Störzer H., Hollenbach D., 1999, *ApJ*, 515, 669
- Strom K. M., Strom S. E., Edwards S., Cabrit S., Skrutskie M. F., 1989, *AJ*, 97, 1451
- Sung H., Stauffer J. R., Bessell M. S., 2009, *AJ*, 138, 1116
- Takahashi K., Portegies Zwart S. F., 2000, *ApJ*, 535, 759
- Tazzari M., et al., 2017, *A&A*, 606, A88
- Throop H. B., Bally J., 2008, *AJ*, 135, 2380
- Tobin J. J., et al., 2020, *ApJ*, 890, 130
- Toonen S., Nelemans G., Zwart S. P., 2012, *A&A*, 546, A70
- Torres S., Cai M. X., Brown A. G. A., Portegies Zwart S., 2019, *A&A*, 629, A139
- Trapman L., Facchini S., Hogerheijde M. R., van Dishoeck E. F., Bruderer S., 2019, *A&A*, 629, A79
- Trapman L., Rosotti G., Bosman A. D., Hogerheijde M. R., van Dishoeck E. F., 2020, *A&A*, 640, A5
- Tritsis A., Tassis K., 2016, *MNRAS*, 462, 3602
- Trumpler R. J., 1930, Leaflet of the Astronomical Society of the Pacific, 1, 117
- Tutukov A. V., 1978, *A&A*, 70, 57
- Tychoniec Ł., et al., 2020, *A&A*, 640, A19
- Van Der Walt S., Colbert S. C., Varoquaux G., 2011, *Computing in Science & Engineering*, 13, 22
- Vázquez-Semadeni E., Palau A., Ballesteros-Paredes J., Gómez G. C., Zamora-Avilés M., 2019, *MNRAS*, 490, 3061
- Vicente S. M., Alves J., 2005, *A&A*, 441, 195
- Vincke K., Pfalzner S., 2016, *ApJ*, 828, 48
- Vincke K., Pfalzner S., 2018, *ApJ*, 868, 1
- Vincke K., Breslau A., Pfalzner S., 2015, *A&A*, 577, A115

- Vink J. S., de Koter A., Lamers H. J. G. L. M., 2001, *A&A*, 369, 574
- Virtanen P., et al., 2019, arXiv:1907.10121 [physics]
- Vorobyov E. I., 2011, *ApJ*, 729, 146
- Wall J. E., McMillan S. L. W., Mac Low M.-M., Klessen R. S., Portegies Zwart S., 2019, *ApJ*, 887, 62
- Wijnen T. P. G., Pols O. R., Pelupessy F. I., Portegies Zwart S., 2016, *A&A*, 594, A30
- Wijnen T. P. G., Pols O. R., Pelupessy F. I., Portegies Zwart S., 2017a, *A&A*, 602, A52
- Wijnen T. P. G., Pols O. R., Pelupessy F. I., Portegies Zwart S., 2017b, *A&A*, 604, A91
- Williams J. P., 2012, *Meteoritics and Planetary Science*, 47, 1915
- Williams J. P., Best W. M. J., 2014, *ApJ*, 788, 59
- Williams J. P., Cieza L. A., 2011, *ARA&A*, 49, 67
- Williams J. P., McKee C. F., 1997, *ApJ*, 476, 166
- Williams J. P., Blitz L., McKee C. F., 2000, *Protostars and Planets IV*, p. 97
- Williams J. P., Cieza L., Hales A., Ansdell M., Ruiz-Rodriguez D., Casassus S., Perez S., Zurlo A., 2019, *ApJ*, 875, L9
- Winkler K.-H. A., Newman M. J., 1980, *ApJ*, 236, 201
- Winston E., et al., 2007, *ApJ*, 669, 493
- Winter A. J., Clarke C. J., Rosotti G., Booth R. A., 2018a, *MNRAS*, 475, 2314
- Winter A. J., Clarke C. J., Rosotti G., Ih J., Facchini S., Haworth T. J., 2018b, *MNRAS*, 478, 2700
- Winter A. J., Booth R. A., Clarke C. J., 2018c, *MNRAS*, 479, 5522
- Winter A. J., Clarke C. J., Rosotti G. P., 2019a, *MNRAS*, 485, 1489
- Winter A. J., Clarke C. J., Rosotti G. P., Hacar A., Alexander R., 2019b, *MNRAS*, 490, 5478
- Winter A. J., Ansdell M., Haworth T. J., Kruijssen J. M. D., 2020a, *MNRASL*, p. slaa110
- Winter A. J., Kruijssen J. M. D., Chevance M., Keller B. W., Longmore S. N., 2020b, *MNRAS*, 491, 903
- Wright N. J., Drake J. J., Drew J. E., Vink J. S., 2010, *ApJ*, 713, 871
- Wright N. J., Parker R. J., Goodwin S. P., Drake J. J., 2014, *MNRAS*, 438, 639
- Wuchterl G., Tscharnutter W. M., 2003, *A&A*, 398, 1081
- Yorke H. W., Bodenheimer P., Laughlin G., 1993, *ApJ*, 411, 274
- Yusef-Zadeh F., Roberts D. A., Wardle M., Cotton W., Schödel R., Royster M. J., 2015, *ApJ*, 801, L26

- Yusef-Zadeh F., Wardle M., Kunneriath D., Royster M., Wootten A., Roberts D. A., 2017, [ApJ](#), 850, L30
- de Juan Ovelar M., Kruijssen J. M. D., Bressert E., Testi L., Bastian N., Cánovas H., 2012, [A&A](#), 546, L1
- van Boekel R., et al., 2017, [ApJ](#), 837, 132
- van Elteren A., Portegies Zwart S., Pelupessy I., Cai M. X., McMillan S. L. W., 2019, [A&A](#), 624, A120
- van Terwisga S. E., Hacar A., van Dishoeck E. F., 2019, [A&A](#), 628, A85
- van Terwisga S. E., et al., 2020, [A&A](#), 640, A27
- van der Marel N., Matthews B., Dong R., Birnstiel T., Isella A., 2018, arXiv:1809.06403 [astro-ph]
- van 't Hoff M. L. R., Tobin J. J., Harsono D., van Dishoeck E. F., 2018, [A&A](#), 615, A83

English summary

CIRCUMSTELLAR discs are structures of gas and dust that surround young stars. It is in these discs where planets will eventually form, so studying their evolution is important to understand the formation of planetary systems. Our own solar system began as a circumstellar disc, spinning around the Sun. These discs develop shortly after their host stars, and in their early years they are immersed in the leftovers of star formation. This environment can be very hostile to the young discs. Most stars form not in isolation but in groups, so nearby stars can pass close to the discs and truncate them, removing their outer layers. If the encountering star has a disc of its own, the two discs might even exchange material. If there are massive stars in the vicinity, the ultraviolet radiation coming from them can heat the surface of nearby discs enough to evaporate material from them, in a process known as external photoevaporation. Even radiation from the host star itself can remove material from the inner regions of the discs, in what is called internal photoevaporation. As they move through the gas in the environment, the ram pressure can strip mass from the outer regions of the discs and harden their surfaces. And, if there happens to be a supernova explosion nearby, the discs in the neighbourhood can be completely destroyed by the blast.

Circumstellar discs also expand due to their inner evolution. Mass flows from the outer parts of the discs to the inner regions, and this matter is accreted, or consumed, by the host star. The outer regions, due to conservation of angular momentum, expand outward. When unperturbed, discs drive material into the star and expand consistently until they are completely drained of mass. In isolation, this process should last around 10 million years. However, observations show that discs disappear much faster than that. This effect can be related to two things. First, planet formation might start very early in the life of a disc, so the mass is quickly used in forming rocky planets and the cores of gas giants. Second, the environmental effects described above might also act rapidly in decreasing the mass of the discs. If the environment is playing an important role, it can literally mean life or death for planetary systems: if the discs lose their mass shortly after their birth, planets simply do not have enough time to form. Constraining the effects of the environment on circumstellar discs will help determine a time scale within which planets must form.

This thesis investigates how the environment affects the evolution of the young circumstellar discs, with the focus being on two particular processes: truncating encounters with other stars, and external photoevaporation caused by the radiation from massive stars in the vicinity. All the work performed in this thesis is based on computational simulations of the astrophysical processes described above. We use the Astrophysical MULTIPurpose Software Environment, AMUSE² to bring together codes to model stellar dynamics, stellar evolution, disc evolution, and photoevaporation. The quantification of the effects of these mechanisms is performed by analysing the distributions of disc masses, sizes, and their lifetimes at the end

²<http://amusecode.org>

of the simulations. All the code developed for this thesis is open source and freely available online³.

In Chapter 2 we model clusters with 1,500 stars where all stars have circumstellar discs. We model the evolution of the discs using a semi-analytical approach, and we look to study how the presence of interstellar gas in the clusters affects the rate of dynamical encounters and disc truncations. We model three types of clusters: one where gas is present during the entire simulation, one without gas, and one where gas is present initially but is expelled halfway through the simulations. The discs are subject to dynamical encounters which can truncate them, and we study how the gas affects the final size distribution of the discs. We find that the results for the three type of regions are relatively similar, since the intrinsic evolution of the discs make them expand faster than they are truncated by encounters. In the models where we consider slowly growing discs, we obtain disc size distributions that are comparable to those observed in real star forming regions.

In Chapter 3 we introduce a new model for the discs that allows us to also implement external photoevaporation. In these new simulations, all low mass stars (less than 2 times the mass of the Sun) have a circumstellar disc, and stars more massive than that emit ultraviolet radiation. This radiation evaporates material from the discs. In these simulations, the discs are subject to their inner evolution, dynamical truncations, and external photoevaporation. We model regions with 100 stars and evolve them for 2 million years. We find that the mass lost from the discs due to external photoevaporation is tens of times higher than that lost by dynamical truncations. This means that external photoevaporation is a much more relevant process in determining final disc mass and size distributions. We also find that photoevaporation is extremely efficient in destroying the discs: around 60% of the discs are dispersed within the first 100,000 years of evolution, and by 2 million years only 10% to 20% of the initial discs are left. This means that in regions with massive stars where discs are subject to photoevaporation, planet formation must start very soon after disc formation. Otherwise, the discs are simply not massive enough to form planets.

Using the same model developed for Chapter 3, in Chapter 4 we simulate a series of clusters with 1,000 stars and different radii, ranging from 0.5 parsec to 5 parsec (one parsec is almost 3.3 lightyears, 210,000 times the distance between the Earth and the Sun, or 31 trillion kilometers). In this way, we explore a larger range of stellar densities. We look to determine how the stellar density of a region affects the lifetimes and masses of the discs. We find that disc masses decrease sharply with increasing stellar density. In particular, in regions where the density is higher than $100 \text{ stars pc}^{-2}$ it is difficult for discs massive enough to form planets to survive for long. We compare our final disc mass distributions and stellar densities to those of observed star forming regions, and we find that both simulations and observations follow a similar trend.

In the first four chapters of this thesis, we consider all the stars in the simulations to form at the same time, and to be initially distributed in a spherical configuration. However, we know that in reality the star formation process results in stars with distributions that are more fractal and filamentary. In Chapter 5 we go one step back from the previous simulations and begin by modelling a simple approximation of the star formation process. This results in two main differences from the previous simulations: the initial spatial distribution of the stars is not be spherical, and not all stars form at the same time. After each star forms, we assign a disc to it which uses the same model as in Chapters 3 and 4. To the inner disc evolution, external photoevaporation, and dynamical encounters, we add the effects of internal photoevaporation and dust evolution inside the discs. We evolve the simulations for 2 million years after the last star has formed. We find that a star formation process that is

³<http://github.com/franciscaconcha>

extended in time allows for the younger discs to live for longer. When star formation ends, the gas left over from the process is expelled from the region. This expulsion makes the clusters expand as they try to regain equilibrium, which reduces the stellar density and the effects of radiation. At the end of these simulations, there are more discs left, and they are more massive than in the previous chapters. The newly implemented dust model also results in the discs having more mass in solids than in previous simulations, which is an important reservoir for the formation of planets.

The results of the simulations performed for this thesis show that the environment is extremely important in determining the survival of circumstellar discs and that the surroundings of these discs constrain the time available for planets to form. These conclusions are also supported by observational surveys of young discs in star forming regions. In particular, external photoevaporation is efficient in quickly destroying circumstellar discs, and so it greatly limits the amount of material and time available to form planets. These results have important consequences for the study of planet formation.



Nederlandse samenvatting

Circumstellaire schijven zijn structuren van gas en stof die zich rondom jonge sterren bevinden. Na verloop van tijd zullen planeten ontstaan in deze schijven. Om de vorming van planetenstelsels, zoals ook ons zonnestelsel, te begrijpen, is het daarom van belang de evolutie van schijven te bestuderen. Schijven ontwikkelen zich kort na het ontstaan van de sterren waaromheen ze zich bevinden. In een eerste fase is de omgeving van de schijf erg vijandig en zijn ze omringd door materiaal dat voortkomt uit het stervormingsproces. Aangezien de meeste sterren in groepen ontstaan, kunnen nabije sterren in de buurt van de schijf de buitenste schijflagen vernietigen. Dit proces noemen we 'afkapping'. Als de nabije ster zelf ook een schijf bevat, kunnen de twee schijven materiaal uitwisselen. Wanneer er zich zware sterren nabij een schijf bevinden, kan de ultraviolette straling van deze zware sterren een schijf zodanig verhitten dat een deel van het schijfmateriaal verdampft. Dit proces noemen we 'externe fotoevaporatie'. Ook straling van de ster zelf kan materiaal uit de binnenste lagen van de schijf verwijderen. Dit proces heet dan interne fotoevaporatie. Wanneer de schijf zich voortbeweegt door de gasrijke omgeving ontstaat zogeheten ramdruk, die leidt tot een verlies van massa in de buitenste lagen van de schijf en een verharding van het schijfoppervlak. Ten slotte is het ook mogelijk dat een schijf volledig wordt vernietigd wanneer er in de omgeving een supernova-explosie plaatsvindt.

Circumstellaire schijven zetten ook uit. Materiaal beweegt vanuit de buitenste schijflagen naar de binnennlagen, waar het uiteindelijk op de ster valt. Door de wet van behoud van impulsmoment verruimen de buitenste lagen hierdoor naar buiten. Zonder verstoring zorgt dit proces ervoor dat materiaal op de ster blijft invallen, en de buitenste lagen blijven uitzetten, tot alle massa is opgebruikt. Dit proces zou ongeveer 10 miljoen jaar duren. Uit waarnemingen blijkt echter dat schijven veel sneller verdwijnen. Hierbij spelen twee andere effecten mogelijk een rol. Ten eerste zou het kunnen dat planeetvorming in de schijf zeer snel van start gaat en dat massa snel opgebruikt wordt om aardachtige planeten en de kernen van gasplaneten te vormen. Ten tweede zou het kunnen dat de vijandige steromgeving die hierboven werd beschreven een rol speelt om de massa in de schijf te verkleinen. De omgeving kan hierbij dus een kwestie van leven of dood betekenen voor planetenstelsels. Als de schijf immers al snel na het ontstaan massa verliest, zal er niet genoeg tijd zijn om planeten te vormen. Als we de invloed van de omgeving op circumstellaire schijven beter begrijpen zal dit dus ook helpen om de tijdschaal te bepalen waarin planeten ontstaan.

In deze thesis onderzoek ik het effect van de omgeving op de evolutie van jonge circumstellaire schijven. De focus ligt daarbij op twee specifieke processen: de afkapping van de buitenste lagen door ontmoetingen met andere sterren, en externe fotoevaporatie door straling van nabije zware sterren. Hiertoe werden computersimulaties van deze processen uitgevoerd, waarbij we vervolgens de resulterende schijfmassa's, schijfgroottes, en levensduurten bestudeerden om deze processen te kwantificeren. Voor deze simulaties werd gebruik

gemaakt van het Astrophysical MULTIPurpose Software Environment, AMUSE⁴. In deze softwaretool wordt code samengebracht die sterodynamica, stereevolutie, schijfevolutie, en fotoevaporatie kan modelleren. De code die werd ontwikkeld als onderdeel van dit thesiswerk is open broncode en vrij beschikbaar⁵.

In Hoofdstuk 2 modelleren we clusters met 1.500 sterren, die allen een circumstellaire schijf bezitten. Om de schijfevolutie te modelleren maken we gebruik van een semi-analytische aanpak. We onderzoeken daarbij de invloed van interstellair gas in de cluster op de hoeveelheid dynamische interacties en schijfafkappingen. We beschouwen drie soorten clusters: een cluster waarbij gas aanwezig is gedurende de gehele simulatie, een cluster zonder gas, en een cluster waarbij gas eerst aanwezig is maar halverwege de simulaties verdwijnt. De schijven ondergaan dynamische interacties die tot afkappingen kunnen leiden. We meten de grootte van de schijven aan het einde van de simulaties en bestuderen hierbij hoe de aanwezigheid van gas de verdeling van schijfgroottes beïnvloedt. Hierbij stellen we vast dat de drie soorten clusters relatief gelijkaardige resultaten opleveren, omdat de intrinsieke evolutie van de schijven leidt tot snellere uitzetting dan de afkapping door interacties. In de modellen waar we traaggroeiende schijven beschouwen, vinden we verdelingen van de schijfgroottes die vergelijkbaar zijn met schijfgroottes die waargenomen zijn in werkelijke stervormingsgebieden.

In Hoofdstuk 3 introduceren we een nieuw schijfmodel. Dit model laat toe om externe fotoevaporatie te modelleren. In deze nieuwe simulaties hebben alle sterren met lage massa (een massa kleiner dan twee zonsmassa's) een circumstellaire schijf. Sterren met hoge massa (groter dan twee zonsmassa's) zenden ultraviolette straling uit. Deze straling leidt tot verdamping van materiaal in de schijven. In deze simulaties ondergaan de schijven zowel interne evolutie als dynamische afkappingen en externe fotoevaporatie. We modelleren hierbij regio's met 100 sterren en volgen deze gedurende 2 miljoen jaar. Hieruit blijkt dat de massa die schijven verliezen als gevolg van externe fotoevaporatie ongeveer een grootteorde hoger ligt dan massaverlies ten gevolge van dynamische afkappingen. Dit betekent dat externe fotoevaporatie van groot belang is om de uiteindelijke verdeling van schijfmassa en schijfstraal te bepalen. Verder leren we dat fotoevaporatie erg effectief is om schijven te vernietigen: ongeveer 60% van de schijven zijn al binnen 100.000 jaar uiteengedreven, en na 2 miljoen jaar blijven slechts ongeveer 10 tot 20% van de oorspronkelijke schijven over. Dit impliceert dat planeetvorming erg vroeg van start moet gaan na de schijf形成, in regio's met sterren met hoge massa's waarbij schijven fotoevaporatie ondergaan. In deze regio's hebben schijven immers al snel niet meer voldoende massa om nog planeten te kunnen vormen.

In Hoofdstuk 4 vertrekken we van hetzelfde model en simuleren we een reeks clusters met 1.000 sterren die verschillende groottes hebben. Deze groottes variëren van 0.5 tot 5 parsec (een parsec is ongeveer 3,3 lichtjaar, 210.000 keer de afstand tussen de aarde en de zon, of 31 biljoen kilometer). Op deze manier onderzoeken we een grotere variatie in ster dichtheid. Hierbij trachten we te bepalen hoe de dichtheid van de sterren in een regio de levensduur en massa van schijven beïnvloedt. Uit deze simulaties blijkt dat de schijfmassa sterk afneemt wanneer de ster dichtheid stijgt. In regio's waar de dichtheid hoger ligt dan 100 sterren per vierkante parsec kunnen schijven met een massa hoog genoeg om planeten te vormen niet lang overleven. We vergelijken de verdeling van de schijfmassa's uit onze simulaties voor verschillende ster dichthesen met waarnemingen van stervormingsgebieden en stellen vast dat beiden een gelijkaardige trend vertonen.

In de eerste vier hoofdstukken van deze thesis namen we aan dat alle sterren in een simulatie tegelijkertijd ontstonden en dat ze een bolvormige verdeling vormden. In werkelijk-

⁴<http://amusecode.org>

⁵<https://github.com/franciscaconcha>

jkheid weten we echter dat stervorming leidt tot een eerder fractale en draadvormige verdeling. In Hoofdstuk 5 nemen we daarom een stap terug ten opzichte van de simulaties uit het vorige hoofdstuk. We modelleren het stervormingsproces volgens enkele vereenvoudigde aannames. Dit leidt tot twee belangrijke verschillen met de eerdere simulaties: de ruimtelijke verdeling van sterren in de simulaties is niet langer bolvormig, en niet elke ster vormt op hetzelfde ogenblik. Nadat een ster zich heeft gevormd, wijzen we ze een schijf toe volgens het model dat we eerder in Hoofdstuk 3 en 4 gebruikten. We modelleren zoals eerder de schijfevolutie, externe fotoevaporatie, en dynamische interacties, maar voegen nu ook de effecten van interne fotoevaporatie en stofevolutie in de schijf toe. De simulaties volgen de sterren voor 2 miljoen jaar nadat de laatste ster zich gevormd heeft. Het gevolg van het verlengen van het stervormingsproces is dat jongere schijven langer leven. Wanneer stervorming ten einde komt, wordt het overgebleven gas verwijderd uit het gebied. Dit proces zorgt ervoor dat de cluster uitzet om een nieuw evenwicht te verkrijgen, waardoor de ster dichtheid verlaagt en het stralingseffect afneemt. Vergelijken met eerdere simulaties blijven in deze simulaties meer schijven over en hebben de schijven een hogere massa. Het nieuwe stofmodel zorgt er ook voor dat schijven meer massa in vaste vorm bevatten, wat belangrijk materiaal is voor de vorming van planeten.

De resultaten van de simulaties die in deze thesis werden uitgevoerd tonen aan dat de omgeving een erg belangrijke rol speelt om te bepalen hoe circumstellaire schijven overleven. De omgeving van deze schijven bepaalt hoeveel tijd beschikbaar is om planeten te vormen. Observaties van jonge schijven in stervormingsgebieden ondersteunen deze conclusies. Externe fotoevaporatie kan circumstellaire schijven snel en effectief vernietigen en limiteert bijgevolg hoeveel materiaal en hoeveel tijd ter beschikking is om planeten te vormen, wat belangrijke gevolgen heeft voor onderzoek naar planeetvorming.



Resumen en español

LOS DISCOS CIRCUMESTELARES son estructuras de gas y polvo que rodean a las estrellas jóvenes. Es en estos discos donde eventualmente se formarán los planetas, por lo que estudiar su evolución es importante para comprender la formación de los sistemas planetarios. Nuestro propio sistema solar comenzó siendo un disco circumestelar rotando en torno al Sol. Estos discos surgen rápidamente luego de la formación de su estrella, y durante sus primeros miles de años de evolución están inmersos en los vestigios del proceso de formación estelar. Este ambiente puede ser muy hostil para los discos. Gran parte de las estrellas no se forman en solitario, sino en grupos. Estrellas vecinas pueden pasar muy cerca de los discos, removiendo material de sus zonas exteriores y truncándolos. Si esta estrella tiene su propio disco, ambos pueden incluso intercambiar material. Si hay estrellas masivas en los alrededores, la radiación ultravioleta que estas emiten puede calentar la superficie de los discos y evaporar parte de su masa, en un proceso llamado fotoevaporación externa. Incluso la radiación proveniente de la estrella que alberga al disco puede remover material de las regiones más internas, en un proceso conocido como fotoevaporación interna. A medida que los discos se mueven a través del gas presente en el ambiente, la fricción puede remover material de sus zonas externas y endurecer su superficie. Y, si hay una explosión de supernova en la región, los discos en las cercanías pueden ser completamente destruidos por la onda expansiva.

Los discos circumestelares también se expanden, debido a su propia evolución interna. La materia fluye desde las regiones externas hacia las internas, y este material es acretado, o consumido, por la estrella central. Las zonas externas del disco se expanden, debido a la conservación de momento angular. Si los discos evolucionan sin perturbaciones, este proceso de mover material desde afuera hacia adentro en conjunto con la expansión continúa hasta que toda su masa inicial ha sido consumida. En aislamiento, este proceso dura alrededor de 10 millones de años. Sin embargo, observaciones de discos en regiones de formación estelar muestran que los discos desaparecen en un tiempo mucho menor, incluso antes de un millón de años de evolución. Este efecto puede estar relacionado con dos procesos. En primer lugar, la formación de planetas puede comenzar muy temprano en la vida de los discos, por lo que la masa está siendo utilizada para formar planetas rocosos y núcleos de planetas gaseosos. En segundo lugar, los efectos ambientales descritos anteriormente pueden ayudar a que la masa de los discos disminuya rápidamente. Si el rol del ambiente es importante, este puede ser de vida o muerte para los sistemas planetarios: si los discos pierden su masa poco después de formarse, no hay suficiente tiempo para que los planetas se formen. Constreñir los efectos que el ambiente tiene sobre los discos permite determinar las escalas de tiempo necesarias para que se formen los planetas.

Esta tesis investiga cómo el ambiente generado por el proceso de formación estelar afecta la evolución de los discos circumestelares recién formados, con un enfoque en dos mecanismos en particular: truncamientos debido a encuentros con otras estrellas, y fotoevaporación

externa causada por la radiación de estrellas masivas en la región. Los efectos de estos procesos son cuantificados analizando las distribuciones finales de masa y tamaño de los discos, además de sus tiempos de vida. Todo el trabajo desarrollado en esta tesis se basa en simulaciones computacionales de los procesos astrofísicos descritos. Usando el framework Astrophysical MULTipurpose Software Environment, AMUSE⁶, integraron códigos para modelar dinámica estelar, evolución estelar, evolución interna de los discos, y el proceso de fotoevaporación. Todo el código desarrollado para esta tesis es abierto y está disponible online⁷.

En el Capítulo 2 modelamos cúmulos estelares con 1.500 estrellas, donde cada una está rodeada por un disco circumestelar. Los cúmulos estelares son conjuntos de estrellas que se mantienen unidas por su fuerza de gravedad. Modelamos la evolución de los discos usando un modelo semi-analítico, que nos permite calcular su masa y tamaño en el tiempo. Buscamos estudiar cómo la presencia de gas entre las estrellas afecta la tasa de encuentros entre discos y de eventuales truncamientos. Modelamos tres tipos de cúmulos: uno donde el gas está presente durante toda la simulación, uno sin gas, y otro donde el gas está presente durante la primera mitad de la simulación y luego es expulsado. Las simulaciones modelan la evolución del sistema por 2 millones de años. Nuestros resultados muestran que los tamaños de los discos son similares en los tres tipos de cúmulo, ya que la evolución intrínseca de los discos hace que se expandan más rápido de lo que son truncados. En los modelos donde los discos se expanden más lentamente, los tamaños finales de los discos son similares a los observados en regiones reales de formación estelar.

En el Capítulo 3 introducimos un nuevo modelo para los discos, que nos permite implementar fotoevaporación externa. En estas nuevas simulaciones, todas las estrellas de poca masa (menos de 2 veces la masa del Sol) tienen un disco circumestelar, y todas las estrellas más masivas emiten radiación ultravioleta. Esta radiación evapora material de los discos cercanos. En estas simulaciones modelamos la evolución interna de los discos, los truncamientos debido a encuentros con otras estrellas, y fotoevaporación externa. Modelamos cúmulos con 100 estrellas que evolucionan por 2 millones de años. Los resultados muestran que la masa que pierden los discos debido a la fotoevaporación es decenas de veces más que la que se pierde debido a truncamientos. Esto significa que la fotoevaporación externa es un proceso mucho más relevante para la evolución de los discos. También determinamos que la fotoevaporación es extremadamente eficiente al evaporar los discos: alrededor del 60% de los discos son destruidos dentro de los primeros 100.000 años de evolución del sistema, y al final de las simulaciones sólo entre un 10% y un 20% de los discos aún poseen algo de masa. Esto demuestra que, en las regiones donde existen estrellas masivas, los planetas deben comenzar a formarse rápidamente una vez que se han formados los discos. De otro modo, los discos simplemente no tendrán suficiente masa para formar sistemas planetarios.

Utilizando el mismo modelo desarrollado para el Capítulo 3, en el Capítulo 4 simulamos una serie de cúmulos con 1.000 estrellas y diferentes radios, desde 0.5 pársec hasta 5 pársec (un pársec es casi 3.3 años luz, 210.000 veces la distancia entre la Tierra y el Sol, o 31 trillones de kilómetros). De esta manera exploramos regiones con distintas densidades estelares. Buscamos determinar cómo la densidad de una región afecta las masas y tiempos de vida de los discos. En nuestros resultados encontramos que la masa de los discos disminuye drásticamente a medida que la densidad estelar aumenta. En particular, en regiones donde la densidad es mayor a 100 estrellas por pársec² es difícil que discos con suficiente masa para formar planetas puedan sobrevivir. Comparamos las distribuciones de las masas en nuestras simulaciones con observaciones de discos en regiones de formación estelar, y encontramos

⁶<http://amusecode.org>

⁷<https://github.com/franciscaconcha>

que las simulaciones y observaciones siguen una tendencia similar en términos de la relación entre masa y densidad estelar: mientras más estrellas hay en un cúmulo, menos masivos son los discos ahí presentes.

En los primeros cuatro capítulos de esta tesis, consideramos que todas las estrellas en las simulaciones se formaron al mismo tiempo, y que inicialmente están distribuidas en una configuración esférica. En la realidad, el proceso de formación estelar resulta en distribuciones más irregulares, con estructuras fractales y filamentos. En el Capítulo 5 tomamos un paso atrás de las simulaciones anteriores, y comenzamos modelando una aproximación simple de formación estelar. Esto otorga dos grandes diferencias con las simulaciones anteriores: la distribución espacial de las estrellas no es esférica, y no todas las estrellas se forman al mismo tiempo. Luego de que una estrella se forma, le asignamos un disco que evoluciona usando el mismo modelo que en los Capítulos 3 y 4, pero además agregamos los procesos de fotoevaporación interna (es decir, debido a la radiación de la misma estrella) y la evolución del polvo separado del gas al interior de los discos. Las simulaciones corren por 2 millones de años después de que se forma la última estrella. Nuestros resultados muestran que extender la formación estelar en el tiempo permite que los discos más jóvenes sobrevivan hasta el final de las simulaciones. Cuando termina el proceso de formación estelar, el gas remanente es expulsado de la región. Esta expulsión hace que los cúmulos se expandan rápidamente, ya que tratan de recuperar su estado de equilibrio. En esta expansión, la distancia entre las estrellas aumenta, lo que reduce la densidad estelar de la región y disminuye los efectos de la radiación sobre los discos. Al final de las simulaciones sobreviven más discos, y estos son más masivos, que en los resultados de los capítulos anteriores. El nuevo modelo para el polvo en los discos también resulta en una mayor retención de masa, lo cual permite a los discos mantener reservas de material para la formación de planetas.

Los resultados de las simulaciones desarrolladas para esta tesis muestran que el ambiente es un factor extremadamente importante para definir la supervivencia de los discos circunestelares. Los procesos que ocurren en los alrededores de los discos acotan el tiempo disponible para la formación de planetas. Conclusiones similares se obtienen al observar discos circumestelares en regiones de formación estelar de distintas edades y densidades. En particular, la fotoevaporación externa es muy eficiente al destruir los discos, y así, limita el tiempo y la masa disponible para formar planetas. Estos resultados tendrán importantes consecuencias para futuros estudios de formación planetaria.



List of publications

First author

1. The viscous evolution of circumstellar discs in young star clusters
Concha-Ramírez, Francisca; Vaher, Eero; Portegies Zwart, Simon
Monthly Notices of the Royal Astronomical Society, Volume 482, Issue 1, p.732-742 (2019)
2. External photoevaporation of circumstellar discs constrains the time-scale for planet formation
Concha-Ramírez, Francisca; Wilhelm, Martijn J. C.; Portegies Zwart, Simon; Haworth, Thomas J.
Monthly Notices of the Royal Astronomical Society, Volume 490, Issue 4, p.5678-5690 (2019)
3. Effects of stellar density on the photoevaporation of circumstellar discs
Concha-Ramírez, Francisca; Wilhelm, Martijn J. C.; Portegies Zwart, Simon; van Terwisga, Sierk E.; Hacar, Alvaro
Monthly Notices of the Royal Astronomical Society, Volume 501, Issue 2, pp.1782-1790 (2021)
4. Evolution of circumstellar discs in young star-forming regions
Concha-Ramírez, Francisca; Portegies Zwart, Simon; Wilhelm, Martijn J. C.
Monthly Notices of the Royal Astronomical Society, in review

Contributor

1. A MODEST review
Varri, Anna Lisa; Cai, Maxwell Xu; **Concha-Ramírez, Francisca**; Dinnbier, František; Lützgendorf, Nora; Pavlík, Václav; Rastello, Sara; Sollima, Antonio; Wang, Long; Zocchi, Alice
Computational Astrophysics and Cosmology, Volume 5, Issue 1, article id. 2 (2018)

Proceedings

1. The size-evolution of circumstellar discs in the Trapezium cluster
Portegies Zwart, Simon; **Concha-Ramírez, Francisca**
Memorie della Societa Astronomica Italiana, Volume 88, p.648 (2017)

* * *

Curriculum Vitae

I was born on the 21st of April of 1988 in Temuco, a city in the south of Chile with a weather remarkably similar to that of Leiden. From a young age I was attracted to astronomy, or rather, to astronomy outreach: during the summer holidays, I would sit my family down and give them short “lectures” about the phases of the Moon.

It was not until my high school years in Colegio Universitario El Salvador, in Santiago de Chile, that I started developing an actual interest for physics and astronomy. The event that sparked my curiosity came about in my first year: I was invited by the only physics teacher in the school, Patricio Arriagada (who used to jokingly call himself “the physics department”), to join a recreation of Eratosthenes’ experiment to measure the radius of the Earth. Simultaneously with a group of students in a city in the north of the country, we measured the length of the shadow cast by a stick on the ground. The last-year students then used trigonometry (which was very impressive to me at that time) to calculate the radius. It was teacher Patricio who awakened my interest in physics, and it was thanks to him that I learned that astronomy was an actual career that I could study. My math teachers, Inés Millán and Marta Quevedo, were also a great support in helping me follow this path.

When I was still in high school, in 2004, I joined the Astronomy Summer School at Universidad de Chile, in which for a month I had the closest to a university education that I had had so far. We learned about the orbits of the planets of the solar system, about stellar evolution, and about galaxy dynamics. It was this course that solidified my interest not only in astronomy, but also in where I would study it. In March 2007 I arrived as a starry-eyed student to the Facultad de Ciencias Físicas y Matemáticas of Universidad de Chile, of which I am a very proud alumna. After the first two years, which were joint with the engineering programmes and consisted of basic physics, mathematics, and engineering courses, I began my specialization in astrophysics.

During my years as a bachelor student, I met some of the people that would be vital in my development as a scientist, in particular Professor Patricio Rojo and Professor María Cecilia Rivara. Professor Rojo taught the Stellar Astrophysics course, and it was thanks to him that I discovered that astronomy was not only looking through telescopes and analysing images, but that a big part of being an astronomer was developing code. Thanks to him I also had the opportunity to dip my toes into observational astronomy, in several observing trips to Cerro Tololo and La Silla to collaborate with his exoplanet research. As fascinating and exciting as those trips were, I was already starting to realize that observational astronomy was not my path. During my bachelor studies I had to carry out a small research project, which I developed with Professor Andrés Escala. While my results of this project were not particularly remarkable, it was here where I had my first approach with actual computational astrophysics: I analysed the formation of clumps in SPH simulation snapshots of galaxy collisions. I did not run the simulations myself, but I became fascinated which how much you could learn using this tool, and with how you could model all kinds of astrophysical

phenomena in a computer.

After that, I decided that computational astronomy was what I wanted to focus on. As a way to prepare, during the last couple of years of my bachelors I enrolled in a series of courses from the Computer Science department. It was in the Computer Graphics course where I would meet Professor Maria Cecilia Rivara, who also became pivotal for my future. After being successful in the class and eventually becoming Teaching Assistant for it for a few terms, I continued to work on research on Computational Geometry with Professor Rivara. I figured that a strong computational background would be key for my development as a computational astronomer, so after receiving my Bachelor in Science degree in 2013 I enrolled in the Master's degree in Computer Science at Universidad de Chile. After taking some courses and carrying out short research projects on computational geometry and graphics processing unit (GPU) accelerated computing, I started working on my thesis project. My Master's thesis consisted in the development of a light curve extraction pipeline powered by the GPU, which I completed under the supervision of Professor Rivara and Professor Rojo.

It was also during my final undergraduate years that my interest in astronomy outreach materialised into actual work. In 2012 I joined the team at Observatorio Astronómico Andino (OAA), a beautiful touristic observatory close to Santiago. There, I had the opportunity to provide astronomical tours and talks to a widely varied audience, ranging from students from the nearby primary school, to local celebrities, to the former president of Chile, Michelle Bachelet, and several ministers. It was at the OAA that I learned how to find my way around the southern sky, how to find constellations and the celestial south pole, how the sky changes during the year, at which moments of the year the solar system planets are visible, and how cold it can get at the foot of the Andes. In 2015 I began my own personal endeavour in astronomy outreach by launching "Primer Fotón"⁸, a blog where I write about astronomy and computer science. With a strong social media presence, I share naked-eyed observable astronomical events with the public, and every month I summarise a news article about astronomy in my podcast⁹. While this project took a back seat in the last year to focus on finishing my PhD, I look forward to continuing sharing astronomy with the public of all backgrounds and ages.

In September 2016 I arrived at the Leiden Observatory in the Netherlands to start my PhD project in the Computational Astrophysics group, supervised by Professor Simon Portegies Zwart. It was here when I finally got to implement my own astrophysical simulations and to bring together my love for both coding and astronomy. In early 2017 I joined the Astronomy on Tap Leiden team, which allowed me to continue sharing astronomy with the public and would become one of the most enriching experiences of my time as a PhD student.

* * *

⁸<http://primerfoton.cl>

⁹<http://podcast.primerfoton.cl>

Acknowledgements

I would like to begin by thanking the teachers, professors, and mentors in my life that helped me get on the path of science in general, and astronomy and computer science in particular: Patricio Arriagada, Inés Millán, Marta Quevedo, Patricio Rojo, María Cecilia Rivara. Thank you for your constant support, encouragement, and advice.

During my PhD years I met so many bright people, doing so many interesting things. With some of them I had the fortune of collaborating, some of them enlightened me with stimulating discussions, and some of them simply inspired me from afar with their work: Thomas Haworth, Sierk van Terwisga, Alvaro Hacar, Steven Rieder, Becky Arnold, Richard Parker, Andrew Winter, James Owen, Leon Trapman, Yanett Contreras, Liz Guzmán, Ewine van Dishoeck, the star formation and discs group at Leiden, Giovanni Rosotti, Yamila Miguel, Elena Sellentin, Pedro Russo, Suzana Filipecki, Michiko Fujii, Silvia Toonen, Stefania Giordini, Michela Mapelli, Elena Maria Rossi, Alessandra Candian, and so many more that I am probably forgetting. Thank you for being an influence in my work and in my development as a scientist, directly and indirectly, evidently or unknowingly.

I would like to thank the team of people at Leiden Observatory that made my arrival in The Netherlands and the completion of this PhD possible: Evelijn, muchísimas gracias por todo tu apoyo tanto en lo académico como en lo personal. Alexandra, thank you for all your work and your help, in particular in arranging the final stages of this PhD. Marjan, Susan, Monica, Liesbeth, thank you for your never-ending work, support, and help. It was thanks to you that my settlement in Leiden and in the observatory went so smoothly. I would also like to thank the ICT team, Eric, Erik, David, Leonardo, for their patience and assistance. Major, major thanks to Valeriu Codreanu, Maxwell Cai, and the whole support team at SURFsara for being of invaluable help in using the Cartesius supercomputer. It is not an exaggeration to say this thesis would not be finished without their friendly and patient support.

To my co-sovereigns of the CAstLe: Santiago, Maxwell, Thomas, Jeroen, Martijn. Thank you for all the lunches, conversations, office therapy sessions, Zoom borrel-breakfasts, for your insistence in taking the stairs instead of the elevator, and for your friendship. I feel incredibly fortunate to have shared these four years with all of you. Martijn, I wish you all the best as the (currently) sole ruler of the CAstLe! Thank you for all your help and all your work, it was great to collaborate with you. Steven, Arjan, and Inti, thank you for being the core that keeps AMUSE together, and for your infinite patience in helping us newcomers (and not so newcomers) use the framework.

One of the most important, formative, and enriching experiences during my PhD was joining Astronomy on Tap Leiden. I was lucky enough to be part of the team when it started and to see it grow into the amazing project that it is today. Liz, Yanett, Vincent, thank you for taking the steps to start AoT Leiden. To all the team that joined with me at the beginning: Eleonora, Sofia, Alex Mechev, Merel, Maaike, Themiyra, Carmen, MJ, Arun, and the ones that joined later: Alex Cridland, Wendy, Lammim, Michał, Marina, Helgi, Turgay. It was a

pleasure to work with all of you. I was also lucky enough to be the one to hand over the reins to a fantastic new team that has already shown they have what it takes to keep AoT going strong: Wendy, Anniek, Marta, Morgan, Marina, and I'm sure there's more of you that I don't know about. You have been doing amazing in this particularly difficult year and I wish you nothing but success in the future events!

A team which I also loved being part of during my PhD were the Borrelinas! Eleonora, Kim, Maria Cristina: it was lovely to be in the Borrel committee with you. It was exhausting at times, but I think we managed to cheer up everyone's Fridays.

To the Agraphia group: Alex, Łukasz, Ylva, Lammim. I know I rarely made it to the 9am writing sessions, but our afternoon meetings helped keep me motivated and organized. Thank you also Sarah for organizing a new writing group!

Marcela, gracias infinitas por ser parte vital de mi doctorado. Tu apoyo constante y nuestras sesiones fueron fundamentales para poder llegar a este momento.

Sarah, thank you for all your help and care when my limbs started going haywire. Our sessions were a relaxing and relieving weekly break.

To all the people from here and there that I crossed paths with during these last four and a half years: Roxanne, Alex, Gaia, Chris, Irene, Lopa, Juliette, Yorine, Jelmer. Thank you for making life in this gray country a lot more colourful.

During my PhD years I deliberately skipped many meetings, conferences, borrels, and even parties, but there is one event that I almost never willingly missed: Tuesday's pub quiz at De Burcht. My dear *Ginteam* (formerly known as *The Drunk Astronomers*): Vincent, Yanett, Max, Pablo, Anne, Caroline, Tim, Eimear, Daniel, and many more that came and went. We might have never made it to first place, but we were always the winners in my heart. Tuesday nights with you were the best mid-week break, even if it made Wednesday mornings a bit harder (thank you, Debbie, for your friendliness and heavy-handed G&Ts; they were both always very appreciated). Thank you also to *The Counts of Monte Quizzto* for adopting me during the last few pub quizzes of the Before Times; I always envied your fantastic team name!

A todos mis amigos que estuvieron siempre cerca, a pesar de la distancia: Laura, Sof, Kam, Sole, Cristi, Paulina, Silvana, Mafe, Valeria, Gaby, Luciano, Rodrigo, Nicho, Cristian, Lea, Jeremías. Gracias por estar siempre, por alegrarme la vida con sus llamadas a horas raras, por hacerme sentir cerca y por su apoyo incondicional.

During my time in Leiden I was fortunate to meet an amazing group of people that became my strongest support net and my closest friends: Cristi, gracias por ser mi confidente, consejera matrimonial, ambulancia, y partner casi oficial. Voy a extrañar nuestros cafecitos, breaks, kit-kats, y conversas tratando de escondernos de nuestros jefes. Gracias por siempre recibirme en tu casa con Claudio y Luquitas y por ser un apoyo super importante en todo. ¡Te voy a echar mucho de menos! Heather, queridísima, además de tu genial amistad me concediste el honor de ser master of ceremony en mi matrimonio. Gracias por estar siempre, por todas las conversas, las risas, los gin & tonic, los desahogos sobre la vida, y las noches viendo videos de Mounir atrooooooo. Te espero para que hagamos el tour de Jane Austen y le sigamos la pista a James Andrews. Julieta, ¡vecina! Gracias por todos los cafecitos y caminatas, los after-office, por cuidar mis plantitas, y por todas esas conversaciones dando vuelta el mundo, las ciencias, y la vida. Admiro tu trabajo y tu pasión por lo que haces y se que llegarás muy lejos. Javi, gracias por todas las risas, los sushis, las conversaciones, los memes que nunca respondí, por las sesiones de belleza, y por ser mi primera gran amiga en Leiden. Gracias por siempre estar y por tu apoyo y amistad. Santi, fuiste mi psicólogo número uno, gracias por todas las conversas, por las terapias en la oficina, por ser mi padrino de PhD y realizar tu labor tan importante llevándome siempre por una cerveza. Yanett y Max, cuando conocí a

Yanett millones de años y vidas atrás nunca me imaginé que en el futuro llegaríamos a tener una amistad. Gracias por siempre recibirme en su casa, por dejarme echarle Coca Cola a su pisco fancy, y por todas las risas, fiestas, y copas que compartimos, espero que sean muchas más. Kelsey, my girl. I feel so lucky and fortunate to have crossed paths with you when we did. Thank you for all the conversations, glasses of wine, nail art videos, and unexpected food euphemisms. Our conversations and your support kept me sane through this rollercoaster. Liz, desde que te conocí que fuiste una inspiración con toda tu fuerza y tu motivación, me siento privilegiada de haber cruzado caminos contigo. To so many more people that made my Leiden years memorable... Pablo, Pedro, Kim, Maria Cristina, Leonora, Jeroen, Thomas, Edwin, Max, Penny, Ylva, Sofia, Anne, Nikita, Jorge, Lina, Marta, Diana, Tomás, Nico, Wi-jnand, Igone, Carmen, Luis, Javier, Alvaro, Sylvia, Daniel, Lammim, Andrés, and so many more that I'm probably forgetting (sorry!). Thank you for all the good times and for making this town feel like home.

All of my achievements would never have been possible without the everlasting and unconditional support and love from my family. Mamá, Pau, Caro: a pesar de la distancia siempre han sido mis mayores fans y mi mayor inspiración, las amo y siempre las he sentido cerca. Papá, todo lo que he logrado y lo que soy hoy en día te lo debo a ti, a tu amor infinito e incondicional por nosotras, a tu apoyo y a tu orgullo. Sé que estuviste conmigo en cada paso de este camino, tu presencia y tus palabras me acompañan siempre.

A todo el resto de mi loca y un poco enredada familia: a mis tíos Nana y Gaby; mis primos Juan Pablo, Jorge Antonio, y sus familias; Jorge Hernán; Olga, Javiera, Pablo. A mis abuelas directas y putativas: Nena, Katty, Inés, tía Silvia; tío Conrado. Me siento orgullosa de ser parte de una familia tan linda, y les doy las gracias a todos por su apoyo y por acompañarme siempre aunque sea a la distancia. Mario, gracias por todo tu apoyo, por tu alegría, por recibirnos con Vincent en tu casa, ¡y por tu rica comida!

To my family in this side of the world, the Van Eylens: Anit, Luk, Wout. Thank you for welcoming me into your home and for making me part of your family since day one.

Four years ago, I never imagined that I would receive a marriage certificate before a doctorate diploma, but life has its way of going with her own plans. Vincent! I am not exaggerating when I say I would have not finished this thesis without your never-ending love and support. Thank you for being my best friend, my # 1 cheerleader, my editor, translator, counsellor, cook, barman, nurse. Knowing that I had you by my side gave me the strength to finish my PhD. I can't thank you enough for all your support! I can't wait to start this new chapter of our life together. I love you with all my heart.

